2013-01-15

Metallization of DNA and DNA Origami Using a Pd Seeding Method

Yanli Geng
Brigham Young University - Provo

Metallization of DNA and DNA Origami

Using a Pd Seeding Method

Yanli Geng

A dissertation submitted to the faculty of
Brigham Young University
in partial fulfillment of the requirements for the degree of

Doctor of Philosophy

Adam T. Woolley, Chair
Robert C. Davis
Roger G. Harrison
Matthew R. Linford
Dean R. Wheeler

Department of Chemistry and Biochemistry

Brigham Young University

January 2013

ABSTRACT

Metallization of DNA and DNA Origami
Using a Pd Seeding Method

Yanli Geng
Department of Chemistry and Biochemistry
Doctor of Philosophy

In this dissertation, I developed a Pd seeding method in association with electroless plating, to successfully metallize both lambda DNA and DNA origami templates on different surfaces.

On mica surfaces, this method offered a fast, simple process, and the ability to obtain a relatively high yield of metallized DNA nanostructures. When using lambda DNA as the templates, I studied the effect of Pd(II) activation time on the seed height and density, and an optimal activation time between 10 and 30 min was obtained. Based on the Pd seeds formed on DNA, as well as a Pd electroless plating solution, continuous Pd nanowires that had an average diameter of ~28 nm were formed with good selectivity on lambda DNA. The selected Pd activation time was also applied to metallize "T"-shape DNA origami, and Au coated branched nanostructures with a length between 200-250 nm, and wire diameters of ~40 nm were also fabricated. In addition, I found that the addition of Mg^{2+} ion into the reducing agent and electroless plating solution could benefit the surface retention of Pd seeded DNA and Au plated DNA structures. This work indicated that DNA molecules were promising templates to fabricate metal nanostructures; moreover, the formation of Au metallized branched nanostructures showed progress towards nanodevice fabrication using DNA origami.

Silicon surfaces were also used as the substrates for DNA metallization. More complex circular circuit DNA origami templates were used. To obtain high enough seed density, multiple Pd seeding steps were applied which showed good selectivity and the seeded DNA origami remained on the surface after seeding steps. I used distribution analysis of seed height to study the effect of seeding steps on both average height and the uniformity of the Pd seeds. Four-repeated palladium seedings were confirmed to be optimal by the AFM images, seed height distribution analysis, and Au electroless plating results. Both Au and Cu metallized circular circuit design DNA origami were successfully obtained with high yield and good selectivity. The structures were maintained well after metallization, and the average diameters of Au and Cu samples were ~32 nm and 40 nm, respectively. Electrical conductivity measurements were done on these Au and Cu samples, both of which showed ohmic behavior. This is the first work to demonstrate the conductivity of Cu metallized DNA templates. In addition, the resistivities were calculated based on the measured resistance and the size of the metallized structures.

My work shows promising progress with metallized DNA and DNA origami templates. The resulting metal nanostructures may find use as conducting interconnects for nanoscale objects as well as in surface enhanced Raman scattering analysis.

Keywords: conductivity measurements, copper, DNA-templated nanofabrication, DNA origami, electroless plating, gold, lambda DNA, metallization, nanocircuits, nanowires

ACKNOWLEDGMENTS

The past five years have been one of the greatest experiences in my whole life.

I thank my family members for their support during my studies when I was down.

I thank my advisor Dr. Adam T. Woolley for his mentorship and patience during the five years at BYU. His scientific guidance helped me to overcome the difficulty in my studies. I also thank him for giving me the trust, the encouragement, and the freedom during the research that I needed along the way to come to the end.

I thank my graduate committee members, Dr. Robert C. Davis, Dr. Roger G. Harrison, Dr. Matthew R. Linford, and Dr. Dean R. Wheeler for their time and suggestions that helped me during my studies.

I thank Dr. John Gardner, Michael Standing, and Dr. Jeffrey Farrer for training and assistance with electron microscope imaging.

I thank Dr. John N. Harb for his kindness and scientific suggestions during my research.

I thank Dr. Robert C. Davis's group for allowing me to use their lab and the electron-beam lithography system.

I thank Elisabeth Gates, Dr. Anthony Pearson, Dr. Ming Yu, Dr. Jianfei Liu, Bibek Uprety, Pamela Nge, Jayson Pagaduan, and Sarah Jamieson for their research assistance and friendship during the past five years.

I thank the Department of Chemistry and Biochemistry of BYU for providing me the opportunity for the graduate study.

I thank National Science Foundation (CBET-0708347) for the funding.

TABLE OF CONTENTS

LIST OF FIGURES

CHAPTER 1: INTRODUCTION

1.1 NANOMATERIALS AND NANOTECHNOLOGY

Nanomaterials and nanotechnology have been attracting increasing interest from governments, research institutions and industry all over the world for several decades. Nanomaterials are substances with at least one dimension between 1 and 100 nm (1 nm=10^{-9} m); in other words, nanomaterials are at or near the atomic or molecular scale, and can achieve functions that are different from bulk materials. As the size of materials decreases close to the size of atoms, the material properties change due to the effects of quantum mechanics. Thus, the properties of nanomaterials such as surface area, electrical conductivity, optical absorbance or emission and mechanical characteristics are different from those of traditional bulk materials. Nanomaterials can be sorted to three categories according to their highly ordered structures: one dimensional materials including thin films, coatings or engineered surfaces; two dimensional materials entailing nanowires and nanotubes; and three dimensional (3D) materials such as nanoparticles, fullerenes, and quantum dots.

The concept of nanotechnology was first introduced by physicist Richard Feynman in his talk "There's Plenty of Room at the Bottom" in 1959.[1] In this talk, he imagined arranging the very "atoms" the way we want and described the hope for fabricating tiny circuits. In 1974, Norio Taniguchi first used the term nanotechnology to describe the ability to fabricate materials at the nanometer scale. Although the idea was presented over 50 years ago, little progress was seen until the mid 1980's. Development of atomic-scale imaging techniques such as scanning tunneling microscopy (STM) and transmission electron microscopy (TEM) has aroused more and more interest in nanotechnology for design and fabrication of nanomaterials. The term

"nanotechnology" can be defined as research, development, manipulation, control or use of nanomaterials.[2] Emphasis is not only on the size of the materials, but also on exploring new features and functions of these materials at the nanometer level. Nowadays, nanotechnology is considered an interdisciplinary area of science (and art) that includes parts of the fields of chemistry, physics, biology, computer science, as well as engineering fields.

1.2 BENEFITS AND APPLICATIONS OF NANOTECHNOLOGY

Nanotechnology as an emerging discipline offers a lot of potential applications that could impact our daily life. These applications span various fields from environment and energy to medical products and electronics.

1.2.1 Environment

Environmental problems such as pollution and energy conservation are global issues that are driven by traditional fossil-energy production, transportation, and pollution. Researchers now are exploring nanotechnology to deal with this problem, and solutions could benefit the environment through more effective pollution control and energy saving improvements. In 2003, Masciangioli and Zhang divided the potential application of nanotechnology for environment into 3 categories: pollution sensing and detection, treatment and remediation, and prevention.[3]

One technique for pollution sensing is surface enhanced Raman spectroscopy (SERS) in which Raman signals from molecules are tremendously increased by attaching to nm-scale metal structures.[4] SERS has attracted interest due to its achievement of single molecule detection as Raman scattering increases of up to10^{15}-fold by growing metal nanostructures on a surface.[5] SERS technique has been used for ultrasensitive detection of toxic pollutants in the

environment.[6-7] For example, Guerrini et al.[6] detected low concentration of pesticide endosulfan via SERS using modified Ag NPs with lucigenine dication as the probe substrate. The detection limit is as low as 20 ppb. Leyton et al.[7] reported the use of humic acids (HA) modified Ag nanoparticles as probe substrate to detect low concentrations of polycyclic aromatic hydrocarbons (PAHs).

Other nanomaterials such as carbon nanotubes[8-10], nanowires[11-12] serve as chemical sensors for pollutant detection. For instance, researchers from Stanford University demonstrated individual semiconducting single-walled carbon nanotubes (S-SWNTs) to detect small concentration of gas molecules by the change of conductance upon exposure to NO_2 or NH_3.[9] Aluri et al.[11] reported the use of TiO_2 nanocluster functionalized Gallium nitride nanowires for sensing aromatic compounds based on the current change when the nanowires were exposed to aromatic compound vapors. The sensitivity of this method could be down to 50 ppb.

Nanomaterials can also aid in pollutant removal. Magnetites are used to absorb organic pollutants due to the convenience of separating them from the medium. Zero-valent iron nanoparticles (NPs) are effective in destroying or reducing chemical pollutants in water due to their high surface area and energy.[13] Applications include aqueous removal of heavy metal ions,[14] arsenic ions,[15-18] halogenated hydrocarbons,[19-21] and organic compounds.[22] Semiconducting light-activated nanoparticles such as TiO_2 are attracting researchers' interest due to their nontoxicity, low cost, chemical inertness and ability to remove organic pollutants in various media. Moreover, catalytic performance can be enhanced by doping, which can extend activity to visible light irradiation.[23] Carbon nanotubes (CNTs) have been demonstrated to be a novel adsorbent for organic pollutants since the first paper on their superior adsorbing ability for

dioxin removal.[24] It has also been reported that CNTs can improve the adsorption capacity of pollutants by chemical modification to form composites with other materials.[25-27]

1.2.2 Energy

Energy challenges including increasing energy demand, increasing oil prices, and decreasing fossil fuel supply combined with environmental impacts are motivating the development of innovative and clean energy resources. Materials at the nanoscale have different properties from the bulk, and can provide new strategies for designing next-generation energy systems.[28] Nanotechnology has been exploited in energy in several ways, including: (1) improving the utilization efficiency of fuels through new nanocatalysts and nanoreactors in refining and during use;[29] (2) improving energy storage and transmission capacity;[30-31] and (3) developing new strategies for solar energy conversion.[32] Studies have been reported in all these areas. For example, nanozeolites with different structures have been used in catalytic cracking of gas oil.[33-34] Carbon nanomaterials such as CNT fibers[35] and graphene sheets[36] have potential application in hydrogen storage due to the increased uptake capacity of H_2 after surface functionalization. Additionally, Peng et al.[37] reported the decoration of 5-10 nm Pt NPs on close packed Si nanowires by electroless plating. The Pt NP coated Si nanowires had enhanced photoconversion efficiency (up to 8.1%), offering a promising hybrid for solar energy conversion. Other nanomaterials are being developed to harvest solar power. For example, Li et al.[38] demonstrated the fabrication of p-n heterojunction by combination of C60-fullerene-encapsualted S-SWNTs with n-type Si. This device showed a promise in conversion of near-infrared light into electrical energy. Additionally, researchers succeeded in printing a Au nanoantenna array onto flexible a polyethylene film, which were then used as nantenna electromagnetic collectors.[39] The devices

were up to 90% efficient for electricity production by collecting solar irradiation in the mid infrared wavelength region.

1.2.3 Medicine

Nanomaterials and nanodevices give unique promise in medical fields such as drug delivery and tissue engineering. One example is mesoporous silica nanoparticles (MSNs) which have large surface area and porous structures. Further functionalization of these materials with biodegradable polymers and proteins provides good biocompatibility for cell internalization, for use as carriers for intracellular controlled release and drug delivery.[40] For instance, Lee et al.[41] demonstrated the pH-dependent loading and controlled release (acidic for loading and neutral for release) of two anionic drug molecules on trimethylammonium functionalized MSNs. The drug release in neutral buffer solution was achieved via strong electrostatic repulsion between negatively charged deprotonated silanol groups on the MSN surface and anionic drug molecules. This carrier is promising for oral delivery drug systems that target the intestine (pH close to neutral) for drug release. Additionally, composite particles of MSNs and superparamagnetic nanocrystals can not only be used in drug delivery but also in simultaneous imaging.[42]

CNTs have also been reported for potential applications in biomedicine. For example, the biocompatibility of CNTs and their effects on cellular function have been studied as well as the potential application in tissue engineering. Collagen-CNT composites could maintain high smooth muscle cell viability.[43] Functionalized CNTs were used as substrates for neuronal growth;[44] in addition, researchers have found that multi-walled CNTs had good compatibility with bone tissue and could accelerate bone formation by interacting with bone morphogenetic protein.[45]

Although nanotechnology for medicine applications has not yet seen much clinical impact, in the future, with the continued development of the technology and understanding of interactions, it would show important benefits in this field.

1.2.4 Information and electronics

According to Moore's law, the number of transistors in integrated circuits doubles 18 months.[46] As the size of electronics gets smaller and smaller, increasing the capabilities of electronic devices while also reducing their dimensions and power consumption becomes a challenge. Nanotechnology has the potential to handle this issue. Although the use of nanotechnology in electronics is still in its early stages, especially in integrated circuit applications such as logic computing and data storage, some exciting studies have been reported in the last ten years. Synthesized nanomaterials can serve as either passive (e.g., data storage media or interconnect) or active (e.g., transistor) components.[47] Since their discovery in the early 1990s,[48-49] CNTs have been intensely investigated due to their metal or semiconducting properties which have potential applications in nanoelectronics. Both single-walled and multi-walled CNTs can serve as field effect transistors.[50-53] Recently, Franklin et al.[54] produced the first sub-10 nm CNT transistor (channel length down to 9 nm), which is superior to Si-based devices at low operating voltage. Other nanostructured materials such as graphenes, and metal/semiconducting nanowires may also find applications in electronics due to their process compatibility with silicon.[55-56]

1.3 OVERVIEW OF TOP-DOWN AND BOTTOM-UP METHODS

Nanofabrication involves processes and methods to construct nanostructures and devices with dimensions smaller than 100 nm. Compared with hundreds of applications mentioned above, the fabrication methods are divided into three major categories: top down, bottom up and hybrid, sorted by the processes applied in nanomaterials fabrication. The last decade has seen the development of a variety of nanofabrication techniques, including either top down, bottom up or their combination, to satisfy the high demand for nanotechnology.

1.3.1 Top-down methods

A top-down approach corresponds to the use of nanolithographic tools to fabricate nanoscaled devices with desired structures starting from macroscaled materials.[57] In this approach, the most commonly used technique is photolithography, which has been widely used in manufacturing structures in silicon-based technology. In semiconductor manufacturing, the overall procedure for lithography typically includes several steps in sequence: surface cleaning, photoresist coating, exposure and developing, etching to remove the uppermost layer that is not protected by photoresist, metal coating by electroplating or deposition, and photoresist removal.

Photolithograhpy is commonly used in today's semiconductor industry. Next-generation lithographic (NGL) techniques refer to nanolithographic methods used in integrated circuit manufacturing that replace photolithography. These techniques include X-ray lithography, electron-beam lithography (EBL), extreme ultraviolet lithography, soft nanoimprint lithography, and liquid immersion lithography. On May 2, 2011, Intel announced the realization of a 22 nm three-dimensional tri-gate transistor in mass production using NGL techniques.[58] Other

nanolithographic methods include scanning probe lithography, block co-polymer lithography, quantum optical lithography, etc. The main drawback of lithography is that it generally requires a combination of instrumentation, cleanroom environment, and materials that remain very expensive to achieve sizes below 50 nm.[59]

1.3.2 Bottom-up methods

In contrast, bottom-up approaches build up more complex multifunctional nano-structural materials or devices by controlling the assembly of molecules or atomic species based on the interaction of the system. The building blocks can be molecules, atoms, or NPs with various compositions and properties (size, shape, or chemical bonding). Bottom-up approaches include atomic layer deposition,[60-61] sol gel nanofabrication,[62] chemical vapor-phase deposition[63-64], and template-mediated nanofabrication.[65] Bottom-up nanofabrication can potentially overcome a main disadvantage of top-down approaches: the fabrication cost. In spite of advantages of bottom-up methods, this nanofabrication strategy has several drawbacks. For example, the resulting nanostructures usually contain defects[66] or errors and lack complexity for self-assembly, which is still in its early stage and less well developed. Other disadvantages also exist such as difficulty of controlling synthesis for sol gel nanofabrication, and long process time for atomic layer deposition.[59]

Alternatively, hybrid approaches, which combine both top-down and bottom-up techniques, are also frequently applied in nanofabrication.[66-68] Hybrid approaches are promising to overcome drawbacks from both top-down and bottom-up approaches, to make nanofabrication higher throughput, more productive and more efficient. For instance, Cheng et al.[66] developed a technique by combining self-assembly of block copolymers with top-down lithography to

fabricate highly ordered block copolymer nanospheres. The nanospheres were confined within linear grooves which were created by lithographic methods, resulting in ordered nanosphere patterns with controlled spatial arrangement. This work demonstrated that hybrid nanofabrication is efficient way to yield defect-free nanostructures. Additionally, Güder et al.[68] reported the use of low-temperature atomic layer deposition and phase-shift lithography to fabricate sub-100nm wide nanochannels with various compositions. The whole procedure had only three steps: generation of sub-100 nm photoresist line patterns by lithography; deposition of metal oxide via ALD; and removal of remaining photoresist. This method was indicated to be low-cost and simple.

1.3.3 Seeding and plating

Electroless plating is a redox reaction process mainly used for metal deposition. It is an autocatalytic reaction in which metal ions in an aqueous solution are selectively reduced only at the surface of a catalytic substrate, and a continuous metal deposition on the substrate is driven by the catalyst.[69] Electroless plating does not require an electrical source, making it different from electroplating. Compared with electroplating, electroless plating needs less equipment and allows metal to deposit evenly and uniformly with low stress over all parts of the substrate with appropriate activation.[70] Coating with different compositions such as Cu, Ni, Au, Pd, etc. have been obtained by electroless plating.

Differences between electroplating and electroless plating process can also be seen through the overall reactions.

In Eq. **(1-1)** for electroplating, the n electrons are provided by an external power supply. The metal ion M^{n+} gains *n* electrons and is reduced to M^0 in the process.

$$M^{n+} + ne^- \xrightarrow{\text{electrode}} M^0 \qquad \textbf{(1-1)}$$

For electroless plating as shown in Eq. (1-2), the metal ion obtains electrons from the reducing agent in the plating solution, which provides electrons to catalytic surface. The catalytic surface can be the surface of a catalytic metal seed M on substrate initially and the surface M itself during the subsequent continued plating.[71]

$$M^{n+} + \text{Red(aq)} \xrightarrow{\text{catalytic surface}} M^0 + \text{Ox(aq)} \qquad \textbf{(1-2)}$$

For electroless plating, an activation of the surface is required prior to plating. This step is called "seeding" in which catalysts or seeds are formed on desired areas of the substrate. Seeds normally are noble metals (Pd, Ag, etc). That can be made on the surface by physical or chemical methods. These approaches have been widely described in the literature. Some examples are: vapor phase deposition such as sputtering or physical vapor deposition,[70] plasma immersion ion implantation,[72-73]photochemical deposition methods such as laser assisted[74-75] or thermal decomposition of photosensitive metal clusters/compounds[76] to form seeds, inkjet printing of solution containing metal nanocolloids,[77-78] etc.

After activation, the surface is ready for electroless plating. An electroless plating bath typically consists of: a metal ion source of the desired plating metal, a reducing agent, complexing agents, stabilizers/inhibitors, and sometimes, a buffer to maintain the pH of the solution.[69] Some commonly used reducing agents in electroless plating solutions are: hypophosphite, boron compounds, formaldehyde, and hydrazine. The complexing agents can (1) serve as a buffering system that maintains the pH of the solution during deposition; (2) prevent

metal salts from precipitating; and (3) reduce the concentration of free metal ion in solution.[69] Additionally, the use of stabilizers can prevent homogeneous reactions that would cause decomposition of the plating solution. The pH of the solution can range from acidic to highly basic, depends on the constituents used, and the pH value is also essential for plating results. Additives are sometimes used to adjust plating rate and improve surface morphology.[79-81] For example, the addition of Cu^{2+} ion into an electroless nickel plating solution can increase the Ni deposition rate and improve surface morphology when the concentration of Cu^{2+} was below a critical value of 536 mg/L.[79]

Although electroless plating method has been commonly used in the metal coating industry, some aspects of the mechanism of the autocatalytic process are still not clear; so far, some understanding has been built up for the basic stages of the process. One requirement of the electroless plating is the localization of the reduction reaction on the catalyst surface which is the only possible place for subsequent metal deposition.[82] One explanation is that an intermediate product such as hydride ion may form and land initially on the catalytic surface, which then donates an electron and reduces metal ions.[83] This hypothesis is consistent with results from some Ni and Cu electroless plating solutions which have hydrogen-containing reducing agents.

A more sophisticated explanation called mixed-potential theory has been used to better understand the process. According to the theory, the metal complex and reducing agent may bind at a distance to the surface while electron exchange between them occurs via the metal catalyst.[84] Thus, the overall reaction of electroless plating of Eq. **(1-2)** is divided into the cathodical reduction reaction and anodical oxidation reaction given by Eq. **(1-3)** and **(1-4)**, respectively.

$$M^{n+} + ne^- \xrightarrow{\text{catalytic surface}} M^0 \qquad \textbf{(1-3)}$$

$$\text{Red(aq)} \xrightarrow{\text{catalytic surface}} \text{Ox(aq)} + m\text{e}^- \qquad \textbf{(1-4)}$$

Both reactions occur on the catalytic metal surface simultaneously, thus resulting in a steady state in the system in which the rates of reduction and oxidation reactions are equal, as well as a compromised potential called the steady state mixed potential, E_m.[82] By introduction of the mixed potential, both partial reactions are shifted from their equilibrium, resulting in non-equilibrium of the system. When the ΔG of the system is negative, the net overall reaction, the autocatalytic process Eq.**(1-2)**, occurs. The mixed-potential theory has been verified for various electroless plating including nickel, gold and copper.[71]

1.3.4 Nanomaterials characterization methods

Characterization of nanomaterials is important for researchers to investigate morphology and properties by means of spectroscopy and microscopy.

1.3.4.1 Overview of atomic force microscopy

Atomic force microscopy (AFM) is a technique for nanometer-resolution surface imaging. Samples being imaged need no special treatment before scanning, and the whole AFM process can be performed under ambient conditions or even in solution. The main components of an AFM instrument include a sharp tip with an end radius of a few nanometers (located at the end of a cantilever), a high sensitivity three-axis piezoelectric scanner, a laser diode, and a photodiode detector. Imaging is based on the repulsive (contact/ tapping mode) or attractive (non-contact mode) interactions between the tip and the sample surface. When the tip is in close proximity to the surface, the repulsive force occurs, and results in deflection of the cantilever. The deflection of the cantilever is then measured using a laser beam reflected on the top surface of the cantilever and onto photodiode detector. The tip-cantilever or the sample is set on a piezoelectric

tube. The three-dimensional X, Y, and Z displacement of the tip (or sample) thus can be controlled by applying voltage to the X, Y, or Z electrodes of the piezoelectric tube.

One of the often-used AFM modes for nanomaterial surface imaging is tapping-mode, which I used for all my samples. In tapping mode, the cantilever/tip oscillates up and down close to its resonance frequency, controlled by piezoelectric scanner. The amplitude is imposed high enough (above 10 nm)[85] so the tip "tap" the surface periodically. During imaging, a constant oscillation amplitude is used as a feedback signal, and is maintained as the tip (or sample) lowers or raises by vertical adjustments of the piezoelectric scanner. Such vertical changes of scanner are recorded as a height image which then represent the topography of the sample surface. Compared with contact mode, the tapping mode, in which the tip does not stick to the surface during imaging, results in less damage to both the sample and the tip as well as less distortion on measurement data. Additionally, in tapping mode, the resolution at Z direction is high enough to detect DNA on surface and to observe the height differences before and after DNA metallization during my research.[86]

1.3.4.2 Overview of scanning electron microscopy

Scanning electron microscopy (SEM) is another useful tool for investigating the morphology of nanostructured samples. SEM uses signals derived from electron-sample interaction to create images that can indicate surface features including morphology, and chemical composition. For a typical SEM, the fundamental principles of operation are as follows. In a vacuum chamber, an electron beam generated from an electron gun is focused by condenser lenses. The focused beam containing primary electrons is scanned across the surface. Energy exchange between incident primary electrons and the sample produces signals such as secondary electrons, back-scattered electrons, and characteristic X-rays. These signals of interest are then detected to generate

images. Characteristic X-rays, which are emitted when the electron beam interacts with inner shell electrons from the sample, can be collected in a technique called energy dispersive SEM-X-ray (EDX) spectroscopy, which is used to determine the chemical composition of sample.

1.4 BOTTOM-UP NANOFABRICATION

Bottom-up nanofabrication usually is the combination of (1) building block fabrication and (2) self-assembly, and these two steps are sometimes used in sequence. Some of the most common bottom-up nanofabrication approaches are described in this section.

1.4.1 Atomic layer deposition

Atomic layer deposition (ALD) is an ultra-thin-film deposition technique for depositing one atomic layer at a time by a self-limiting mechanism, which distinguishes it from other chemical vapor deposition methods. ALD works through chemical gas phase deposition by alternating saturating surface reactions.[87] A typical ALD reaction involves two volatile precursors, for example, organometallic compounds, which react with a surface one-at-a-time, sequentially. Each precursor reaction is followed by a purge step in which excess precursor is evacuated. ALD nanofabrication has several advantages, including accurate thickness film control to atomic level precision, high reproducibility, and adhesion with the surface due to chemical bond formation at the first atomic layer.[59] ALD has been a useful technique to generate functional devices of hollow structures.[88-89] For example, Nam et al.[89] demonstrated the use of self-limiting ALD to fabricate sub-10-nm nanochannels. The fabrication process included: (1) fabrication of trench-pipe feature on SiO_2 with a thin Si coating; and (2) ALD of a conformal film inside of the structure to make nanochannels with controlled diameter. These nanochannel structures have

potential application as ion-field effect transistors. In addition, ALD is also used to make core-shell heterostructures.[90-91] Weber et al.[90] fabricated supported core/shell Pt/Pd nanoparticles using ALD via: (1) island growth of Pd NPs Al_2O_3, and (2) a selective deposition of the Pt shell around the Pd NPs. The core/shell bimetallic NPs can be used in catalysis.[90]

1.4.2 Sol gel nanofabrication

Sol-gel is a wet chemical technique that forms products (mainly metal oxides) from sol-precursors. During the process, a gel is obtained by mixing the precursors (sol) followed by hydrolysis or poly-condensation reactions in which a gel-like diphasic system forms. The structure and properties of the gel then are changed by aging, during which stiffening and coarsening occur. To form the final product, the resulting gel usually needs further drying and sintering.[92] The sol-gel method has attracted growing interest in nanofabrication because it is relatively low cost and has the ability to mass produce nanomaterials with non-toxicity, high purity and reproducibility. So far, nanomaterials with different structures such as films[93] and nanowires[94] have been fabricated. Ansari et al.[93] reported the use of sol-gel to obtain nanoporous ZnO film on indium tin oxide coated glass. The film was further modified with thiolated ssDNA and used as bioelectrode for a DNA biosensor, and the results indicated promising performance.

1.4.3 Template-assisted nanofabrication

Materials that contain nano-sized pores or reactive functional groups can be used as a template to form nanostructures. For example, porous anodic aluminum oxide (AAO) has been used for the production of nanowire arrays,[95] or carbon/silicon nanotube arrays.[96] Materials are formed in AAO templates through electrodeposition, which gives a controllable and low-cost technique for

metal nanowire array fabrication. Metal nanowire arrays such as copper,[97-98] palladium,[99] and alloys[95, 100] have been produced. For example, the production of highly ordered, well-aligned and parallel copper nanowire arrays by AAO template-assisted electrodeposition method was demonstrated.[98] The resulting nanowires had an average width of ~100 nm, and electrical conductivity measurements showed a lack of ohmic behavior. Thus, although the paper demonstrated templated Cu nanowire arrays, more work needed to be focused on both single nanowire production and improvement of conductivity for electronic applications. Micelles and block copolymers are also used as templates for fabrication of variety of nanostructural composites or nanoparticles due to their particular configurations.[101-103] For example, Koh et al.[101] demonstrated the fabrication of Pt/Au bimetallic nanospheres by using a triblock copolymer where one block coordinated with Pt(II), while the other block coordinated with Au(III) when the two metal ion solutions were added to system one after the other. The TEM images indicated that the inner diameters of nanosphere ranged from 20 to 40 nm. Additionally, biomolecules such as peptides and proteins are also frequently used in template-mediated nanofabrication.[104-107] Patolsky et al.[106] demonstrated the used of G-actin as a template to form Au nanowires and Au containing filaments. Metallization was achieved by polymerization of Au NP-functionalized G-actin monomer units, followed by catalytic plating on the NPs in Au^{3+} solution. The resulting nanowires had a thickness of 80 to 200 nm and showed high electrical conductivity. Similar to proteins, DNA molecules are also used frequently as templates for nanofabrication. In following section, I will talk more about DNA nanofabrication.

1.5 FUNDAMENTALS OF DNA MOLECULES

DNA is a biomolecule that contains and carries the genetic information for living organisms. Due to its unique features such as molecular recognition, programmability and self-assembly, DNA holds promise for designing nanostructures.

1.5.1. DNA structure

The ability of DNA to build up nanostructures through self-assembly is due to the unique double-stranded helix architecture, first described by Watson and Crick in 1953.[108] Natural DNA has a double helical structure with a sugar phosphate backbone that carries four nitrogenous bases, adenine (A), thymine (T), cytosine (C) and guanine (G), with hydrogen bonds between complementary bases to form base pairs (A-T and C-G). Figure 1.1 shows schematics of DNA structures. The distance between base pairs is 0.34 nm, and one full turn of the helix is about 3.5 nm, or 10 to 10.5 base pairs long.

1.5.2 Properties of DNA

1.5.2.1 Physical properties

Two different base-base interactions exist in DNA structure. One is vertical π-stacking interaction (dashed lines in Figure 1A), and the other is planar hydrogen bonding interaction (also seen in Figure 1C-D), both interactions are non-covalent. Variables such as ionic strength, pH, dielectric constant of the solvent and temperature can break the base-base interactions, resulting in a helix to coil transition which is called DNA denaturation (melting). In most cases, this only disrupts the non-covalent interactions, i.e., the double helical structure, not the bases or

the sugar phosphate backbone. DNA denaturation caused by temperature is related to base composition. G- C pairs are more stable than A-T (three vs. two hydrogen bonds) under heating; thus, the melting temperature (T_m) is related to G+C content percentage.[109] The denaturation of DNA is usually reversible, for example, by slow cooling; however, in certain circumstances of organic solvents, DNA cannot return to its normal helical structure.[110] DNA condensation, the formation of a highly ordered toroidal structure, can happen if the negative charges of the phosphate groups are neutralized by metal ions.[111]

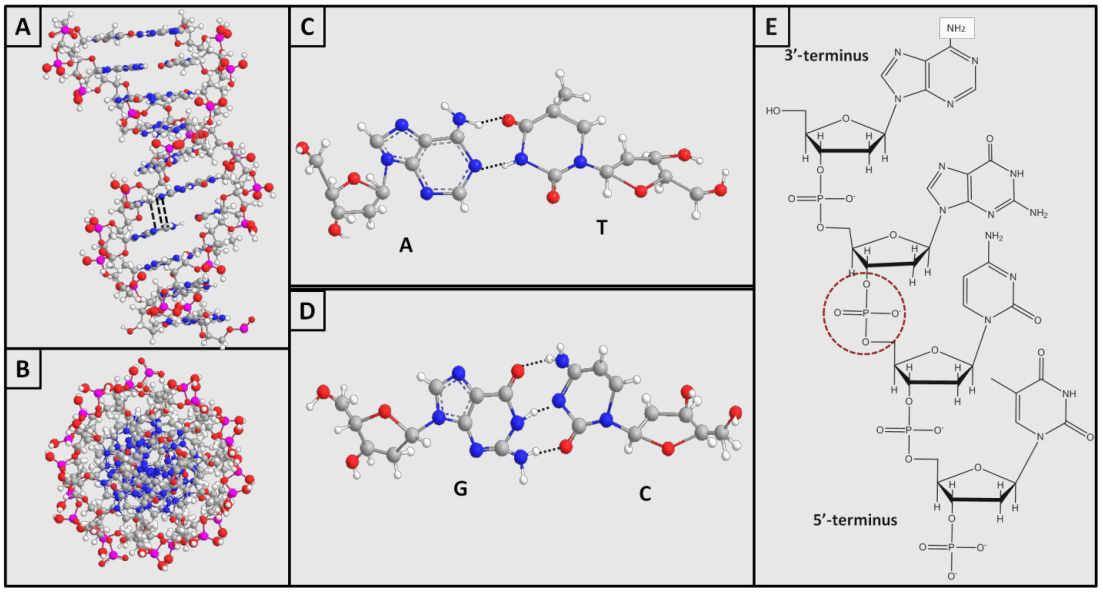

Figure 1.1. Schematics of DNA structure. (A) 3D view of DNA helical structure. Dashed lines represent π-orbital overlaps between two bases. (B) Axial view of (A). (C-D) The formation of Watson-Crick base pairing between complementary bases via hydrogen bonds. (E) Single stranded DNA with sequence 3'-AGCT-5' indicating phosphate backbone link and structural information for each base.

1.5.2.2 Electronic properties

The last two decades have seen an increasing effort to understand the electronic properties of DNA molecules.[112-114] It was suggested that DNA had the potential to be conductive due to the π-orbital overlaps between bases (Figure 1.1A)[115] and thus could transport electrons. However,

this conclusion has not yet been confirmed, and contradictory results have been obtained by different studies as well as divergent outcomes from theoretical work and experiments. Reported conductivity properties range widely from insulating[114, 116] and semiconducting[117-120] to conducting,[113, 121-122] or even to proximity-induced superconducting.[123] Storm et al.[124] observed the absence of any electrical conductivity of DNA molecules on silicon or mica using Au or Pt electrodes, and concluded that both single and small bundles of DNA are insulating.

Lee et al.[120] found that DNA conductance can be changed by several orders of magnitudes using oxygen hole doping (oxygen adsorption). The experiment was based on previously observed results[125] showing that holes were generated on some polymers adsorbed oxygen molecules. Thus for a p-type semiconducting DNA, an increase in conductance should be observed due to an increase in holes by oxygen adsorption; whereas, for DNA of a *n*-type semiconducting property, conductance should decrease. The result indicated that DNA acts as *p*-type semiconductor when the oxygen adsorption experiment was carried out on poly(dG)-poly(dC) DNA molecules, whereas for poly(dA)-poly(dT), it has *n*-type semiconducting properties.

Although it's still an unsolved problem, some other factors have been reported to influence the conductivity of DNA, such as the type of DNA sequence, aggregation of DNA molecules (ropes vs. single molecules), DNA molecule length, and temperature.[126-128] So far, since no solid evidence proves that reasonable conductivity exists in native DNA molecules on a large length scale, the application of DNA for nanodevices in electronics has been limited. Thus, more work must be done to solve this problem. For instance, DNA contains many functional groups and allows the specific formation of base pairs, both of which can allow DNA modification and thus

expand the use of DNA in nanofabrication. In this regard, the past 15 years have witnessed a dramatically growing interest in manipulation of DNA for further nanofabrication.

1.5.3 Interactions of DNA with metal ions

Metal ions interact with two main groups on nucleic acids: (1) phosphate backbones and (2) nitrogen, and oxygen atoms on nucleobases. Figure 1.2 shows base chemical structures. Each A-T base pair has two non-covalent hydrogen bonds (dashed lines), and each G-C base pair has three hydrogen bonds. Phosphate groups are deprotonated in solution when the pH is above 2.5, and thus are negatively charged. These anions have electrostatic interactions with cations, including those of Group 1A (Li^+, Na^+, K^+, etc.), and 2A (Mg^{2+}, Ca^{2+}, etc.). These cations can stabilize the DNA double helix by neutralizing the negative charges on sugar-phosphate backbone, but have little effect on DNA conformation.[129] However, at typical concentrations, it was demonstrated that a high concentration of Li^+ or Na^+ ion caused the conformation change of B-DNA to Z-DNA.[130]

Besides the electrostatic interactions mentioned above, metal cations also interact with DNA through coordination and form complexes with DNA bases. Most transition metal ions are in the latter category, forming complexes with DNA bases through their totally or partially empty d orbtials, which can serve as electron acceptors from nitrogen or oxygen atoms on the bases. The nucleophilic sites on the bases that coordinate with metal ions include the N7 position on guanine or adenine bases, O6 on guanine, N3 on cytosine and deprotonated N3 on thymine.[131] Cations may also interact with other sites such as N3 on cytosine and N1 on adenine, which are not approachable under base pairing.[132] The strength/stability of base binding site interaction with transition metal ions has the following order: N7/O6(G)>N3(C)>N7(A)>N1(A)>N3(A,

G).[133] In addition, coordination of metal cations to the binding sites involved in hydrogen bonding, such as N3(C) and N1(A), decreases the melting temperature of the DNA double helix,[131] making thermal denaturation easier.[129]

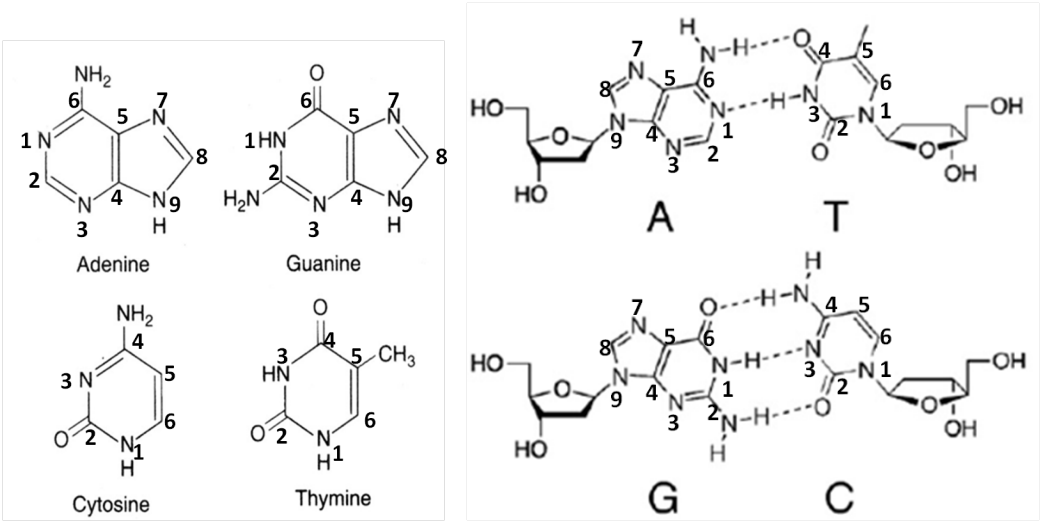

Figure 1.2. Chemical structures of nucleobases. (Left) The chemical structures of adenine, guanine, cytosine, and thymine; (right) A-T base pair with two non-covalent hydrogen bonds (dashed lines), and G-C base pair with three hydrogen bonds (dashed lines).

In addition, soft transition metal ions such as Pt(II), Pd(II) and Ru(II) prefer to bind with N7 of the guanine and adenine on DNA.[134-135] Transition-metal ions with less softness are also able to bind with the oxygen atoms of phosphate backbones through electrostatic interaction. The preference for phosphate over base association was found to decrease in the order Mg(II)>Co(II)>Ni(II)>Mn(II)>Zn(II)>Cd(II)>Cu(II).[136]

1.6 STRUCTURAL DNA NANOTECHNOLOGY

Seeman pioneered structural DNA nanotechnology in the 1980s, by making branched junctions and cube-like molecular complexes.[137-138] Structural DNA nanotechnology, in principle, is the use of DNA motifs to build complex shapes and arrangement of nanoscale sizes,

as well as self-assembly of periodic arrays.[139] The object of research in this area now has been extended to various nanofabrication strategies that use DNA as the basic constructing material, many of which share the same ultimate goal for making functional nanodevices. DNA nanofabrication technology has grown dramatically since it was first raised over 20 years ago.

1.6.1 DNA self-assembly/scaffolding

1.6.1.1 DNA structural development

The molecular recognition through base pairing in DNA molecules provides accurate self-assembly properties. Figure 1.3 illustrates the sticky end association of DNA molecules by hybridization and ligation. The ligation step involves formation of a phosphodiester bond between one nucleotide and another. The Watson-Crick complementarity of DNA molecules gives rise to diverse intermolecular interactions with highly specificity. This specific and powerful molecular recognition can be used to program and construct double helices and simple branched junctions from single stranded DNA via hydrogen bonding and ligation. Additionally, the idea of using Watson-Crick complementary association of single-stranded sticky ends provides a predictable geometry.[140] With complementary single stranded overhangs (sticky ends) to direct the association between junctions or intermolecular structural units, more stable and intricate structures can be made. Such structures include cubes and octahedra[138, 141] or DNA tiles[142-144] for periodic structure synthesis. The typical process for fabricating structures entails several steps: (1) design of oligonucleotides with complementary sequences for assembly; (2) combination of these oligonucleotides in appropriate stoichiometry in solution; and (3) hybridization of the sequences into the intended structures via temperature control. The ordered

and periodic DNA motifs produced by the above techniques have been used to direct the assembly of nanostructures for use in protein detection[142] and electronics.[145]

Regardless of these achievements, however, there still exist problems that need to be addressed such as low yield and resulting motif defects caused by less than perfect yields during fabrication, especially in producing large structures. To minimize these experimental errors, the oligonucleotides must be mixed in perfect stoichiometry, and thus, more purification steps are needed, which results in a time-consuming and inefficient process.[146] For this reason, more sophisticated techniques are needed to improve DNA structural assembly. One of the most innovative strategies, called scaffolded DNA origami was developed by Rothemund,[147] producing a big advance in DNA assembly. I will talk more about this in the following section.

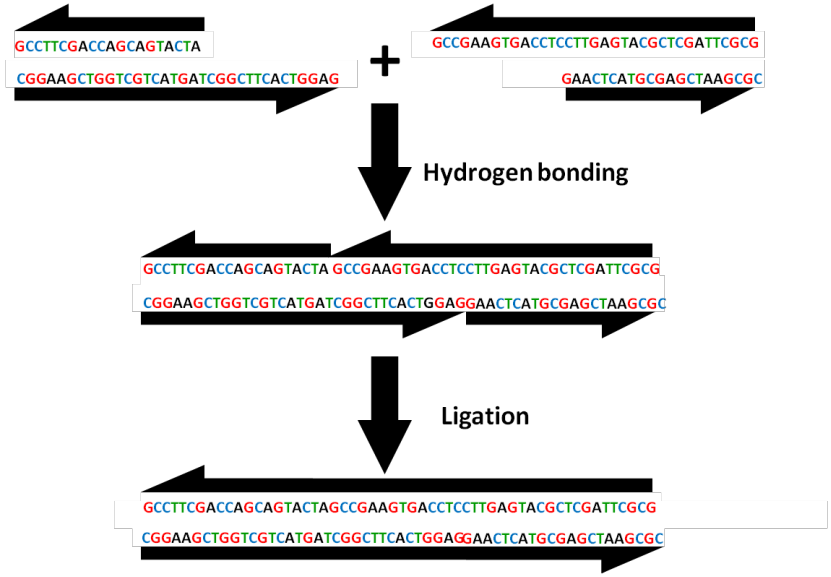

Figure 1.3. Sticky-ended hybridization and ligation.

1.6.1.2 Overview of DNA origami

In 2006, DNA origami was introduced, wherein a long single-stranded DNA scaffold (M13mp18) is folded into a two dimensional shape with the aid of many short single strands that

are sequence complementary with specific part of the scaffold.[147] The scaffold and staple strands are formed into DNA origami with arbitrary structures by programmed self-assembly based on hydrogen bonding between base pairs. DNA origami is a revolutionary advance through which arbitrary patterns just 100 nm wide can be produced with less effort and expense than the traditional DNA assembly methods. Rothemund demonstrated the versatility of this method by creating a number of different structures such as smiley faces, stars, maps, and snowflakes, etc.[147]

Different from the DNA structural assembly processes mentioned in 1.6.1.1, DNA origami is a simpler one-pot reaction between a mixture of scaffold and complementary staple strands, requiring only annealing. In addition, the short staple strands can be used in excess without stoichiometry concerns which shortens and simplifies the whole process, and at the same time results in intended structures with fewer defects as well as higher yields.[146]

For my work, DNA origami were designed in Dr. Woolley's lab. The basic design of DNA origami to form a "T" shape is illustrated in Figure 1.4. The design includes: (1) the layout of the desired shape in a computer program to fit the long, single-stranded DNA scaffold of known sequence; (2) the addition of short single stranded oligonucleotides (staple strands) with complementary sequences to specific regions of the DNA scaffold to "staple" the scaffold in place in the layout; and (3) display of the sequences of all staples needed for the desired shape within the program; then, during folding, scaffold, staples, and buffer solution are mixed together and annealed under a temperature program for several hours to generate the DNA origami structures.

Since the initial demonstration in 2006, the past 6 years have seen rapid progress in DNA origami. For folding technique, Jungmann et al.[148] demonstrated the use of an isothermal

assembly method instead of the often used thermal annealing to generate DNA origami, via slowly lowering the concentration of denaturing agent (formamide). Additionally, several DNA origami design software programs have been developed such as caDNAno (http://cadnano.org/) and SARSE (http://cdna.au.dk/software/). For example, Andersen et al.[149] used SARSE software to design dolphin structures and indicated that specific docking of DNA origami structures can stabilize flexible region conformations by forming dimers through sticky end interactions. With the development of the folding and programming techniques, almost any 2D DNA origami with arbitrary nanostructures can be fabricated.

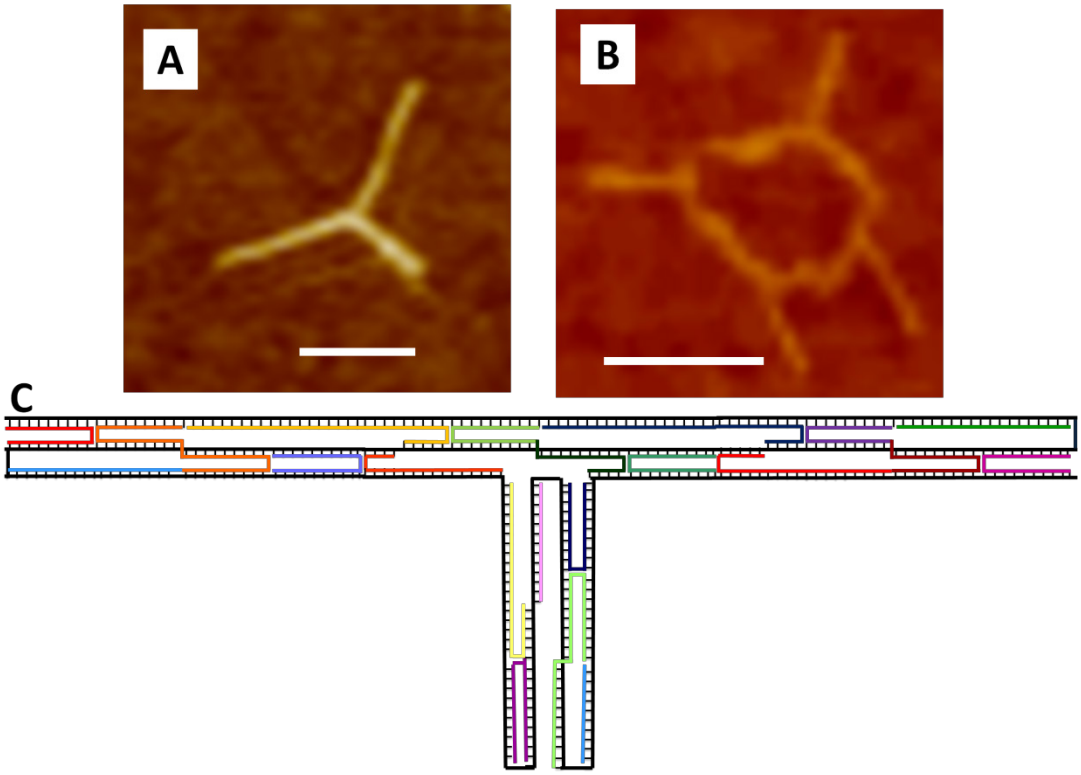

Figure 1.4. DNA origami method for fabricating nanostructures. (A-B) AFM images of "T"-shape and circular circuit DNA origami. Scale bar for both images: 100 nm. (C) Schematic of DNA origami layout to fold a "T" shape using the caDNAno program. The ssDNA scaffold that goes across the area of the shape is immobilized by staple strands.

In spite of these success, there is one limitation of DNA origami that may restrict functional development of DNA origami technology, and that is the size of DNA origami. The single-stranded scaffolds used normally in folding are the bacteriophage M13mp18 which has a ~7 kb length, thus, the sizes of DNA origami are determined and restricted by this length. Zhao and coworkers[150] demonstrated a strategy called "origami of origami" to produce larger DNA origami structures by combining preformed origami tiles with preformed scaffold frames via sticky end association of these preformed structures. Although the yield still needs to be improved, this “origami of origami” technique has potential for use in nanoscale integrated circuit fabrication. Via this super origami folding, smaller DNA origami structures can be interconnected and combined into a larger and high ordered structure, which can be used as a template for selective and specific coating by metal or localizing by CNTs, as well as for assembling proteins and other molecules.

DNA origami was originally developed for 2D structures, but it is not restricted only to the 2D area. A series of papers demonstrating 3D structures have been published since 2009. The formation of first 3D DNA origami shapes were described by different groups.[151-154] For instance, Andersen et al.[153] used SARSE software to create a 3D DNA "cuboid" box structure using the entire M13 sequence and designed staple stands to fold the structure by bridging the edges. The box had a size of 42×36×36 nm^3, and the lid would be opened by an external DNA oligonucleotide. Another study by Dietz et al.[154] demonstrated the use of DNA origami to fabricate twisted and curved DNA bundles. They designed tunable global bending-angle structures by site-directed base-pair deletions and insertions, followed by creation of more complex gear structures by combination of these bent modules.

1.6.2 DNA assisted assembly of other nanostructures

The molecular recognition characteristics of DNA combined with diverse functional sites also allow it to create addressable nanostructures with nanoscale precision.[155] The past 10 years have witnessed a number of successful examples of nanomaterial assembly.

1.6.2.1 Oligonucleotide functionalized NPs for DNA assisted assembly

The conjugation of nanoparticles with oligonucleotides is a key part of the assembly process, providing NPs with unique molecular recognition properties that allow them to be specifically recognized and attach (i.e., hybridization) to the sticky-end linkers on a DNA platform.[65, 156] DNA oligonucleotides can be modified with chemical substituents such as thiol groups attached to the 3'-or 5'-terminus. These thiols can bond covalently to Au/Ag nanoparticles. Since the first paper on DNA based assembly of nanoparticles by Mirkin et al.[157], much has been developed to use this technique for assembly of NPs into two or three dimensional architectures. Pal et al.[158] demonstrated the production of bimetallic Ag-Au core-satellite nanostructures by the complementary sequence recognition between Ag-and Au-linked DNA.

1.6.2.2 DNA-based assembly of proteins and CNTs

Besides NPs, DNA can also assist in the assembly of other nanomaterials such as proteins[159-160], and CNTs[161-164] with proper attachment chemistry. For instance, Yan et al.[159] reported the use of DNA nanogrids containing biotinylated oligonucleotides at the tile center to assemble streptavidin and form periodic arrays. A study showed that DNA origami assembled functional groups or sites could be used for single-molecule chemical reactions, in which a DNA origami breadboard serves as a locally addressable solid support.[160] Li et al.[161] oxidized CNTs to have carboxylic acid end groups for ssDNA grafting, in which the oxidized CNTs were chemical

bonded to amino-end functionalized ssDNA chains. The ssDNA attached CNTs then hybridized with the complementary sequence on DNA-coated Au NPs. However, for this method the chemical modification of CNTs and subsequent assembly only occurred at the cut ends; so the resulting structures lacked rigidity, and the shapes were difficult to control. Additionally, the CNTs aligned in this way had limited complexity, constraining their potential application in nanoelectronic devices. Eskelinen et al.[165] demonstrated the use of streptavidin-biotin interaction to assemble CNTs on DNA origami. The process included: (1) fabrication of a DNA origami structure with biotin patterned at a specific location; (2) attachment of streptavidin onto the biotin on the DNA origami; (3) the wrapping of biotin-functionalized ssDNA around CNTs; and (4) localization of ssDNA wrapped CNTs onto streptavidin defined binding sites on the DNA origami. This method could assemble CNT cross-junctions on DNA origami at desired locations. Although this strategy still has a relatively low yield, such made CNT-origami structures have potential for use in fabrication of nano-transistors.

1.6.3 Continuous nanostructures coated on DNA templates

DNA is an ideal building material for templating nanostructure due to the versatile binding sites on its strands that can interact with other species. However, some properties of DNA like conductivity have not been fully elucidated and are not understood yet. Thus, the use of DNA or DNA origami as a template for fabrication of other materials can create features with new electronic, photonic and magnetic properties. As mentioned in Section 1.5.3, the major binding sites on DNA include: (1) negative charges on the phosphate backbone; and (2) nitrogen atoms on the bases.

1.6.3.1 Nonmetal nanostructures coated on DNA templates

Nonmetallic nanostructures have been generated using DNA templates, usually via electrostatic interaction of positively charged nanostructures with negatively charged DNA backbone. The deposited materials, including polymers[166-168] and nonmetal inorganic materials (ZnO, CdS, and CdSe),[169-170] confer electrical or magnetic properties. He and coworkers[166] fabricated polyaniline nanowires using surface DNA molecules as templates. DNA was aligned on Si and incubated with protonated aniline monomer solution to localize aniline molecules through electrostatic interaction, followed by enzymatic polymerization to produce polyaniline nanowires. These materials have electrical conductivity that is sensitive to acid or base doping. Kundu et al.[170] developed a rapid microwave method to generate CdS nanowires on DNA. Nanowire fabrication was achieved by microwave irradiating a solution of DNA, Cd(II) and an organosulfur compound which decomposed to provide S^{2-} to form CdS.

The studies reported in this area have shown some promise for DNA templates. However, deposition of metal on DNA templates has attracted even greater interest due to the potential use of metal nanostructures in nanoelectronic devices. I will discuss DNA metallization in detail below.

1.6.3.2. Process of DNA metallization

Although metallization of DNA in solution has been reported,[171] more work has been focused on metallization of surface DNA mainly because the localization and orientation of DNA molecules on surfaces before metallization are relatively easy. The basic process for metallization of surface DNA basically includes: (1) immobilization of DNA molecules on surfaces; (2) deposition of seeds on DNA that serve as catalysts; and (3) further plating to form continuous metal nanostructures.

1.6.3.3 Immobilization of DNA molecules on surfaces

The manipulation of DNA molecules on a surface is usually precedes metallization steps. A number of DNA alignment methods have been developed on different surfaces.

A simple and reproducible DNA alignment process called molecular combing is a method in which the ends of DNA molecules are anchored to a surface and a receding meniscus of an air-water interface then stretches and aligns the DNA molecules.[172] The force applied on DNA molecules when stretching (estimated to be ~ 160 pN) is sufficient to align DNA (DNA is bonded to the surface) but small enough not to break the bonds between DNA and surfaces. [172] Combing methods can be used on surfaces such as silicon[173] or glass, and silanized,[174] amine-terminated,[175] poly-L-lysine treated,[176] or unmodified mica surfaces.[177] Ouyang et al.[178] demonstrated the use of a modified molecular combing method to align DNA into linear patterns on mica surfaces without the anchoring of the DNA end. A droplet of DNA solution was placed onto a glass coverslip and was then placed onto the surface. The solution was spread by the weight of the cover and a pressure was applied on the cover while combing to form DNA molecule lines.

Spin stretching, a rapid and effective method developed by Yokota et al.,[179] is also used to put DNA on surfaces. Stretching of DNA was achieved by spinning a droplet of DNA solution on a $MgCl_2$-soaked mica surface with a dc motor at 4000-7000 rpm, during which the centrifugal force on the droplet can remove excess solution from the surface.[175, 180] A water droplet is necessary to provide water flow that favors the stretching of DNA molecules on surfaces as well as flushing the remaining salts. The centrifugal force that is proportional to the angular velocity of the disk thus can generate radial DNA molecule patterns.

The methods to align DNA nanostructures such as DNA rafts, DNA tiles and DNA origami can be greatly extended by the association of other techniques such as printing and lithography, in which DNA can be transferred, stretched, or patterned onto desired sites on the substrates.[181-184] For example, Guan et al.[182] used a modified molecular combing method associated with soft lithography to produce DNA nanostrand arrays on mica or glass surfaces. During the process, DNA molecules were first transferred from glass slips to polydimethylsiloxane (PDMS) stamps either by fast or by slow peeling, which would then generate long or short DNA strands on surfaces during the subsequent step in which PDMS stamps were pressed onto surfaces. The arrangement and orientation of individual triangular DNA origami structures were also realized using EBL and etching of the surfaces.[184] Triangular or other binding site shapes such as rhombi, double-sized triangles, or hexagons were generated on SiO_2 or diamond-like carbon surfaces using EBL followed by O_2 plasma etching. The etching step provided hydrophilic surface locations for later DNA binding while leaving non-etched areas hydrophobic. The patterned surfaces were then incubated aqueous $MgCl_2$ which only adsorbed onto the hydrophilic areas to help the selective attachment of DNA origami. These methods offer a promising way to both arrange and orient DNA origami on surfaces.

1.6.3.4 Seeding and electroless plating on DNA templates

The last 15 years have seen a number of approaches to form seeds on DNA templates. All these approaches fall into four basic methods. They are (1) thiol-oligonucleotide functionalized NPs serving as seeds are assembled on DNA molecules through molecular recognition;[185-187] (2) activation of DNA by the binding of positively charged NPs[188] through electrostatic forces; (3) electrostatic interaction of metal cations with the DNA phosphate backbone, followed by reduction of the attached cations to make seeds; and (4) activation of DNA molecules by the

binding of transition metal complexes to DNA bases through coordination, followed by a reduction step to form metal seeds. The activation and seeding steps are crucial in generating as many seeds as possible.[84]

Although the assembly of NPs on DNA has been developed for over ten years (see Section 1.6.2), the use of these NPs as seeds for site-specific metallization is a relatively new area. Only recently has this seeding method been used for metallization of DNA origami.[185, 189]

Few papers have been published for seeding via electrostatic assembly of NPs; for example, some research groups reported[188, 190] that lysine-capped colloidal Au NPs were assembled on DNA templates through electrostatic interaction. The limited usage of this seeding method may be due to needed complex modifications of the NPs that makes the process less simple.

For DNA activated with transition metal cations, the metal species generally used are platinum, palladium, and silver. The activation time ranges from minutes to days;[84, 191-193] for instance, Mertig et al.[194] found that the nucleation upon reduction of $PtCl_4^{2-}$ bound to DNA is controlled by Pt(II)•DNA adducts formed in an activation step. It is suggested that longer DNA activation time can improve the seeding selectivity due to the preferential heterogeneous nucleation of DNA-Pt(II) instead of Pt(II)-Pt(II) in solution. Additionally, the reduction steps after activation can also influence seeding. For example, more continuous Pd clusters were formed by aggregation of seeds when the duration of the reduction step was extended.[84]

Other seeding methods were also reported. Keren et al.[195] developed a different seeding strategy where a reducing agent (aldehyde) was localized on DNA first, which was followed by activation with Ag^+ solution, producing Ag seeds on the DNA. This seeding method was also applied by other groups, who fabricated Ag[143] and Au[196] nanostructures on DNA templates.

Complete metallization of DNA usually requires electroless plating, during which the continuity and conductance would be improved by a thicker metal coating. I have already discussed electroless plating in section 1.3.3. Some factors of electroless plating including temperature, pH value and plating time are of most important variables that may affect plating results especially for DNA templating methods.

1.6.4 Fabrication and characterization of metallic DNA nanostructures for nanoelectronic application

DNA metallization for nanoelectronic applications, although still in its early stage, has focused on the ultimate integration with semiconductors.[197] The synthesis of conductive metal nanowires that have potential use in nanocircuits has gained increasing interest since the first paper reported conducting silver wires on a DNA template in 1998.[197] Lambda DNA was attached between two Au electrodes through hybridization to surface bound oligonucleotides. The use of fluorescently labeled lambda DNA was used to image the DNA bridge between the electrodes. Silver ions were bound to DNA through Na^+/Ag^+ ion exchange on the DNA backbone and reduced to silver metal catalysts for further silver wire growth. The Ag wires had a diameter of 60-100 nm, and were conductive though had a resistance of several MΩ for a 15-μm length. Since then, a remarkable progress in DNA metallization has been noted, as discussed below with respect to selected studies.

In 2001, Richter et al.[198] reported electrical conductivity measurements on nanowires made on lambda DNA positioned between Au electrodes, followed by Pd metallization. The contact resistance between the Pd nanowires and Au electrodes was decreased by pinning the nanowires at the electrodes with electron-beam-induced carbon lines. The nanowires exhibited low

resistance (below 1 kΩ) at room temperature. The resulting conductance was 2×10^4 S/cm, which is only 5 times smaller than that of bulk Pd. This study showed further promise to use DNA as a template for conductive metal nanowire fabrication.

Using similar approaches, research groups have fabricated metal nanowires made of Au,[191, 199-200] Ag,[143, 159, 201] Ni,[202] Cu,[203-204] Co,[171, 205] and Pd,[191] some of which showed electrical conductivity.[159, 199] Another study was reported later on the realization of a DNA-templated CNT field-effect transistor.[55] RecA monomers were first polymerized on ssDNA to form a nucleoprotein filament, and lambda DNA templates were treated with glutaraldehyde to introduce reducing agent on the DNA. The nucleoprotein filament with a sequence complementary to the lambda DNA then underwent homologous recombination to bind the filament at a desired location. A streptavidin-modified SWNT was localized on the RecA-bound DNA through RecA-antiRecA-biotin-streptavidin interaction. During seeding with Ag^+, template regions not covered by RecA were seeded with silver metal which was followed by electroless Au plating in which Au nanowires were formed. The whole process succeeded in the integration of a field-effect transistor by combining metal nanowires with semiconducting SWNTs.

The studies mentioned above show big progress in fabrication of conductive metal nanowires using linear DNA templates. However, with only linear DNA, it is difficult to produce sophisticated nanocircuitry with interconnections to multiple components. Therefore, more complex templates are needed. As described in Section 1.6.1.2, DNA origami[147] may extend the use of DNA as a self-assembly template and advance the application of DNA in the construction of nanoelectronic circuits. Very recently, progress has been made in metallizing these nanostructures. A group at BYU was the first[196] to show metallization of DNA origami. Although this was the first demonstration, the surfaces used in this work were mica, the yield of

metallized nanostructures was low, and the metallization process was complicated. Later, work done by Finkelstein's group[185] showed the metallization of a small number up to 14 of Au NPs attached to DNA origami deposited on silicon surfaces. The seeds were localized in predesigned regions of the DNA origami template for selective and site-specific plating process to produce silver nanostructures. However, more complex designs had more feature defects. Furthermore, the overall sites of nanostructures were limited to what would fit in a ~100×100 nm^2 tile, thus, more work is needed for templating complex structures. Recently, the BYU team[189] demonstrated the use of a higher density Au NP seeding method to selectively metallize DNA origami on desired locations. The method generated defined gaps in metal lines at desired locations within DNA origami, which offers the door to fabrication of heterogeneous transistors by filling the gap with semiconductor switch components. The resulting Au nanowires were also electrically conductive, demonstrating the formation of conductive nanowires on DNA origami for the first time. However, in this seeding method, spacing between the neighboring Au NPs was still large, and defects were sometimes observed. Thus, more work needs to be done in optimization of the seeding process. In summary, DNA origami shows promise in templating and producing more complex nanostructures, but further work is still needed in key areas of seeding and plating. Importantly, my dissertation addresses these key issues.

1.7 DISSERTATION OVERVIEW

Chapter 2 describes metallization of DNA on mica surfaces. A rapid Pd seeding method was applied to produce catalytic seeds on both lambda DNA and branched DNA origami structures.

The Pd seeds on the DNA then were developed through electroless plating, leading to a transition from noncontinuous lines into continuous metal nanostructures. Two different electroless plating solutions were applied for Pd or Au coating.

Chapter 3 details the use of a modified Pd seeding method from Chapter 2 for metallization of DNA origami structures on Si surfaces. Multiple seeding steps were applied. The results of each seeding step and their optimization are discussed in detail. Selective and continuous Au or Cu metal nanostructures were obtained. Electron beam lithography and Au vapor deposition were applied to pattern electrodes on top of these structures, and the electrical conductivity was successfully measured.

Chapter 4 completes my research by drawing conclusions and discussing future work on DNA metallized nanostructures towards the realization of nanoelectronic device fabrication.

1.8 REFERENCES

1. Gilbert, D. H., *There's Plenty of Room at the Bottom*. Reinhold Publishing Corporation: New York, 1961; p 282-296.
2. Hannah, W.; Thompson, P. B., Nanotechnology, risk and the environment: a review. *J Environ Monitor* **2008,** *10* (3), 291-300.
3. Masciangioli, T.; Zhang, W. X., Environmental technologies at the nanoscale. *Environ Sci Technol* **2003,** *37* (5), 102a-108a.
4. Xie, Y. F.; Wang, X.; Han, X. X.; Xue, X. X.; Ji, W.; Qi, Z. H.; Liu, J. Q.; Zhao, B.; Ozaki, Y., Sensing of polycyclic aromatic hydrocarbons with cyclodextrin inclusion complexes on silver nanoparticles by surface-enhanced Raman scattering. *Analyst* **2010,** *135* (6), 1389-1394.
5. Nie, S. M.; Emery, S. R., Probing single molecules and single nanoparticles by surface-enhanced Raman scattering. *Science* **1997,** *275* (5303), 1102-1106.
6. Guerrini, L.; Aliaga, A. E.; Carcamo, J.; Gomez-Jeria, J. S.; Sanchez-Cortes, S.; Campos-Vallette, M. M.; Garcia-Ramos, J. V., Functionalization of Ag nanoparticles with the bis-acridinium lucigenin as a chemical assembler in the detection of persistent organic pollutants by surface-enhanced Raman scattering. *Anal Chim Acta* **2008,** *624* (2), 286-293.
7. Leyton, P.; Cordova, I.; Lizama-Vergara, P. A.; Gomez-Jeria, J. S.; Aliaga, A. E.; Campos-Vallette, M. M.; Clavijo, E.; Garcia-Ramos, J. V.; Sanchez-Cortes, S., Humic acids as

molecular assemblers in the surface-enhanced Raman scattering detection of polycyclic aromatic hydrocarbons. *Vib Spectrosc* **2008,** *46* (2), 77-81.
8. Zanolli, Z.; Leghrib, R.; Felten, A.; Pireaux, J. J.; Llobet, E.; Charlier, J. C., Gas Sensing with Au-Decorated Carbon Nanotubes. *ACS Nano* **2011,** *5* (6), 4592-4599.
9. Kong, J.; Franklin, N. R.; Zhou, C. W.; Chapline, M. G.; Peng, S.; Cho, K. J.; Dai, H. J., Nanotube molecular wires as chemical sensors. *Science* **2000,** *287* (5453), 622-625.
10. Hernandez, S. C.; Kakoullis, J.; Lim, J. H.; Mubeen, S.; Hangarter, C. M.; Mulchandani, A.; Myung, N. V., Hybrid ZnO/SWNT Nanostructures Based Gas Sensor. *Electroanal* **2012,** *24* (7), 1613-1620.
11. Aluri, G. S.; Motayed, A.; Davydov, A. V.; Oleshko, V. P.; Bertness, K. A.; Sanford, N. A.; Rao, M. V., Highly selective GaN-nanowire/TiO2-nanocluster hybrid sensors for detection of benzene and related environment pollutants. *Nanotechnology* **2011,** *22* (29), 1-11.
12. Jin, C.; Park, S.; Kim, H.; An, S.; Lee, C., CO Gas-Sensor Based on Pt-Functionalized Mg-Doped ZnO Nanowires. *B Korean Chem Soc* **2012,** *33* (6), 1993-1997.
13. Homhoul, P.; Pengpanich, S.; Hunsom, M., Treatment of Distillery Wastewater by the Nano-Scale Zero-Valent Iron and the Supported Nano-Scale Zero-Valent Iron. *Water Environ Res* **2011,** *83* (1), 65-74.
14. Scott, T. B.; Popescu, I. C.; Crane, R. A.; Noubactep, C., Nano-scale metallic iron for the treatment of solutions containing multiple inorganic contaminants. *J Hazard Mater* **2011,** *186* (1), 280-287.
15. Kanel, S. R.; Greneche, J. M.; Choi, H., Arsenic(V) removal kom groundwater using nano scale zero-valent iron as a colloidal reactive barrier material. *Environ Sci Technol* **2006,** *40* (6), 2045-2050.
16. Lackovic, J. A.; Nikolaidis, N. P.; Dobbs, G. M., Inorganic arsenic removal by zero-valent iron. *Environ Eng Sci* **2000,** *17* (1), 29-39.
17. Gupta, A.; Yunus, M.; Sankararamakrishnan, N., Zerovalent iron encapsulated chitosan nanospheres - A novel adsorbent for the removal of total inorganic Arsenic from aqueous systems. *Chemosphere* **2012,** *86* (2), 150-155.
18. Giasuddin, A. B. M.; Kanel, S. R.; Choi, H., Adsorption of humic acid onto nanoscale zerovalent iron and its effect on arsenic removal. *Environ Sci Technol* **2007,** *41* (6), 2022-2027.
19. Schrick, B.; Blough, J. L.; Jones, A. D.; Mallouk, T. E., Hydrodechlorination of trichloroethylene to hydrocarbons using bimetallic nickel-iron nanoparticles. *Chem Mater* **2002,** *14* (12), 5140-5147.
20. Lowry, G. V.; Johnson, K. M., Congener-specific dechlorination of dissolved PCBs by microscale and nanoscale zerovalent iron in a water/methanol solution. *Environ Sci Technol* **2004,** *38* (19), 5208-5216.
21. Lien, H. L.; Zhang, W. X., Transformation of chlorinated methanes by nanoscale iron particles. *J Environ Eng-Asce* **1999,** *125* (11), 1042-1047.
22. Joo, S. H.; Feitz, A. J.; Sedlak, D. L.; Waite, T. D., Quantification of the oxidizing capacity of nanoparticulate zero-valent iron. *Environ Sci Technol* **2005,** *39* (5), 1263-1268.
23. Xu, H.; Zheng, Z.; Zhang, L. Z.; Zhang, H. L.; Deng, F., Hierarchical chlorine-doped rutile TiO2 spherical clusters of nanorods: Large-scale synthesis and high photocatalytic activity. *J Solid State Chem* **2008,** *181* (9), 2516-2522.
24. Long, R. Q.; Yang, R. T., Carbon nanotubes as superior sorbent for dioxin removal. *J Am Chem Soc* **2001,** *123* (9), 2058-2059.

25. Hu, J.; Shao, D. D.; Chen, C. L.; Sheng, G. D.; Li, J. X.; Wang, X. K.; Nagatsu, M., Plasma-Induced Grafting of Cyclodextrin onto Multiwall Carbon Nanotube/Iron Oxides for Adsorbent Application. *J Phys Chem B* **2010,** *114* (20), 6779-6785.
26. Salipira, K. L.; Mamba, B. B.; Krause, R. W.; Malefetse, T. J.; Durbach, S. H., Carbon nanotubes and cyclodextrin polymers for removing organic pollutants from water. *Environ Chem Lett* **2007,** *5* (1), 13-17.
27. Peng, X. J.; Luan, Z. K.; Di, Z. C.; Zhang, Z. G.; Zhu, C. L., Carbon nanotubes-iron oxides magnetic composites as adsorbent for removal of Pb(II) and Cu(II) from water. *Carbon* **2005,** *43* (4), 880-883.
28. Zach, M.; Hagglund, C.; Chakarov, D.; Kasemo, B., Nanoscience and nanotechnology for advanced energy systems. *Curr Opin Solid St M* **2006,** *10* (3-4), 132-143.
29. Wang, J. W.; Liu, Y.; Zhang, X. W.; Mi, Z. T.; Wang, L., Facile preparation of hydrocarbon fuel-soluble nano-catalyst and its novel application in catalytic combustion of JP-10. *Catal Commun* **2009,** *10* (11), 1518-1522.
30. Ma, S. B.; Nam, K. W.; Yoon, W. S.; Bak, S. M.; Yang, X. Q.; Cho, B. W.; Kim, K. B., Nano-sized lithium manganese oxide dispersed on carbon nanotubes for energy storage applications. *Electrochem Commun* **2009,** *11* (8), 1575-1578.
31. Chang, J. K.; Wu, C. M.; Sun, I. W., Nano-architectured Co(OH)(2) electrodes constructed using an easily-manipulated electrochemical protocol for high-performance energy storage applications. *J Mater Chem* **2010,** *20* (18), 3729-3735.
32. Knight, M. W.; Sobhani, H.; Nordlander, P.; Halas, N. J., Photodetection with Active Optical Antennas. *Science* **2011,** *332* (6030), 702-704.
33. Vuong, G. T.; Hoang, V. T.; Nguyen, D. T.; Do, T. O., Synthesis of nanozeolites and nanozeolite-based FCC catalysts, and their catalytic activity in gas oil cracking reaction. *Appl Catal a-Gen* **2010,** *382* (2), 231-239.
34. Vuong, G. T.; Do, T. O., A new route for the synthesis of uniform nanozeolites with hydrophobic external surface in organic solvent medium. *J Am Chem Soc* **2007,** *129* (13), 3810-3811.
35. Leonard, A. D.; Hudson, J. L.; Fan, H.; Booker, R.; Simpson, L. J.; O'Neill, K. J.; Parilla, P. A.; Heben, M. J.; Pasquali, M.; Kittrell, C.; Tour, J. M., Nanoengineered Carbon Scaffolds for Hydrogen Storage. *J Am Chem Soc* **2009,** *131* (2), 723-728.
36. Jin, Z.; Lu, W.; O'Neill, K. J.; Parilla, P. A.; Simpson, L. J.; Kittrell, C.; Tour, J. M., Nano-Engineered Spacing in Graphene Sheets for Hydrogen Storage. *Chem Mater* **2011,** *23* (4), 923-925.
37. Peng, K. Q.; Wang, X.; Wu, X. L.; Lee, S. T., Platinum Nanoparticle Decorated Silicon Nanowires for Efficient Solar Energy Conversion. *Nano Lett* **2009,** *9* (11), 3704-3709.
38. Li, Y. F.; Kodama, S.; Kaneko, T.; Hatakeyama, R., Harvesting Infrared Solar Energy by Semiconducting Single-Walled Carbon Nanotubes. *Appl Phys Express* **2011,** *4* (6), 1-3.
39. Kotter, D. K.; Novack, S. D.; Slafer, W. D.; Pinhero, P., Solar Nantenna Electromagnetic Collectors. *ASME Conference Proceedings* **2008,** *2008* (43208), 409-415.
40. Slowing, I. I.; Trewyn, B. G.; Giri, S.; Lin, V. S. Y., Mesoporous silica nanoparticles for drug delivery and biosensing applications. *Adv Funct Mater* **2007,** *17* (8), 1225-1236.
41. Lee, C. H.; Lo, L. W.; Mou, C. Y.; Yang, C. S., Synthesis and Characterization of Positive-Charge Functionalized Mesoporous Silica Nanoparticles for Oral Drug Delivery of an Anti-Inflammatory Drug. *Adv Funct Mater* **2008,** *18* (20), 3283-3292.

42. Kim, J.; Kim, H. S.; Lee, N.; Kim, T.; Kim, H.; Yu, T.; Song, I. C.; Moon, W. K.; Hyeon, T., Multifunctional Uniform Nanoparticles Composed of a Magnetite Nanocrystal Core and a Mesoporous Silica Shell for Magnetic Resonance and Fluorescence Imaging and for Drug Delivery. *Angew Chem Int Edit* **2008,** *47* (44), 8438-8441.
43. MacDonald, R. A.; Laurenzi, B. F.; Viswanathan, G.; Ajayan, P. M.; Stegemann, J. P., Collagen-carbon nanotube composite materials as scaffolds in tissue engineering. *J Biomed Mater Res A* **2005,** *74A* (3), 489-496.
44. Hu, H.; Ni, Y. C.; Mandal, S. K.; Montana, V.; Zhao, N.; Haddon, R. C.; Parpura, V., Polyethyleneimine functionalized single-walled carbon nanotubes as a substrate for neuronal growth. *J Phys Chem B* **2005,** *109* (10), 4285-4289.
45. Usui, Y.; Aoki, K.; Narita, N.; Murakami, N.; Nakamura, I.; Nakamura, K.; Ishigaki, N.; Yamazaki, H.; Horiuchi, H.; Kato, H.; Taruta, S.; Kim, Y. A.; Endo, M.; Saito, N., Carbon nanotubes with high bone-tissue compatibility and bone-formation acceleration effects. *Small* **2008,** *4* (2), 240-246.
46. Kanellos, M. Moore's Law to roll on for another decade. http://news.cnet.com/2100-1001-984051.html (accessed Nov. 12).
47. Yu, B.; Meyyappan, M., Nanotechnology: Role in emerging nanoelectronics. *Solid State Electron* **2006,** *50* (4), 536-544.
48. Iijima, S.; Ichihashi, T., Single-Shell Carbon Nanotubes of 1-Nm Diameter. *Nature* **1993,** *363* (6430), 603-605.
49. Bethune, D. S.; Klang, C. H.; de Vries, M. S.; Gorman, G.; Savoy, R.; Vazquez, J.; Beyers, R., Cobalt-catalysed growth of carbon nanotubes with single-atomic-layer walls. *Nature* **1993,** *363* (6430), 605-607.
50. Wei, X. J.; Aoki, N.; Yahagi, T.; Maeda, K.; Bird, J. P.; Ishibashi, K.; Ochiai, Y., Analysis of Operation Mechanism of Field Effect Transistor Composed of Network of High-Quality Single Wall Carbon Nanotubes by Scanning Gate Microscopy. *Jpn J Appl Phys* **2012,** *51* (4), 1-4.
51. Liu, Q. H.; Yu, L. L.; Li, H.; Qin, R.; Jing, Z.; Zheng, J. X.; Gao, Z. X.; Lu, J., All-Metallic High-Performance Field Effect Transistor Based on Telescoping Carbon Nanotubes: An ab Initio Study. *J Phys Chem C* **2011,** *115* (14), 6933-6938.
52. Cui, J. B.; Burghard, M.; Kern, K., Room temperature single electron transistor by local chemical modification of carbon nanotubes. *Nano Lett* **2002,** *2* (2), 117-120.
53. Ahlskog, M.; Tarkiainen, R.; Roschier, L.; Hakonen, P., Single-electron transistor made of two crossing multiwalled carbon nanotubes and its noise properties. *Appl Phys Lett* **2000,** *77* (24), 4037-4039.
54. Franklin, A. D.; Luisier, M.; Han, S. J.; Tulevski, G.; Breslin, C. M.; Gignac, L.; Lundstrom, M. S.; Haensch, W., Sub-10 nm Carbon Nanotube Transistor. *Nano Lett* **2012,** *12* (2), 758-762.
55. Keren, K.; Berman, R. S.; Buchstab, E.; Sivan, U.; Braun, E., DNA-templated carbon nanotube field-effect transistor. *Science* **2003,** *302* (5649), 1380-1382.
56. Pribat, D.; Cojocaru, C. S., Carbon Nanotubes, Semiconductor Nanowires and Graphene for Thin Film Transistor and Circuit Applications. *Jpn J Appl Phys* **2011,** *50* (3).
57. Gates, B. D.; Xu, Q. B.; Stewart, M.; Ryan, D.; Willson, C. G.; Whitesides, G. M., New approaches to nanofabrication: Molding, printing, and other techniques. *Chem Rev* **2005,** *105* (4), 1171-1196.

58. IntelPR Intel 22nm 3-D Tri-Gate Transistor Technology. http://newsroom.intel.com/docs/DOC-2032 (accessed Oct. 09).
59. Biswas, A.; Bayer, I. S.; Biris, A. S.; Wang, T.; Dervishi, E.; Faupel, F., Advances in top-down and bottom-up surface nanofabrication: Techniques, applications & future prospects. *Adv Colloid Interfac* **2012,** *170* (1-2), 2-27.
60. Shin, H. J.; Jeong, D. K.; Lee, J. G.; Sung, M. M.; Kim, J. Y., Formation of TiO2 and ZrO2 nanotubes using atomic layer deposition with ultraprecise control of the wall thickness. *Adv Mater* **2004,** *16* (14), 1197-1200.
61. Knez, M.; Niesch, K.; Niinisto, L., Synthesis and surface engineering of complex nanostructures by atomic layer deposition. *Adv Mater* **2007,** *19* (21), 3425-3438.
62. Davis, M.; Gumeci, C.; Kiel, C.; Hope-Weeks, L. J., Preparation of porous manganese oxide nanomaterials by one-pot synthetic sol-gel method. *J Sol-Gel Sci Techn* **2011,** *58* (2), 535-538.
63. Tao, X. Y.; Zhang, X. B.; Cheng, J. P.; Liu, F.; Luo, J. H.; Luo, Z. Q., Morphology-controllable CVD synthesis of carbon nanomaterials on an alkali-element-doped Cu catalyst. *Chem Vapor Depos* **2006,** *12* (6), 353-356.
64. Yu, H. K.; Kim, J. S.; Oh, S. G.; Ryu, H., Effects of mechanochemical treatment of Ni-Al(OH)(3) on the preparation of carbon nanomaterials by thermal CVD. *Powder Technol* **2003,** *129* (1-3), 30-36.
65. Becerril, H. A.; Woolley, A. T., DNA-templated nanofabrication. *Chem Soc Rev* **2009,** *38* (2), 329-337.
66. Cheng, J. Y.; Mayes, A. M.; Ross, C. A., Nanostructure engineering by templated self-assembly of block copolymers. *Nat Mater* **2004,** *3* (11), 823-828.
67. Li, C. B.; Hasegawa, T.; Tanaka, H.; Miyazaki, H.; Odaka, S.; Tsukagoshi, K.; Aono, M., Toward sub-20 nm hybrid nanofabrication by combining the molecular ruler method and electron beam lithography. *Nanotechnology* **2010,** *21* (49).
68. Guder, F.; Yang, Y.; Kruger, M.; Stevens, G. B.; Zacharias, M., Atomic Layer Deposition on Phase-Shift Lithography Generated Photoresist Patterns for 1D Nanochannel Fabrication. *Acs Appl Mater Inter* **2010,** *2* (12), 3473-3478.
69. Mallory, G. O.; Hajdu, J. B., *Electroless plating: fundamentals and applications*. American Electroplaters and Surface Finishers Society: New York, 1990.
70. Thomas, R. R.; Park, J. M., Vapor-Phase Deposition of Palladium for Electroless Copper Plating. *J Electrochem Soc* **1989,** *136* (6), 1661-1666.
71. Paunovic, M.; Schlesinger, M., *Fundamentals of Electrochemical Deposition*. 2nd ed. ed.; Wiley-Interscience: Hoboken, New Jersey, 2006.
72. Kiang, M. H.; Lieberman, M. A.; Cheung, N. W.; Qian, X. Y., Pd/Si Plasma Immersion Ion-Implantation for Selective Electroless Copper Plating on SiO2. *Appl Phys Lett* **1992,** *60* (22), 2767-2769.
73. Lin, J. H.; Tsai, Y. Y.; Chiu, S. Y.; Lee, T. L.; Tsai, C. M.; Chen, P. H.; Lin, C. C.; Feng, M. S.; Kou, C. S.; Shih, H. C., Palladium seeding on the tantalum-insulated silicon oxide film by plasma immersion ion implantation for the growth of electroless Copper. *Thin Solid Films* **2000,** *377*, 592-596.
74. Schrott, A. G.; Braren, B.; Osullivan, E. J. M.; Saraf, R. F.; Bailey, P.; Roldan, J., Laser-Assisted Seeding for Electroless Plating on Polyimide Surfaces. *J Electrochem Soc* **1995,** *142* (3), 944-949.

75. Schrott, A. G.; Braren, B.; Saraf, R., Laser-Assisted Pd Seeding for Electroless Plating on Sio2. *Appl Phys Lett* **1994,** *64* (12), 1582-1584.
76. Kondo, K.; Ishikawa, F.; Ishida, N.; Irie, M., Photoreductive Deposition of Palladium for Electroless Copper Plating. *Chem Lett* **1992,** (6), 999-1002.
77. Kao, C. Y.; Chou, K. S., Electroless copper plating onto printed lines of nanosized silver seeds. *Electrochem Solid St* **2007,** *10* (3), D32-D34.
78. Busato, S.; Belloli, A.; Ermanni, P., Inkjet printing of palladium catalyst patterns on polyimide film for electroless copper plating. *Sensor Actuat B-Chem* **2007,** *123* (2), 840-846.
79. Chen, C. H.; Chen, B. H.; Hong, L., Role of Cu^{2+} as an additive in an electroless nickel-phosphorus plating system: A stabilizer or a codeposit? *Chem Mater* **2006,** *18* (13), 2959-2968.
80. Nelson, K. A.; Linford, M. R.; Wheeler, D. R.; Harb, J. N., Use of a plating additive to enable continuous metallization of nanoscale electrochemically patterned chemical templates. *Electrochim Acta* **2012,** *69* (0), 320-327.
81. Bird, E. J.; Nelson, K. A.; Harb, J. N.; Wheeler, D. R., Investigation of additives for electroless plating of nanowires. *Electrochim Acta* **2012,** *70* (0), 69-75.
82. Vakelis, A., Electroless Plating. In *Coatings Technology Handbook, Third Edition*, CRC Press: 2005; pp 27-1-27-12.
83. Lukes, R. M., The mechanism for the autocatalytic reduction of nickel by hypophosphite ion. *plating* **1964,** *51*, 969-971.
84. Richter, J., Metallization of DNA. *Physica E* **2003,** *16* (2), 157-173.
85. Pishkenari, H. N.; Meghdari, A., Tip and sample flexibility effects on tapping mode (amplitude modulation) AFM measurements. *Micro Nano Lett* **2011,** *6* (12), 1023-1028.
86. Becerril, H. A.; Ludtke, P.; Willardson, B. M.; Woolley, A. T., DNA-templated nickel nanostructures and protein assemblies. *Langmuir* **2006,** *22* (24), 10140-10144.
87. Becker, J. S.; Gordon, R. G., Diffusion barrier properties of tungsten nitride films grown by atomic layer deposition from bis(tert-butylimido)bis(dimethylamido)tungsten and ammonia. *Appl Phys Lett* **2003,** *82*, 2239.
88. Ras, R. H. A.; Kemell, M.; de Wit, J.; Ritala, M.; ten Brinke, G.; Leskela, M.; Ikkala, O., Hollow inorganic nanospheres and nanotubes with tunable wall thicknesses by atomic layer deposition on self-assembled polymeric templates. *Adv Mater* **2007,** *19* (1), 102-106.
89. Nam, S. W.; Lee, M. H.; Lee, S. H.; Lee, D. J.; Rossnagel, S. M.; Kim, K. B., Sub-10-nm Nanochannels by Self-Sealing and Self-Limiting Atomic Layer Deposition. *Nano Lett* **2010,** *10* (9), 3324-3329.
90. Weber, M. J.; Mackus, A. J. M.; Verheijen, M. A.; van der Marel, C.; Kessels, W. M. M., Supported Core/Shell Bimetallic Nanoparticles Synthesis by Atomic Layer Deposition. *Chem Mater* **2012,** *24* (15), 2973-2977.
91. Lee, J.; Farhangfar, S.; Yang, R. B.; Scholz, R.; Alexe, M.; Gosele, U.; Lee, J.; Nielsch, K., A novel approach for fabrication of bismuth-silicon dioxide core-shell structures by atomic layer deposition. *J Mater Chem* **2009,** *19* (38), 7050-7054.
92. Brinker, C. J., *Sol-gel science: the physics and chemistry of sol-gel processing*. Academic Press: Boston, 1990.
93. Ansari, A. A.; Singh, R.; Sumana, G.; Malhotra, B. D., Sol-gel derived nano-structured zinc oxide film for sexually transmitted disease sensor. *Analyst* **2009,** *134* (5), 997-1002.
94. Fu, C. L.; Cai, W.; Zhou, L. L.; Chen, H. Q.; Liu, Z. R., Synthesis of self-assembly BaTiO3 nanowire by sol-gel and microwave method. *Appl Surf Sci* **2009,** *255* (23), 9444-9446.

95. Guo, L. M.; Wang, X. H.; Zhong, C. F.; Li, L. T., Template-based synthesis and magnetic properties of Mn-Zn ferrite nanotube and nanowire arrays. *J Appl Phys* **2012,** *111* (2).
96. Hu, W. C.; Gong, D. W.; Chen, Z.; Yuan, L. M.; Saito, K.; Grimes, C. A.; Kichambare, P., Growth of well-aligned carbon nanotube arrays on silicon substrates using porous alumina film as a nanotemplate. *Appl Phys Lett* **2001,** *79* (19), 3083-3085.
97. Gao, T.; Meng, G. W.; Zhang, J.; Wang, Y. W.; Liang, C. H.; Fan, J. C.; Zhang, L. D., Template synthesis of single-crystal Cu nanowire arrays by electrodeposition. *Appl Phys a-Mater* **2001,** *73* (2), 251-254.
98. Lotey, G.; Kumar, S.; Verma, N., Fabrication and electrical characterization of highly ordered copper nanowires. *Applied Nanoscience* **2012,** *2* (1), 7-13.
99. Tasaltin, N.; Ozturk, S.; Kilinc, N.; Yuzer, H.; Ozturk, Z. Z., Fabrication of vertically aligned Pd nanowire array in AAO template by electrodeposition using neutral electrolyte. *Nanoscale Res Lett* **2010,** *5* (7), 1137-1143.
100. Yue, E. H.; Yu, G.; Ouyang, Y. J.; Weng, B. C.; Si, W. W.; Ye, L. Y., Electrochemical Fabrication of Pd-Ag Alloy Nanowire Arrays in Anodic Alumina Oxide Template. *J Mater Sci Technol* **2008,** *24* (6), 850-856.
101. Koh, H. D.; Park, S.; Russell, T. P., Fabrication of Pt/Au Concentric Spheres from Triblock Copolymer. *ACS Nano* **2010,** *4* (2), 1124-1130.
102. Lee, J. H.; Kim, I. T.; Tannenbaum, R.; Shofner, M. L., Synthesis of polymer-decorated hydroxyapatite nanoparticles with a dispersed copolymer template. *J Mater Chem* **2012,** *22* (23), 11556-11560.
103. Zhang, S. Y.; Zhao, Y., Template Synthesis of Subnanometer Gold Clusters in Interfacially Cross-Linked Reverse Micelles Mediated by Confined Counterions. *Langmuir* **2012,** *28* (7), 3606-3613.
104. McMillan, R. A.; Paavola, C. D.; Howard, J.; Chan, S. L.; Zaluzec, N. J.; Trent, J. D., Ordered nanoparticle arrays formed on engineered chaperonin protein templates. *Nat Mater* **2002,** *1* (4), 247-252.
105. Shemetov, A. A.; Nabiev, I.; Sukhanova, A., Molecular Interaction of Proteins and Peptides with Nanoparticles. *ACS Nano* **2012,** *6* (6), 4585-4602.
106. Patolsky, F.; Weizmann, Y.; Willner, I., Actin-based metallic nanowires as bio-nanotransporters. *Nat Mater* **2004,** *3* (10), 692-695.
107. Bhattacharya, R.; Patra, C. R.; Wang, S. F.; Lu, L. C.; Yaszemski, M. J.; Mukhopadhyay, D.; Mukherjee, P., Assembly of gold nanoparticles in a rod-like fashion using proteins as templates. *Adv Funct Mater* **2006,** *16* (3), 395-400.
108. Watson, J. D.; Crick, F. H. C., Molecular Structure of Nucleic Acids: A Structure for Deoxyribose Nucleic Acid. *Nature* **1953,** *171* (4356), 737-738.
109. Cavalleri, L. F.; Rosenberg, B. H., Nucleic acid: molecular biology of DNA. *Annual review of biochemistry* **1962,** *31*, 247-270.
110. Mcghee, J. D.; Vonhippel, P. H., Formaldehyde as a Probe of DNA-Structure .4. Mechanism of Initial Reaction of Formaldehyde with DNA. *Biochemistry-Us* **1977,** *16* (15), 3276-3293.
111. Besteman, K.; Van Eijk, K.; Lemay, S. G., Charge inversion accompanies DNA condensation by multivalent ions. *Nat Phys* **2007,** *3* (9), 641-644.
112. Guo, X. F.; Gorodetsky, A. A.; Hone, J.; Barton, J. K.; Nuckolls, C., Conductivity of a single DNA duplex bridging a carbon nanotube gap. *Nat Nanotechnol* **2008,** *3* (3), 163-167.

113. Fink, H. W.; Schonenberger, C., Electrical conduction through DNA molecules. *Nature* **1999,** *398* (6726), 407-410.
114. de Pablo, P. J.; Moreno-Herrero, F.; Colchero, J.; Gomez-Herrero, J.; Herrero, P.; Baro, A. M.; Ordejon, P.; Soler, J. M.; Artacho, E., Absence of dc-conductivity in lambda-DNA. *Phys Rev Lett* **2000,** *85* (23), 4992-4995.
115. Mallajosyula, S. S.; Pati, S. K., Toward DNA Conductivity: A Theoretical Perspective. *J Phys Chem Lett* **2010,** *1* (12), 1881-1894.
116. Eley, D. D.; Leslie, R. B., Conduction in Nucleic Acid Components. *Nature* **1963,** *197* (4870), 898-898.
117. Iguchi, K., Semiconductivity and band gap of a double strand of DNA. *J Phys Soc Jpn* **2001,** *70* (2), 593-597.
118. Rakitin, A.; Aich, P.; Papadopoulos, C.; Kobzar, Y.; Vedeneev, A. S.; Lee, J. S.; Xu, J. M., Metallic conduction through engineered DNA: DNA nanoelectronic building blocks. *Phys Rev Lett* **2001,** *86* (16), 3670-3673.
119. Wang, J. X., Electrical conductivity of double stranded DNA measured with ac impedance spectroscopy. *Phys Rev B* **2008,** *78* (24).
120. Lee, H. Y.; Tanaka, H.; Otsuka, Y.; Yoo, K. H.; Lee, J. O.; Kawai, T., Control of electrical conduction in DNA using oxygen hole doping. *Appl Phys Lett* **2002,** *80* (9), 1670-1672.
121. Hwang, J.; Ahn, D.; Hong, S.; Kim, H.; Hwang, S., Electrical conduction of thiol modified 60bp poly (dG) - Poly (dC) DNA molecules through Au nanoparticles. *J Mech Sci Technol* **2005,** *19* (11), 2138-2144.
122. Yoo, K. H.; Ha, D. H.; Lee, J. O.; Park, J. W.; Kim, J.; Kim, J. J.; Lee, H. Y.; Kawai, T.; Choi, H. Y., Electrical conduction through poly(dA)-poly(dT) and poly(dG)-poly(dC) DNA molecules. *Phys Rev Lett* **2001,** *87* (19).
123. Kasumov, A. Y.; Kociak, M.; Gueron, S.; Reulet, B.; Volkov, V. T.; Klinov, D. V.; Bouchiat, H., Proximity-induced superconductivity in DNA. *Science* **2001,** *291* (5502), 280-282.
124. Storm, A. J.; van Noort, J.; de Vries, S.; Dekker, C., Insulating behavior for DNA molecules between nanoelectrodes at the 100 nm length scale. *Appl Phys Lett* **2001,** *79* (23), 3881-3883.
125. Sadaoka, Y.; Sakai, Y.; Yamazoe, N.; Seiyama, T., Effect of adsorbed oxidative gases on electrical-properties of evaporated-films of phthalocyanines. *Denki Kagaku* **1982,** *50* (6), 457-462.
126. Endres, R. G.; Cox, D. L.; Singh, R. R. P., Colloquium: The quest for high-conductance DNA. *Rev Mod Phys* **2004,** *76* (1), 195-214.
127. Tran, P.; Alavi, B.; Gruner, G., Charge transport along the lambda-DNA double helix. *Phys Rev Lett* **2000,** *85* (7), 1564-1567.
128. Yu, Z. G.; Song, X. Y., Variable range hopping and electrical conductivity along the DNA double helix. *Phys Rev Lett* **2001,** *86* (26), 6018-6021.
129. Duguid, J.; Bloomfield, V. A.; Benevides, J.; Thomas, G. J., Raman Spectral Studies of Nucleic-Acids .44. Raman-Spectroscopy of DNA-Metal Complexes .1. Interactions and Conformational Effects of the Divalent-Cations - Mg, Ca, Sr, Ba, Mn, Co, Ni, Cu, Pd, and Cd. *Biophys J* **1993,** *65* (5), 1916-1928.

130. Patel, D. J.; Kozlowski, S. A.; Nordheim, A.; Rich, A., Right-handed and left-handed DNA: studies of B- and Z-DNA by using proton nuclear Overhauser effect and P NMR. *P Natl Acad Sci USA* **1982,** *79* (5), 1413-1417.
131. Burda, J. V.; Sponer, J.; Hobza, P., Ab Initio study of the interaction of guanine and adenine with various mono- and bivalent metal cations (Li^+, Na^+, K^+, Rb^+, Cs^+; Cu^+, Ag^+, Au^+; Mg^{2+}, Ca^{2+}, Sr^{2+}, Ba^{2+}; Zn^{2+}, Cd^{2+}, and Hg^{2+}). *J Phys Chem-Us* **1996,** *100* (17), 7250-7255.
132. Potaman, V. N.; Soyfer, V. N., Divalent Metal-Cations Upon Coordination to the N7 of Purines Differentially Stabilize the Pypupu DNA Triplex Due to Unequal Hoogsteen-Type Hydrogen-Bond Enhancement. *J Biomol Struct Dyn* **1994,** *11* (5), 1035-1040.
133. Burda, J. V.; Sponer, J.; Leszczynski, J.; Hobza, P., Interaction of DNA base pairs with various metal cations (Mg^{2+}, Ca^{2+}, Sr^{2+}, Ba^{2+}, Cu^+, Ag^+, Au^+, Zn^{2+}, Cd^{2+}, and Hg^{2+}): Nonempirical ab initio calculations on structures, energies, and nonadditivity of the interaction. *J Phys Chem B* **1997,** *101* (46), 9670-9677.
134. Onoa, G. B.; Cervantes, G.; Moreno, V.; Prieto, M. J., Study of the interaction of DNA with cisplatin and other Pd(II) and Pt(II) complexes by atomic force microscopy. *Nucleic Acids Res* **1998,** *26* (6), 1473-1480.
135. Corduneanu, O.; Chiorcea-Paquim, A. M.; Diculescu, V.; Fiuza, S. M.; Marques, M. P. M.; Oliveira-Brett, A. M., DNA Interaction with Palladium Chelates of Biogenic Polyamines Using Atomic Force Microscopy and Voltammetric Characterization. *Anal Chem* **2010,** *82* (4), 1245-1252.
136. Eichhorn, G. L.; Shin, Y. A., Interaction of metal ions with polynucleotides and related compounds. XII. The relative effect of various metal ions on DNA helicity. *J Am Chem Soc* **1968,** *90* (26), 7323-7328.
137. Seeman, N. C., Nucleic acid junctions and lattices. *Journal of Theoretical Biology* **1982,** *99* (2), 237-247.
138. Chen, J. H.; Seeman, N. C., Synthesis from DNA of a Molecule with the Connectivity of a Cube. *Nature* **1991,** *350* (6319), 631-633.
139. Seeman, N. C., An overview of structural DNA Nanotechnology. *Mol Biotechnol* **2007,** *37* (3), 246-257.
140. LaBean, T. H.; Yan, H.; Kopatsch, J.; Liu, F. R.; Winfree, E.; Reif, J. H.; Seeman, N. C., Construction, analysis, ligation, and self-assembly of DNA triple crossover complexes. *J Am Chem Soc* **2000,** *122* (9), 1848-1860.
141. Zhang, Y. W.; Seeman, N. C., Construction of a DNA-Truncated Octahedron. *J Am Chem Soc* **1994,** *116* (5), 1661-1669.
142. Lin, C. X.; Liu, Y.; Rinker, S.; Yan, H., DNA tile based self-assembly: Building complex nanoarchitectures. *Chemphyschem* **2006,** *7* (8), 1641-1647.
143. Park, S. H.; Barish, R.; Li, H. Y.; Reif, J. H.; Finkelstein, G.; Yan, H.; LaBean, T. H., Three-helix bundle DNA tiles self-assemble into 2D lattice or 1D templates for silver nanowires. *Nano Lett* **2005,** *5* (4), 693-696.
144. Winfree, E.; Liu, F. R.; Wenzler, L. A.; Seeman, N. C., Design and self-assembly of two-dimensional DNA crystals. *Nature* **1998,** *394* (6693), 539-544.
145. Liu, D.; Park, S. H.; Reif, J. H.; LaBean, T. H., DNA nanotubes self-assembled from triple-crossover tiles as templates for conductive nanowires. *P Natl Acad Sci USA* **2004,** *101* (3), 717-722.

146. Nangreave, J.; Han, D. R.; Liu, Y.; Yan, H., DNA origami: a history and current perspective. *Curr Opin Chem Biol* **2010,** *14* (5), 608-615.
147. Rothemund, P. W. K., Folding DNA to create nanoscale shapes and patterns. *Nature* **2006,** *440* (7082), 297-302.
148. Jungmann, R.; Liedl, T.; Sobey, T. L.; Shih, W.; Simmel, F. C., Isothermal assembly of DNA origami structures using denaturing agents. *J Am Chem Soc* **2008,** *130* (31), 10062-10063.
149. Andersen, E. S.; Dong, M. D.; Nielsen, M. M.; Jahn, K.; Lind-Thomsen, A.; Mamdouh, W.; Gothelf, K. V.; Besenbacher, F.; Kjems, J., DNA origami design of dolphin-shaped structures with flexible tails. *ACS Nano* **2008,** *2* (6), 1213-1218.
150. Zhao, Z.; Liu, Y.; Yan, H., Organizing DNA Origami Tiles into Larger Structures Using Preformed Scaffold Frames. *Nano Lett* **2011,** *11* (7), 2997-3002.
151. Douglas, S. M.; Dietz, H.; Liedl, T.; Hogberg, B.; Graf, F.; Shih, W. M., Self-assembly of DNA into nanoscale three-dimensional shapes. *Nature* **2009,** *459* (7245), 414-418.
152. Ke, Y. G.; Sharma, J.; Liu, M. H.; Jahn, K.; Liu, Y.; Yan, H., Scaffolded DNA Origami of a DNA Tetrahedron Molecular Container. *Nano Lett* **2009,** *9* (6), 2445-2447.
153. Andersen, E. S.; Dong, M.; Nielsen, M. M.; Jahn, K.; Subramani, R.; Mamdouh, W.; Golas, M. M.; Sander, B.; Stark, H.; Oliveira, C. L. P.; Pedersen, J. S.; Birkedal, V.; Besenbacher, F.; Gothelf, K. V.; Kjems, J., Self-assembly of a nanoscale DNA box with a controllable lid. *Nature* **2009,** *459* (7243), 73-U75.
154. Dietz, H.; Douglas, S. M.; Shih, W. M., Folding DNA into Twisted and Curved Nanoscale Shapes. *Science* **2009,** *325* (5941), 725-730.
155. Aldaye, F. A.; Palmer, A. L.; Sleiman, H. F., Assembling materials with DNA as the guide. *Science* **2008,** *321* (5897), 1795-1799.
156. Sharma, J.; Chhabra, R.; Liu, Y.; Ke, Y. G.; Yan, H., DNA-templated self-assembly of two-dimensional and periodical gold nanoparticle arrays. *Angew Chem Int Edit* **2006,** *45* (5), 730-735.
157. Mirkin, C. A.; Letsinger, R. L.; Mucic, R. C.; Storhoff, J. J., A DNA-based method for rationally assembling nanoparticles into macroscopic materials. *Nature* **1996,** *382* (6592), 607-609.
158. Pal, S.; Sharma, J.; Yan, H.; Liu, Y., Stable silver nanoparticle-DNA conjugates for directed self-assembly of core-satellite silver-gold nanoclusters. *Chem Commun* **2009,** (40), 6059-6061.
159. Yan, H.; Park, S. H.; Finkelstein, G.; Reif, J. H.; LaBean, T. H., DNA-Templated Self-Assembly of Protein Arrays and Highly Conductive Nanowires. *Science* **2003,** *301* (5641), 1882-1884.
160. Voigt, N. V.; Torring, T.; Rotaru, A.; Jacobsen, M. F.; Ravnsbaek, J. B.; Subramani, R.; Mamdouh, W.; Kjems, J.; Mokhir, A.; Besenbacher, F.; Gothelf, K. V., Single-molecule chemical reactions on DNA origami. *Nat Nano* **2010,** *5* (3), 200-203.
161. Li, S.; He, P.; Dong, J.; Guo, Z.; Dai, L., DNA-Directed Self-Assembling of Carbon Nanotubes. *J Am Chem Soc* **2004,** *127* (1), 14-15.
162. Chen, Y.; Liu, H.; Ye, T.; Kim, J.; Mao, C., DNA-Directed Assembly of Single-Wall Carbon Nanotubes. *J Am Chem Soc* **2007,** *129* (28), 8696-8697.
163. Li, Y.; Han, X.; Deng, Z., Grafting Single-Walled Carbon Nanotubes with Highly Hybridizable DNA Sequences: Potential Building Blocks for DNA-Programmed Material Assembly. *Angewandte Chemie* **2007,** *119* (39), 7625-7628.

164. Maune, H. T.; Han, S.-p.; Barish, R. D.; Bockrath, M.; Goddard, I. I. A.; RothemundPaul, W. K.; Winfree, E., Self-assembly of carbon nanotubes into two-dimensional geometries using DNA origami templates. *Nat Nano* **2010,** *5* (1), 61-66.
165. Eskelinen, A. P.; Kuzyk, A.; Kaltiaisenaho, T. K.; Timmermans, M. Y.; Nasibulin, A. G.; Kauppinen, E. I.; Torma, P., Assembly of Single-Walled Carbon Nanotubes on DNA-Origami Templates through Streptavidin-Biotin Interaction. *Small* **2011,** *7* (6), 746-750.
166. Ma, Y. F.; Zhang, J. M.; Zhang, G. J.; He, H. X., Polyaniline nanowires on Si surfaces fabricated with DNA templates. *J Am Chem Soc* **2004,** *126* (22), 7097-7101.
167. Pruneanu, S.; Al-Said, S. A. F.; Dong, L. Q.; Hollis, T. A.; Galindo, M. A.; Wright, N. G.; Houlton, A.; Horrocks, B. R., Self-assembly of DNA-templated polypyrrole nanowires: Spontaneous formation of conductive nanoropes. *Adv Funct Mater* **2008,** *18* (16), 2444-2454.
168. Hassanien, R.; Al-Hinai, M.; Al-Said, S. A. F.; Little, R.; Siller, L.; Wright, N. G.; Houlton, A.; Horrocks, B. R., Preparation and Characterization of Conductive and Photoluminescent DNA-Templated Polyindole Nanowires. *ACS Nano* **2010,** *4* (4), 2149-2159.
169. Hassanien, R.; Al-Said, S. A. F.; Siller, L.; Little, R.; Wright, N. G.; Houlton, A.; Horrocks, B. R., Smooth and conductive DNA-templated Cu2O nanowires: growth morphology, spectroscopic and electrical characterization. *Nanotechnology* **2012,** *23* (7).
170. Kundu, S.; Lee, H.; Liang, H., Synthesis and Application of DNA-CdS Nanowires within a Minute using Microwave Irradiation. *Inorg Chem* **2009,** *48* (1), 121-127.
171. Gu, Q.; Haynie, D. T., Palladium nanoparticle-controlled growth of magnetic cobalt nanowires on DNA templates. *Mater Lett* **2008,** *62* (17-18), 3047-3050.
172. Strick, T.; Allemand, J. F.; Croquette, V.; Bensimon, D., Twisting and stretching single DNA molecules. *Prog Biophys Mol Bio* **2000,** *74* (1-2), 115-140.
173. Xiao, Z. W.; Xu, M. X.; Ohgi, T.; Fujita, D., Influence of silicon surface structure on long deoxyribonucleic acid molecule alignment. *Jpn J Appl Phys 1* **2003,** *42* (7B), 4748-4751.
174. Hu, J.; Wang, M.; Weier, H. U. G.; Frantz, P.; Kolbe, W.; Ogletree, D. F.; Salmeron, M., Imaging of single extended DNA molecules on flat (aminopropyl)triethoxysilane-mica by atomic force microscopy. *Langmuir* **1996,** *12* (7), 1697-1700.
175. Ye, J. Y.; Umemura, K.; Ishikawa, M.; Kuroda, R., Atomic force microscopy of DNA molecules stretched by spin-coating technique. *Anal Biochem* **2000,** *281* (1), 21-25.
176. Woolley, A. T.; Kelly, R. T., Deposition and characterization of extended single-stranded DNA molecules on surfaces. *Nano Lett* **2001,** *1* (7), 345-348.
177. Li, J. W.; Bai, C. L.; Wang, C.; Zhu, C. F.; Lin, Z.; Li, Q.; Cao, E. H., A convenient method of aligning large DNA molecules on bare mica surfaces for atomic force microscopy. *Nucleic Acids Res* **1998,** *26* (20), 4785-4786.
178. Ouyang, Z. Q.; Hu, J.; Chen, S. F.; Sun, J. L.; Li, M. Q., Molecular patterns by manipulating DNA molecules. *J Vac Sci Technol B* **1997,** *15* (4), 1385-1387.
179. Yokota, H.; Sunwoo, J.; Sarikaya, M.; van den Engh, G.; Aebersold, R., Spin-stretching of DNA and protein molecules for detection by fluorescence and atomic force microscopy. *Anal Chem* **1999,** *71* (19), 4418-4422.
180. Kim, J. H.; Shi, W. X.; Larson, R. G., Methods of stretching DNA molecules using flow fields. *Langmuir* **2007,** *23* (2), 755-764.
181. Nakao, H.; Gad, M.; Sugiyama, S.; Otobe, K.; Ohtani, T., Transfer-printing of highly aligned DNA nanowires. *J Am Chem Soc* **2003,** *125* (24), 7162-7163.

182. Guan, J. J.; Lee, J., Generating highly ordered DNA nanostrand arrays. *P Natl Acad Sci USA* **2005,** *102* (51), 18321-18325.
183. Sarveswaran, K.; Hu, W. C.; Huber, P. W.; Bernstein, G. H.; Lieberman, M., Deposition of DNA rafts on cationic SAMs on silicon [100]. *Langmuir* **2006,** *22* (26), 11279-11283.
184. Kershner, R. J.; Bozano, L. D.; Micheel, C. M.; Hung, A. M.; Fornof, A. R.; Cha, J. N.; Rettner, C. T.; Bersani, M.; Frommer, J.; Rothemund, P. W. K.; Wallraff, G. M., Placement and orientation of individual DNA shapes on lithographically patterned surfaces. *Nat Nanotechnol* **2009,** *4* (9), 557-561.
185. Pilo-Pais, M.; Goldberg, S.; Samano, E.; LaBean, T. H.; Finkelstein, G., Connecting the Nanodots: Programmable Nanofabrication of Fused Metal Shapes on DNA Templates. *Nano Lett* **2011,** *11* (8), 3489-3492.
186. Weizmann, Y.; Patolsky, F.; Popov, I.; Willner, I., Telomerase-generated templates for the growing of metal nanowires. *Nano Lett* **2004,** *4* (5), 787-792.
187. Schreiber, R.; Kempter, S.; Holler, S.; Schuller, V.; Schiffels, D.; Simmel, S. S.; Nickels, P. C.; Liedl, T., DNA Origami-Templated Growth of Arbitrarily Shaped Metal Nanoparticles. *Small* **2011,** *7* (13), 1795-1799.
188. Kumar, A.; Pattarkine, M.; Bhadbhade, M.; Mandale, A. B.; Ganesh, K. N.; Datar, S. S.; Dharmadhikari, C. V.; Sastry, M., Linear superclusters of colloidal gold particles by electrostatic assembly on DNA templates. *Adv Mater* **2001,** *13* (5), 341-344.
189. Pearson, A. C.; Liu, J.; Pound, E.; Uprety, B.; Woolley, A. T.; Davis, R. C.; Harb, J. N., DNA Origami Metallized Site Specifically to Form Electrically Conductive Nanowires. *The Journal of Physical Chemistry B* **2012,** *116* (35), 10551-10560.
190. Sastry, M.; Kumar, A.; Datar, S.; Dharmadhikari, C. V.; Ganesh, K. N., DNA-mediated electrostatic assembly of gold nanoparticles into linear arrays by a simple drop-coating procedure. *Appl Phys Lett* **2001,** *78* (19), 2943-2945.
191. Geng, Y. L.; Liu, J. F.; Pound, E.; Gyawali, S.; Harb, J. N.; Woolley, A. T., Rapid metallization of lambda DNA and DNA origami using a Pd seeding method. *J Mater Chem* **2011,** *21* (32), 12126-12131.
192. Richter, J.; Seidel, R.; Kirsch, R.; Mertig, M.; Pompe, W.; Plaschke, J.; Schackert, H. K., Nanoscale palladium metallization of DNA. *Adv Mater* **2000,** *12* (7), 507-510.
193. Nguyen, K.; Monteverde, M.; Filoramo, A.; Goux-Capes, L.; Lyonnais, S.; Jegou, P.; Viel, P.; Goffman, M.; Bourgoin, J. P., Synthesis of thin and highly conductive DNA-based palladium nanowires. *Adv Mater* **2008,** *20* (6), 1099-1104.
194. Mertig, M.; Ciacchi, L. C.; Seidel, R.; Pompe, W.; De Vita, A., DNA as a selective metallization template. *Nano Lett* **2002,** *2* (8), 841-844.
195. Keren, K.; Krueger, M.; Gilad, R.; Ben-Yoseph, G.; Sivan, U.; Braun, E., Sequence-specific molecular lithography on single DNA molecules. *Science* **2002,** *297* (5578), 72-75.
196. Liu, J. F.; Geng, Y. L.; Pound, E.; Gyawali, S.; Ashton, J. R.; Hickey, J.; Woolley, A. T.; Harb, J. N., Metallization of Branched DNA Origami for Nanoelectronic Circuit Fabrication. *ACS Nano* **2011,** *5* (3), 2240-2247.
197. Braun, E.; Eichen, Y.; Sivan, U.; Ben-Yoseph, G., DNA-templated assembly and electrode attachment of a conducting silver wire. *Nature* **1998,** *391* (6669), 775-778.
198. Richter, J.; Mertig, M.; Pompe, W.; Monch, I.; Schackert, H. K., Construction of highly conductive nanowires on a DNA template. *Appl Phys Lett* **2001,** *78* (4), 536-538.

199. Ongaro, A.; Griffin, F.; Beeeher, P.; Nagle, L.; Iacopino, D.; Quinn, A.; Redmond, G.; Fitzmaurice, D., DNA-templated assembly of conducting gold nanowires between gold electrodes on a silicon oxide substrate. *Chem Mater* **2005,** *17* (8), 1959-1964.
200. Aherne, D.; Satti, A.; Fitzmaurice, D., Diameter-dependent evolution of failure current density of highly conducting DNA-templated gold nanowires. *Nanotechnology* **2007,** *18* (12).
201. Park, S. H.; Prior, M. W.; LaBean, T. H.; Finkelstein, G., Optimized fabrication and electrical analysis of silver nanowires templated on DNA molecules. *Appl Phys Lett* **2006,** *89* (3).
202. Gu, Q.; Cheng, C. D.; Suryanarayanan, S.; Dai, K.; Haynie, D. T., DNA-templated fabrication of nickel nanocluster chains. *Physica E* **2006,** *33* (1), 92-98.
203. Monson, C. F.; Woolley, A. T., DNA-templated construction of copper nanowires. *Nano Lett* **2003,** *3* (3), 359-363.
204. Kudo, H.; Fujihira, M., DNA-Templated copper nanowire fabrication by a two-step process involving electroless metallization. *Ieee T Nanotechnol* **2006,** *5* (2), 90-92.
205. Gu, Q.; Cheng, C. D.; Haynie, D. T., Cobalt metallization of DNA: toward magnetic nanowires. *Nanotechnology* **2005,** *16* (8), 1358-1363.

CHAPTER 2: RAPID METALLIZATION OF LAMBDA DNA AND DNA ORIGAMI USING A PD SEEDING METHOD*

2.1 INTRODUCTION

The bottom-up approach is an emerging way to produce nanomaterials, combining atomic or molecular species to construct desired systems via chemical reactions.[1] Using objects with designed complexity as templates to direct the self-assembly of nanomaterials is one method to synthesize such nanometre-scale structures. In particular, DNA is a promising template to fabricate metal nanostructures.[2] Many studies on the metallization of DNA have been reported since the first DNA-templated nanowires were fabricated by Braun et al.[3] Metal nanowires with different compositions, such as Au,[4-10] Ag,[3, 11-14] Cu,[15, 16] Co,[17, 18] Pd,[19-23] Pt,[24] Ni[25, 26] and multiple segments,[27, 28] have been created using DNA scaffolding. These studies indicate broad applicability of DNA as a template to fabricate diverse metal nanowire systems.

The first paper to show the formation of Pd clusters on a DNA template was published by Richter and co-workers,[20] in which they activated DNA with Pd for 2 h, followed by reduction. The diameter of the Pd metallized clusters was ~40 nm. In 2008, Nguyen et al.[22] developed a method to fabricate Pd nanowires with higher conductance, using the selective precipitation of PdO followed by reduction. This approach yielded ~25-nm-diameter, Pd-coated DNA nanowires , and minimized parasitic metal cluster growth in adjacent areas. However, the metallization process was slow, taking nearly 2 days.

---

* This chapter is adapted with permission from Geng, Y. L.; Liu, J. F.; Pound, E.; Gyawali, S.; Harb, J. N.; Woolley, A. T., *J Mater Chem* **2011,** *21* (32), 12126-12131. Copyright 2011 The Royal Society of Chemistry.

Interfaces between metals and semiconductors are needed to fabricate nanoelectronic systems. In 2003, DNA was used as a template to make a linear transistor; the DNA served to precisely localize carbon nanotubes and also to template Au nanowire metallization.[4] More sophisticated nanocircuitry will require multiple interconnections and branching, necessitating more complex template designs. In 2006, Rothemund[29] developed a method called "scaffolded DNA origami" wherein arbitrary two-dimensional structures are created through programmed self-assembly based on hydrogen bonding between base pairs in a long scaffold strand and numerous shorter staple strands. Scaffolded DNA origami shows great promise for the creation of complex nanostructures including circuit-like shapes, which makes this approach especially desirable for application in templated nanofabrication, for example, in making nanocircuits. A group at BYU recently demonstrated a silver seeding method to metallize branched DNA origami structures with good selectivity,[30] which is a key step toward the realization of DNA-templated nanocircuits. However, although this was an important advance, there were also drawbacks, such as the somewhat complicated metallization process and relatively low density of metallized nanostructures that remained on the surface after plating.

In this paper, I developed a quick and efficient Pd seeding method to obtain continuous and uniform Pd nanowires with small (~30 nm) diameters. To further highlight the versatility of this Pd seeding method, I also employed it in making Au-metallized lambda DNA and branched DNA origami with higher surface density than in earlier work. My approach for DNA metallization consists of three steps: (1) Pd activation, (2) Pd reduction to form seeds, and (3) electroless plating. **Figure 2.1** outlines the process to obtain metal nanowires using Pd seeds on DNA. In the seeding step, the DNA is activated by a Pd(II) solution, wherein Pd(II) forms coordination complexes with Lewis bases on the DNA.[31] The activation is followed by exposure

to a reducing agent to form Pd seeds on the DNA. In the electroless plating step, these metal seeds serve as nucleation sites for the electroless deposition of a thicker metal coating. Specifically my work provides two key advances. First, I decrease the Pd activation time to <30 min, giving rise to more rapid and efficient metallization. Second, I obtain increased surface density of metallized, branched nanostructures made from DNA origami templates.

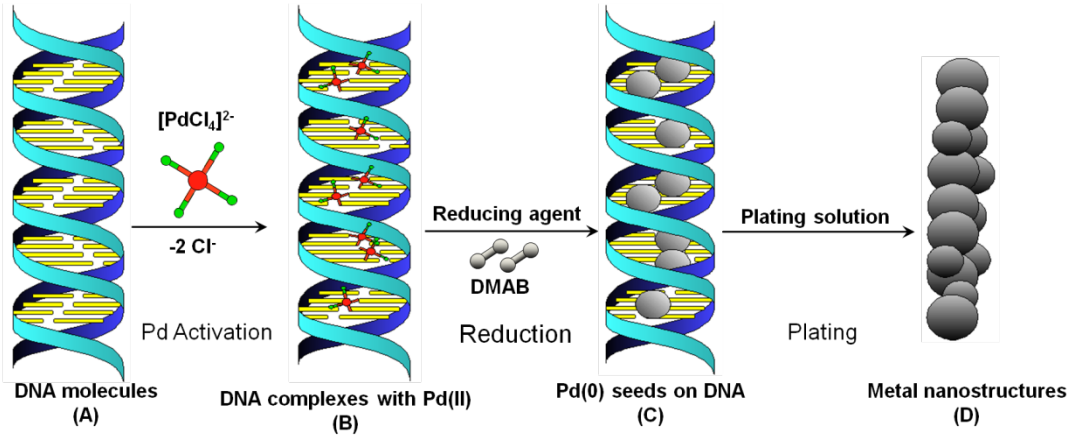

Figure 2.1 Schematic of Pd seeding and plating on double-stranded DNA. Pd(II): red; Cl: green; Pd(0): silver. (A) Double-stranded DNA; base pairs are represented by yellow bars. (B) Interaction between DNA and Pd(II) (in the form of $PdCl_4^{2-}$) to form complexes. (C) Pd seeds on DNA strands after reducing. (D) More metal is deposited to form nanostructures on the Pd(0) seeds upon treatment with plating solution.

2.2 EXPERIMENTAL SECTION

2.2.1 Materials

Muscovite mica surfaces were bought from S&J Trading (Glen Oaks, NY). Lambda DNA samples came from New England Biolabs (Ipswich, MA), and DNA origami were formed similarly to work that was described previously.[32] NH_4OH and HEPES were obtained from Mallinckrodt Baker (Phillipsburg, NJ). NH_4F and NH_4Cl were bought from EM Science

(Gibbstown, NJ). $MgCl_2$ was acquired from EMD Chemicals (Gibbstown, NJ). H_2SO_4 was bought from Mallinckrodt Chemicals (Phillipsburg, NJ), and H_2O_2 (30%) was obtained from Fisher Scientific (Pittsburgh, PA). Gold plating solution was obtained from Nanoprobes (Yaphank, NY). Any other chemicals not previously mentioned were obtained from Sigma-Aldrich (St. Louis, MO). Water (18.3 MΩ cm) treated by an EASYPure UV/UF purification system (Barnstead, Dubuque, IA) was employed for all rinsings and aqueous solution preparations.

DNA templates. Lambda DNA and DNA origami were used as templates to fabricate metal nanostructures. For lambda DNA, a 500 μg/mL stock solution was first diluted to 60 μg/mL and then dissolved in 30 mM $MgCl_2$ and 10 mM HEPES (pH 6.5), making a final DNA concentration of 2 μg/mL. This solution (5 μL) was placed on freshly cleaved mica. After 30 s, surfaces were rinsed with water and then dried with air. DNA origami solutions (10 nM scaffold strand, 100 nM staple strands) were mixed with 30 mM $MgCl_2$ at a 1:1 volume ratio. A 5 μL aliquot of the resulting solution was placed on freshly cleaved mica. After 1 min surfaces were rinsed, first with 4 mM $MgCl_2$ and then with water, followed by air drying.

DNA metallization. For both lambda DNA and DNA origami metallization, the fundamental process consists of three steps: Pd activation, reduction to form seeds, and electroless plating. During activation, 15-20 μL of Pd(II) solution[25] (1 mM $PdCl_2$ and 1 M NH_4Cl in HEPES buffer, pH 6.5) was pipetted onto a surface having deposited DNA templates and left to stand for an activation time of 5 to 30 min in a humidified container at room temperature. Next, the liquid on the surface was absorbed using filter paper. After activation, the palladinized DNA templates were incubated in 15-20 μL of reducing agent (40 mM DMAB, dimethylamine borane, and 5 mM $MgCl_2$) for 1 min. The reaction was quenched by rinsing with 4 mM $MgCl_2$ solution,

followed by water rinsing and drying under a stream of air. A repeated, second Pd seeding step was done for DNA origami samples to ensure sufficient numbers and sizes of seeds on these small structures. I utilized two different electroless plating solutions (Pd and Au) on seeded DNA templates. The Pd plating solution (pH 10)[33] was made by dissolving 50 mM $PdCl_2$, 110 mM $Na_4P_2O_7$ (a complexing agent to stabilize Pd^{2+}), 0.1 M NH_4OH and 0.3 M NH_4F in water for 16 h, and then adding enough NaH_2PO_2 to yield a 50 mM final concentration. The Au plating solution was from a commercial source, as noted previously. $MgCl_2$ was added to both the Pd and Au plating solutions to make a 10 mM concentration before use. Either the electroless Au or Pd plating solution (40-50 μL) was pipetted onto surfaces having Pd-seeded DNA samples, with the reaction proceeding for 5-15 min at 60-70 °C (Pd) or room temperature (Au). Afterward, the sample was rinsed with H_2O for 5 s, followed by drying using a stream of air.

Atomic force microscopy (AFM) imaging. All AFM images were obtained using a Multimode Nanoscope IIIa atomic force microscope under tapping mode in air. AFM tips were purchased from Nanoscience Instruments (Phoenix, AZ).

Scanning electron microscopy (SEM). SEM images were taken using a XL30 ESEM FEG (Philips, Hillsboro, OR). Energy-dispersive X-ray (EDX) analysis was performed by spot scanning. SEM images were taken in low-vacuum mode to avoid surface charging.

2.3 RESULTS AND DISCUSSION

2.3.1 Seeding and plating on Lambda DNA

I used lambda DNA templates in initial experiments to test the feasibility of the Pd seeding method[25, 34] and to provide a robust foundation for subsequent DNA origami metallization work.

I focused on obtaining seeding continuity and selectivity, as well as on retaining large numbers of nanostructures on the surface after metallization. Several factors thought to affect the results were evaluated, including Pd activation time and magnesium ion concentration in the DMAB reducing solution, as well as in the plating bath.

Seeding selectivity is essential for the selectivity of the subsequent metallization step. Pd activation, in which Pd(II) species coordinate with N atoms on nucleobases, is a key step in the metallization process. The extent of reaction between Pd(II) and DNA is time dependent. The time of activation reported in the literature[17, 20, 22] varied from 2 h[20] to one,[17] or more days[22] at room temperature or lower. I explored a range of short activation times (2-180 min) to make this step more efficient, while still achieving high seeding density. For the shortest activation times, Pd seeding density was low, and the height of the seeds after reduction was <3 nm (**Figure 2.2A**); For a 5 min activation time (**Figure 2.2B**), seeding density increased, and the average seed height was >3 nm. For activation times of 10 and 30 min (**Figure 2.2C-D**), seeding density and continuity went up further, compared with 5 min activation. Lengthening the activation time beyond 10 min did not affect the seeding density significantly, and seed aggregation occurred, leading to an increase in the average size. I also found that when the activation time was increased to 3 h (**Figure 2.2E**), the underlying DNA strands were partially removed from the surface. This may be due to DNA cleavage during the extended exposure (3 h vs. 30 min) to Pd(II).[35] Based on my analysis, sufficient Pd activation occurs within 10 to 30 min; these shorter activation times are also desirable for DNA origami metallization.

I also studied the stability of lambda DNA on mica during the step of reduction to form seeds. I found that Mg^{2+} played an important role in keeping DNA on the surface throughout the DMAB reducing bath treatment (**Figure 2.3**). Without Mg^{2+} in the reducing solution, the amount

of DNA left on the surface after DMAB treatment decreased (**Figure 2.3B**). By comparing AFM images of DNA before and after DMAB treatment (**Figure 2.3**), I found that 5 mM Mg^{2+} improved DNA retention on the surface. This is due to the reported ability of Mg^{2+} to act as an ion bridge between negatively charged mica and DNA phosphate groups,[36] preventing the Pd(II)-DNA complexes from being removed from the surface during reduction and rinsing.

Additional experiments were performed to investigate the effect of Mg^{2+} in the plating solution on surface adherence of the resulting nanostructures. Without Mg^{2+} in the plating solution, only a few particles were seen on the surface (**Figure 2.4A**). Similarly, with 2 mM Mg^{2+}, largely nonspecific particles were left on the surface, with very little metallized DNA observable after Au plating (**Figure 2.4B**). In contrast, with 10 mM Mg^{2+} in the plating solution, linear metallized nanostructures were obtained (**Figure 2.4C**). Thus, a moderate concentration of Mg^{2+} in the Au plating solution allows Pd-seeded DNA to remain on the surface, without negatively impacting plating effectiveness. It may also be possible to plate DNA in solution and then deposit it on surfaces, although I have not yet succeeded in demonstrating this approach. The need for Mg^{2+} in the seeding and plating solutions would likely be eliminated, but procedures would need to be developed to purify seeded material from the seeding solution, to rapidly quench the plating reaction, and to selectively deposit the metal structures on surfaces.

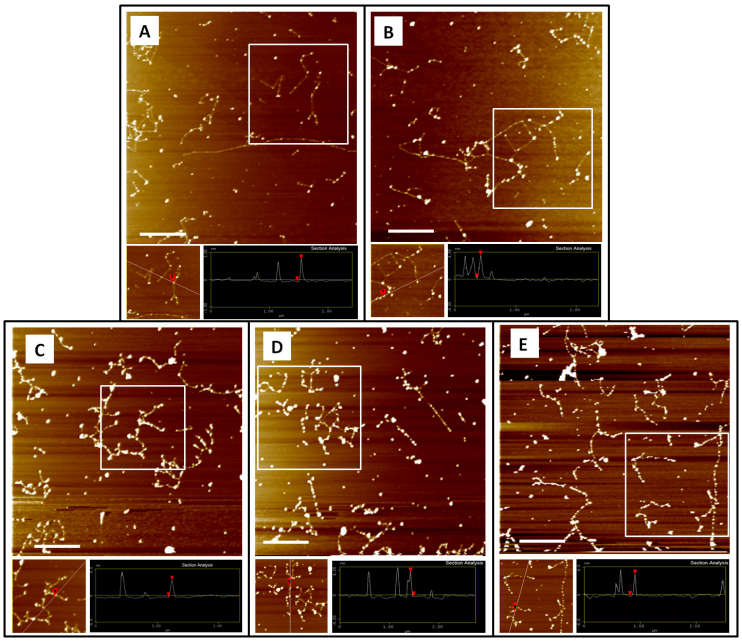

Figure 2.2 Influence of Pd activation time on surface DNA after seeding. Activation times are (A) 2, (B) 5, (C) 10, (D) 30 and (E) 180 min. DMAB reduction for 1 min was done after activation. Height scale: 6 nm. Scale bars: 1 µm. (Left insets) Views of the white squares marked in each image, with the white lines showing the paths of the cross-section traces. (Right insets) Cross-sectional traces along the indicated paths.

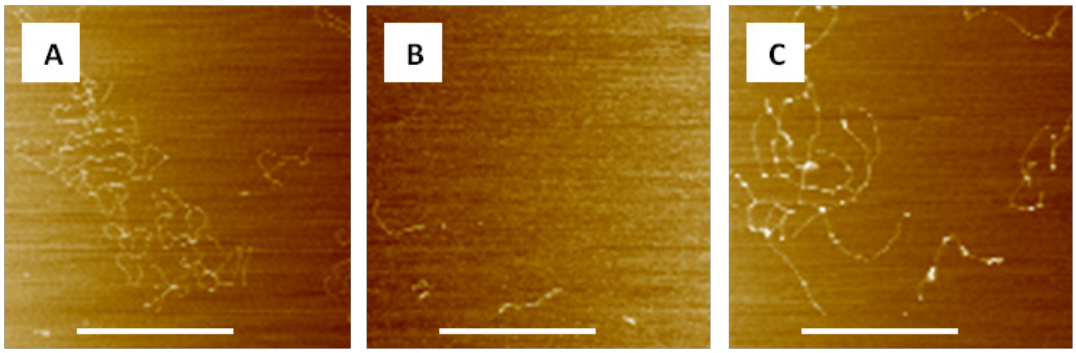

Figure 2.3 The effect of Mg^{2+} on surface DNA attachment after DMAB reduction. AFM images of lambda DNA on mica (A) before DMAB treatment, (B) after DMAB treatment for 1 min with no added Mg^{2+}, and (C) after DMAB treatment with 5 mM Mg^{2+} in the reducing solution. Scale bars: 1 µm; height scale: 5 nm.

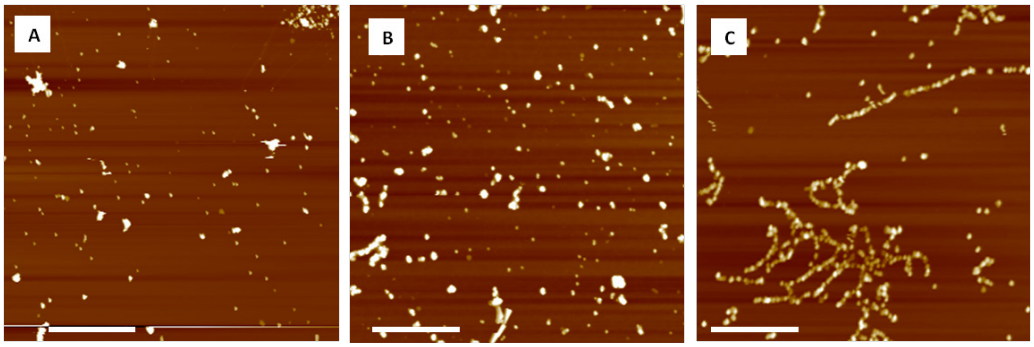

Figure 2.4 AFM images of metallized lambda DNA after Au plating for 5 min in a bath having (A) no Mg^{2+}, (B) 2 mM Mg^{2+} and (C) 10 mM Mg^{2+}. Scale bars: 1 μm. Height scale: 80 nm.

Given the importance of Mg^{2+} in the Au plating solution, I also added 10 mM Mg^{2+} to my Pd plating bath, which I used on Pd-seeded lambda DNA. My optimization of metallization process variables resulted in the selective and continuous coating of lambda DNA with Pd, as seen from AFM and SEM data (**Figure 2.5**). The average height of the nanowires (n=5) is ~28 nm (**Figure 2.5A** inset). The SEM image shows continuous strings of Pd nanoparticles along the DNA strands (**Figure 2.5B**). The EDX spectrum (**Figure 2.5C**) has multiple peaks for Pd (in addition to characteristic mica signals), which confirms the composition of the nanowires.

2.3.2 Seeding and plating on DNA origami

To fabricate more complex metal nanostructures that satisfy the more sophisticated needs of nanocircuit fabrication, I used branched, "T"-shaped DNA origami[32] as a template with my optimized Pd seeding and Au plating methods. The results shown in **Figure 2.6** demonstrate the formation of branched metal nanostructures from a DNA origami template. Comparison of **Figure 2.6A-B** clearly indicates that DNA origami T structures retained their shapes after Pd seeding, and that the size of the T shapes decreased somewhat after seeding (**Figure 2.6A-B**). I also noted that the height of the structures increased with a second seeding step as additional

Pd(0) formed and was deposited.[34, 37] A higher nonspecific background of deposition was found after the second seeding step (**Figure 2.6C**) compared to after one seeding (**Figure 2.6B**). I hypothesize that this is due to a combination of slow DNA cleavage by Pd(II) during the seeding process[35] and nonspecific Pd(0) deposition on the surface from the activation solution. Under identical seeding conditions, the nucleation site density was higher on DNA origami (1 seed per 70 nm, 26 seeds counted) than on lambda DNA (1 seed per 115 nm, 44 seeds counted). Thus, moving to denser DNA motifs such as six-helix bundles[38] or three-dimensional DNA origami[3939] may provide even greater nucleation site density that should result in smoother plated structures. **Figure 2.6D** shows an AFM image after Au plating of twice-seeded T-shape DNA origami. The lateral size of the Au metallized nanostructures was around 200-250 nm in length, and the height was ~40 nm. These results demonstrate the promise of my approach for increasing the density of metallized DNA origami on surfaces.

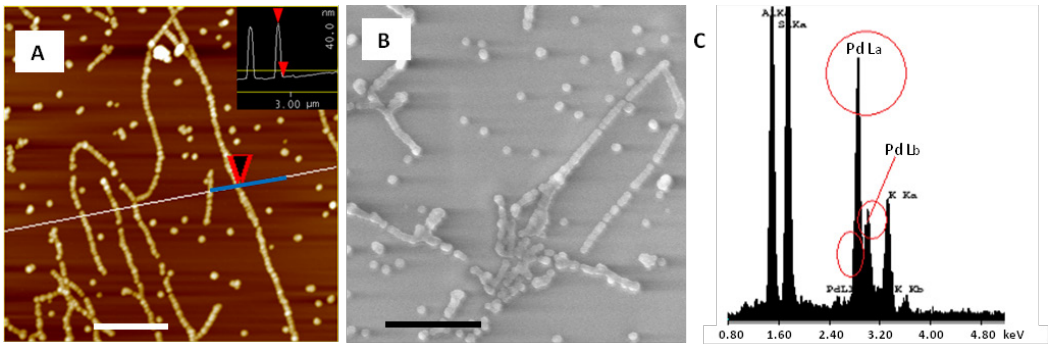

Figure 2.5 DNA-templated Pd nanowires formed through Pd activation and seeding, followed by Pd plating for 10 min. (A) AFM image of continuous Pd nanowires on mica; inset: height analysis along the blue line in (A). Height scale: 80 nm. (B) SEM image of Pd nanowires on mica. (C) EDX spectrum of nanowires in (B) by spot scanning. Scale bars for (A–B): 1 μm.

SEM was also used to observe the morphology and continuity of Au-plated T-shape DNA origami, as indicated in **Figure 2.7**. The SEM data show metal nanostructures that have the same T shape as the unplated branched DNA origami template. Additionally, the SEM images show that the metal clusters generally formed continuous structures along the DNA origami, especially in the zoom-view SEM (**Figure 2.7C**). Finally, EDX results provide confirmation of the presence of Au in the templated nanostructures (**Figure 2.7D**). The electron microscopy data provide confirming evidence that my DNA origami nanostructures have continuous plating of gold metal.

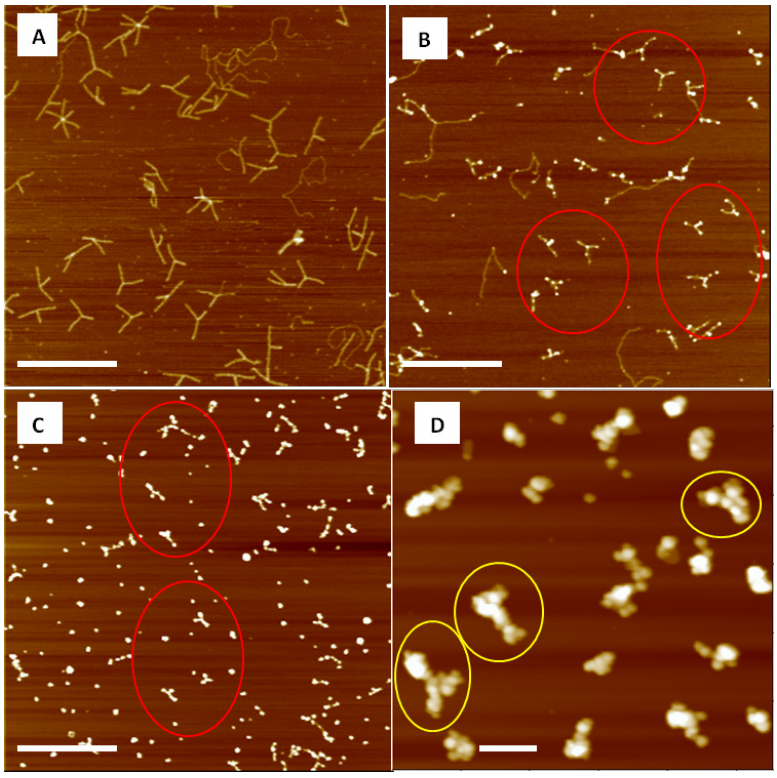

Figure 2.6 AFM images of metallization of T-shape DNA origami on mica. (A) DNA origami. (B) Single Pd seeding. (C) Double Pd seeding. (D) Gold metallized. Scale bars for (A–C): 1 μm. Scale bar for (D): 200 nm. Height scales for (A–C): 6 nm. Height scale for (D): 80 nm.

2.4 CONCLUSIONS

I have demonstrated the metallization of lambda DNA with both Pd and Au, after Pd seeding. Continuous Pd nanowires with small diameters were obtained, and the whole process was relatively simple and fast. Additionally, I found that Mg^{2+} played an important role in both the seeding and plating steps. I have applied these methods to metallize T-shaped DNA origami with Au, resulting in improved yields over previous work. Furthermore, the metallized DNA origami appear continuous and retain the branched template structure. This work represents an attractive approach to achieve rapid metallzation of DNA origami nanostructures with good yields.

Ongoing efforts focus on electrical conductivity characterization of these metal nanostructures. I am applying the mica surface procedures for DNA origami deposited on oxidized silicon, to enable more straightforward electron-beam patterning of contact electrodes. Confirmation of electrical properties will be a key step in moving toward the full realization of DNA-templated nanoelectronic circuits.

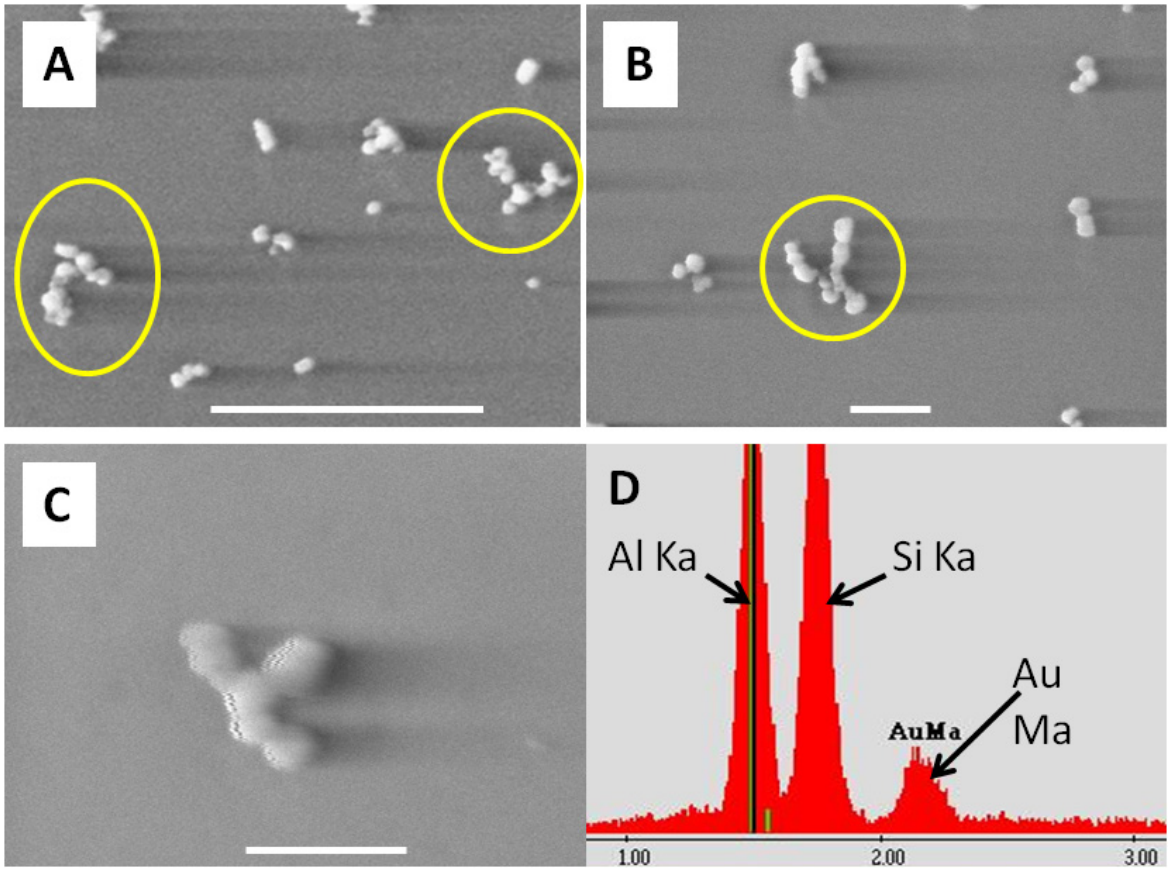

Figure 2.7 Characterization of Au-metallized T-shape DNA origami on mica. (A–C) SEM images in low-vacuum mode. Scale bars: (A) 700 nm; (B–C): 200 nm. (D) EDX of the plated DNA origami in (B).

2.5 REFERENCES

1. Seeman, N. C., DNA in a material world. *Nature* **2003,** *421* (6921), 427-431.
2. Becerril, H. A.; Woolley, A. T., DNA-templated nanofabrication. *Chem Soc Rev* **2009,** *38* (2), 329-337.

3. Braun, E.; Eichen, Y.; Sivan, U.; Ben-Yoseph, G., DNA-templated assembly and electrode attachment of a conducting silver wire. *Nature* **1998,** *391* (6669), 775-778.
4. Keren, K.; Berman, R. S.; Buchstab, E.; Sivan, U.; Braun, E., DNA-templated carbon nanotube field-effect transistor. *Science* **2003,** *302* (5649), 1380-1382.
5. Nishinaka, T.; Takano, A.; Doi, Y.; Hashimoto, M.; Nakamura, A.; Matsushita, Y.; Kumaki, J.; Yashima, E., Conductive metal nanowires templated by the nucleoprotein filaments, complex of DNA and RecA protein. *J Am Chem Soc* **2005,** *127* (22), 8120-8125.
6. Ongaro, A.; Griffin, F.; Beeeher, P.; Nagle, L.; Iacopino, D.; Quinn, A.; Redmond, G.; Fitzmaurice, D., DNA-templated assembly of conducting gold nanowires between gold electrodes on a silicon oxide substrate. *Chem Mater* **2005,** *17* (8), 1959-1964.
7. Aherne, D.; Satti, A.; Fitzmaurice, D., Diameter-dependent evolution of failure current density of highly conducting DNA-templated gold nanowires. *Nanotechnology* **2007,** *18* (12), 125205.
8. Satti, A.; Aherne, D.; Fitzmaurice, D., Analysis of scattering of conduction electrons in highly conducting bamboolike DNA-templated gold nanowires. *Chem Mater* **2007,** *19* (7), 1543-1545.
9. Kundu, S.; Liang, H., Microwave synthesis of electrically conductive gold nanowires on DNA scaffolds. *Langmuir* **2008,** *24* (17), 9668-9674.
10. Mohammadzadegan, R.; Mohabatkar, H.; Sheikhi, M. H.; Safavi, A.; Khajouee, M. B., DNA-templated gold nanowires. *Physica E* **2008,** *41* (1), 142-145.
11. Yan, H.; Park, S. H.; Finkelstein, G.; Reif, J. H.; LaBean, T. H., DNA-templated self-assembly of protein arrays and highly conductive nanowires. *Science* **2003,** *301* (5641), 1882-1884.
12. Park, S. H.; Barish, R.; Li, H. Y.; Reif, J. H.; Finkelstein, G.; Yan, H.; LaBean, T. H., Three-helix bundle DNA tiles self-assemble into 2D lattice or 1D templates for silver nanowires. *Nano Lett* **2005,** *5* (4), 693-696.
13. Park, S. H.; Prior, M. W.; LaBean, T. H.; Finkelstein, G., Optimized fabrication and electrical analysis of silver nanowires templated on DNA molecules. *Appl Phys Lett* **2006,** *89* (3), 033901-1 -033901-3.
14. Becerril, H. A.; Stoltenberg, R. M.; Monson, C. F.; Woolley, A. T., Ionic surface masking for low background in single- and double-stranded DNA-templated silver and copper nanorods. *J Mater Chem* **2004,** *14* (4), 611-616.
15. Monson, C. F.; Woolley, A. T., DNA-templated construction of copper nanowires. *Nano Lett* **2003,** *3* (3), 359-363.
16. Becerril, H. A.; Stoltenberg, R. M.; Wheeler, D. R.; Davis, R. C.; Harb, J. N.; Woolley, A. T., DNA-templated three-branched nanostructures for nanoelectronic devices. *J Am Chem Soc* **2005,** *127* (9), 2828-2829.
17. Gu, Q.; Cheng, C. D.; Haynie, D. T., Cobalt metallization of DNA: toward magnetic nanowires. *Nanotechnology* **2005,** *16* (8), 1358-1363.
18. Gu, Q.; Haynie, D. T., Palladium nanoparticle-controlled growth of magnetic cobalt nanowires on DNA templates. *Mater Lett* **2008,** *62* (17-18), 3047-3050.
19. Richter, J.; Mertig, M.; Pompe, W.; Monch, I.; Schackert, H. K., Construction of highly conductive nanowires on a DNA template. *Appl Phys Lett* **2001,** *78* (4), 536-538.
20. Richter, J.; Seidel, R.; Kirsch, R.; Mertig, M.; Pompe, W.; Plaschke, J.; Schackert, H. K., Nanoscale palladium metallization of DNA. *Adv Mater* **2000,** *12* (7), 507-510.

21. Richter, J.; Mertig, M.; Pompe, W.; Vinzelberg, H., Low-temperature resistance of DNA-templated nanowires. *Appl Phys A-Mater* **2002,** *74* (6), 725-728.
22. Nguyen, K.; Monteverde, M.; Filoramo, A.; Goux-Capes, L.; Lyonnais, S.; Jegou, P.; Viel, P.; Goffman, M.; Bourgoin, J. P., Synthesis of thin and highly conductive DNA-based palladium nanowires. *Adv Mater* **2008,** *20* (6), 1099-1104.
23. Kundu, S.; Lee, H.; Liang, H., Synthesis and Application of DNA-CdS Nanowires within a Minute using Microwave Irradiation. *Inorg Chem* **2009,** *48* (1), 121-127.
24. Mertig, M.; Ciacchi, L. C.; Seidel, R.; Pompe, W.; De Vita, A., DNA as a selective metallization template. *Nano Lett* **2002,** *2* (8), 841-844.
25. Gu, Q.; Cheng, C. D.; Suryanarayanan, S.; Dai, K.; Haynie, D. T., DNA-templated fabrication of nickel nanocluster chains. *Physica E* **2006,** *33* (1), 92-98.
26. Becerril, H. A.; Ludtke, P.; Willardson, B. M.; Woolley, A. T., DNA-templated nickel nanostructures and protein assemblies. *Langmuir* **2006,** *22* (24), 10140-10144.
27. Fischler, M.; Simon, U.; Nir, H.; Eichen, Y.; Burley, G. A.; Gierlich, J.; Gramlich, P. M.; Carell, T., Formation of bimetallic Ag-Au nanowires by metallization of artificial DNA duplexes. *Small* **2007,** *3* (6), 1049-1055.
28. Lee, J.; Wang, A. A.; Rheem, Y.; Yoo, B.; Mulchandani, A.; Chen, W.; Myung, N. V., DNA assisted assembly of multisegmented nanowires. *Electroanal* **2007,** *19* (22), 2287-2293.
29. Rothemund, P. W. K., Folding DNA to create nanoscale shapes and patterns. *Nature* **2006,** *440* (7082), 297-302.
30. Liu, J. F.; Geng, Y. L.; Pound, E.; Gyawali, S.; Ashton, J. R.; Hickey, J.; Woolley, A. T.; Harb, J. N., Metallization of Branched DNA Origami for Nanoelectronic Circuit Fabrication. *ACS Nano* **2011,** *5* (3), 2240-2247.
31. Richter, J., Metallization of DNA. *Physica E* **2003,** *16* (2), 157-173.
32. Pound, E.; Ashton, J. R.; Becerril, H. A.; Woolley, A. T., Polymerase Chain Reaction Based Scaffold Preparation for the Production of Thin, Branched DNA Origami Nanostructures of Arbitrary Sizes. *Nano Lett* **2009,** *9* (12), 4302-4305.
33. Mallory, G. O.; Hajdu, J. B., *Electroless plating: fundamentals and applications*. American Electroplaters and Surface Finishers Society: New York, 1990.
34. Kind, H.; Bittner, A. M.; Cavalleri, O.; Kern, K.; Greber, T., Electroless deposition of metal nanoislands on aminothiolate-functionalized Au(111) electrodes. *J Phys Chem B* **1998,** *102* (39), 7582-7589.
35. Gao, E. J.; Wang, K. H.; Gu, X. F.; Yu, Y.; Sun, Y. G.; Zhang, W. Z.; Yin, H. X.; Wu, Q.; Zhu, M. C.; Yan, X. M., A novel binuclear palladium complex with benzothiazole-2-thiolate: Synthesis, crystal structure and interaction with DNA. *J Inorg Biochem* **2007,** *101* (10), 1404-1409.
36. Bezanilla, M.; Drake, B.; Nudler, E.; Kashlev, M.; Hansma, P. K.; Hansma, H. G., Motion and Enzymatic Degradation of DNA in the Atomic-Force Microscope. *Biophys J* **1994,** *67* (6), 2454-2459.
37. Ford, W. E.; Harnack, O.; Yasuda, A.; Wessels, J. M., Platinated DNA as precursors to templated chains of metal nanoparticles. *Adv Mater* **2001,** *13* (23), 1793-1797.
38. Mathieu, F.; Liao, S. P.; Kopatscht, J.; Wang, T.; Mao, C. D.; Seeman, N. C., Six-helix bundles designed from DNA. *Nano Lett* **2005,** *5* (4), 661-665.
39. Douglas, S. M.; Dietz, H.; Liedl, T.; Hogberg, B.; Graf, F.; Shih, W. M., Self-assembly of DNA into nanoscale three-dimensional shapes. *Nature* **2009,** *459* (7245), 414-418.

CHAPTER 3: ELECTRICALLY CONDUCTIVE GOLD AND COPPER METALLIZED DNA ORIGAMI NANOSTRUCTURES*

3.1 INTRODUCTION

Bottom-up nanofabrication by self-assembly has shown promise in the production of structures with nanoscale features.[1] Among bottom-up methods, DNA-based nanofabrication[2, 3] to create complex shapes with nanometer sizes has attracted increasing interest for fabricating nanodevices, as complex shapes are enabling for creating multiple interconnections. DNA metallization is a key area of interest, offering a promising route to designed metal nanostructures. DNA-templated nanowires with diverse compositions have been reported;[4-6] in some instances, the electrical conductivity of these DNA-templated nanowires (Ag, Au, and Pd) has also been measured.[4-9] Although these resistivities were larger than that of the bulk metal by one to four orders of magnitude, these prior results still show promise. However, among these studies no paper has been published demonstrating conductive Cu nanowires formed on DNA.

In particular, the method of scaffolded DNA origami[10-13] has opened a new area for fabricating complex patterns of metal nanostructures. In brief, this technique can fold a long single-stranded DNA "scaffold" into an arbitrary nanostructure through the use of numerous complementary, short oligonucleotide pieces known as "staple strands". I was part of the first group to show that DNA origami could be metallized, using a silver seeding method and then plating with gold.[14] I also metallized DNA origami using a palladium seeding and gold plating method,[15] which showed good selectivity. Concurrent with this latter work, Pilo-Pais et al.[16] used oligonucleotide

---

* This chapter is adapted from Geng, Y. L.; Pearson, A. C.; Gates, E. P.; Uprety, B.; Davis, R. C.; Harb, J. N.; Woolley, A. T., Electrically conductive gold and copper metallized DNA origami nanostructures (submitted).

functionalized gold nanoparticles (NPs) for site-specific seeding on DNA origami tiles, followed by silver plating to produce nanostructures such as rings, parallel bars, and "H" shapes. Recently, the BYU group applied a hybridization-based strategy with higher seeding density than prior work,[16] and a Au electroless plating bath to site-specifically metallize DNA origami, resulting in both continuous wires and metal segments with designed gaps.[9] This paper also reported the first electrical conductivity measurements on metallized DNA origami linear wires. A circular circuit (CC) DNA origami template was further used and produced circuit-like structures with gaps. However, the yield of the resulting metallized nanostructures was somewhat low. In addition, no paper has been published on DNA origami templated Cu nanostructures; moreover, no work has been published on conductance measurements on Cu metallized DNA.

Herein, I describe the metallization of the same CC DNA origami structure on silicon surfaces using a modification of a Pd seeding method I reported previously.[15] The process entails the formation of DNA origami and their placement on a surface; the use of multiple Pd seeding steps; and finally, Au or Cu electroless plating. The DNA origami CC structures were placed on surfaces with high yield using a spin stretching technique. The spinning was also applied after Pd activation, simplifying seeding as well. I addressed the relatively low seeding density of Pd on DNA origami on silicon surfaces by using multiple seeding steps, which increased seeding density with both good selectivity and reproducibility. The seeding and subsequent plating were studied by size distribution analysis to determine optimal conditions. The seeded DNA origami were further electrolessly plated with either Au or Cu, resulting in continuous metal nanostructures with small and well-defined features as well as high yield. I measured the electrical conductivity of both Au and Cu metallized DNA origami, and both showed typical ohmic behavior and electrical conductivity. Importantly, my work is the first demonstration of

conductive Cu nanostructures made from DNA or DNA origami templates. This work on making plated DNA origami structures shows promise for making connections to individual nanostructures, and for tailoring or enhancing surface plasmons.

3.2 EXPERIMENTAL

3.2.1 Materials

M13mp18 was purchased from New England Biolabs (Ipswich, MA). Staple strands (100 μM in Tris-EDTA buffer) were ordered from Operon Biotechnologies (Huntsville, AL). Ammonium hydroxide, formaldehyde, potassium sodium tartrate, and 4-(2-hydroxyethyl)-1-piperazineethanesulfonic acid (HEPES) were obtained from Mallinckrodt Baker (Phillipsburg, NJ). Ammonium chloride was bought from EM Science (Gibbstown, NJ). Copper sulfate and sodium hydroxide were purchased from Spectrum Chemical (Gardena, CA). Magnesium chloride was acquired from EMD Chemical (Gibbstown, NJ). Concentrated sulfuric acid was bought from Mallinckrodt Chemicals (Phillipsburg, NJ), and 30% hydrogen peroxide solution was obtained from Fisher Scientific (Pittsburgh, PA). A gold electroless plating solution (GoldEnhance EM, Catalog #2113) was obtained from Nanoprobes (Yaphank, NY). Silicon wafers with a 500 nm thick oxidized layer were purchased from Silicon Wafer Enterprises (El Dorado Hills, CA). ZEP-520 electron beam resist and ZED-N50 developer were bought from Zeon Chemicals (Louisville, KY). The 1165 Microposit remover was obtained from MicroChem (Newton, MA). Hydroxylamine hydrochloride, chloroauric acid, 2-propanol, ethylenediaminetetraacetic acid (EDTA), palladium chloride, and dimethylaminoborane were obtained from Sigma-Aldrich (St. Louis, MO). Water (18.3 MΩ cm) treated by an EASYPure

UV/UF purification system (Barnstead, Dubuque, IA) was employed for all rinsings and aqueous solution preparations.

3.2.2 Methods

Scheme 3.1 offers an overview of the entire DNA origami metallization process. Briefly, fabrication includes: (1) DNA origami formation and deposition on a surface, (2) Pd seeding via multiple Pd activation and reduction steps, and (3) electroless plating.

CC DNA origami folding. M13mp18 ssDNA was used as the scaffold for CC DNA origami folding.[9] The structures were folded by combining a mixture of 2 nM M13mp18 and 20 nM of all staple strands in 1× Tris-acetate-EDTA (TAE)-Mg^{2+} buffer (12.5 mM Mg^{2+}) and putting the mixture through a temperature program in a thermal cycler as described previously.[9]

DNA origami surface deposition. Undiluted DNA origami solution was placed onto Si surfaces by spinning. Prior to use, Si surfaces were cleaned with piranha solution (70% H_2SO_4, 30% H_2O_2) at ~150 °C for 10 min. For spin coating, Si surfaces were first pretreated by spinning 20 µL of 4 mM magnesium chloride for 20 s at 2,000 rpm. Then, 4.5 µL of the DNA origami solution was pipetted onto the surface and allowed to stand for 2 min, and the substrate was spun for 15 s at 1,500 rpm. After that, the surface was rinsed twice by spinning 35 µL of water for 35 s at 3,500 rpm.

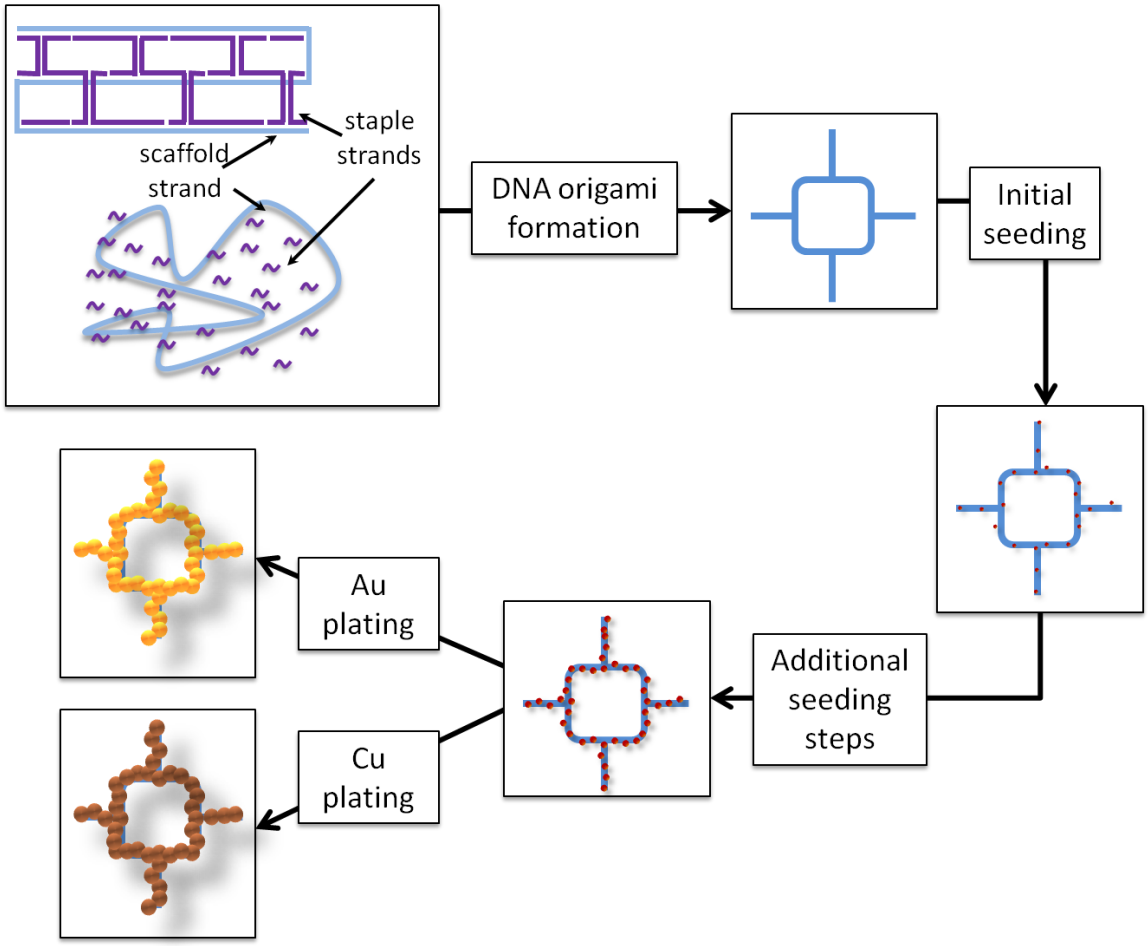

Scheme 3.1 Fabrication and metallization of DNA origami. The process starts with the formation of DNA origami, which is deposited on a Si surface. Next, Pd seeding steps are done, during which Pd seeds grow on the DNA template. Then, either Au or Cu electroless plating is used to enhance and develop seeds into thicker and continuous nanostructures.

DNA origami metallization. The overall process consists of three steps: Pd activation, Pd reduction to form seeds, and electroless plating.[15, 17] During activation, 20 µL of Pd solution (1 mM palladium chloride and 1 M ammonium chloride in HEPES buffer, pH 6.5) was pipetted onto surface DNA templates and let stand for the desired activation time in a humidified container at room temperature. After activation, the samples were spun at 1,500 rpm for 15 s to remove residual liquid. For reduction, 20 µL of reducing agent (40 mM dimethylaminoborane and 5 mM magnesium chloride) were transferred to the surface and left for 1 min. The reaction

was quenched through water rinsing for 4 s and drying under a stream of air. After reduction, the Pd seeded DNA origami were plated as described below. To optimize Pd seeding, I used multiple successive seeding steps. The activation time for the first seeding step was 2.5 h, and 25 min for the other four steps.

I used two different Au electroless plating solutions. One was from a commercial source, and the other (0.4 mM hydroxylamine hydrochloride and 0.01% chloroauric acid) was prepared following a published procedure.[9, 18] The reducing agent was added to the solution just before use. The second plating solution was applied for 5 min on samples that had already been treated for 10 min with the commercial solution.

Before Cu plating, I first treated the Pd-seeded DNA with the commercial Au electroless plating solution for 10-15 s to enlarge the seeds. The Cu plating solution contained a mixture of 3.2 g/L copper sulfate, 25 g/L potassium sodium tartrate tetrahydrate, and 7 g/L sodium hydroxide. For 1 mL of plating solution, 10 μL of formaldehyde (37%) was added to the mixture right before use. The Cu electroless plating time was 1 min.

For electroless plating, the Au or Cu plating solution (40-50 μL) was pipetted onto seeded DNA samples, with the reaction proceeding for the designated time at room temperature. Afterwards, the sample was rinsed with water for 8 s, followed by drying using a stream of air.

Atomic force microscopy (AFM) imaging. All AFM images were obtained using a Multimode Nanoscope IIIa instrument (Santa Barbara, CA) under tapping mode in air. AFM tips were purchased from Nanoscience Instruments (Phoenix, AZ).

Scanning electron microscopy (SEM). SEM images were taken using a XL30 ESEM FEG (Philips, Hillsboro, OR). Energy-dispersive X-ray (EDX) analysis was performed by spot scanning.

Electrical conductivity measurements. Au electrode deposition was carried out after electron beam lithography using a nanometer pattern generation system on the SEM. ZEP-520 and ZED-N50 were used as electron beam resist and developer, respectively. Following exposure and resist developing, a CHA-600 thermal evaporator (Fremont, CA) was used to deposit a 7 nm chromium adhesion layer followed by 75 nm of gold. The resulting samples were then immersed in 1165 Microposit remover at room temperature overnight for lift-off. After that, surfaces were rinsed with 2-propanol and dried by a stream of air. Samples after lift-off were stored in a vacuum desiccator until conductivity measurements were done. For Cu metallized DNA, electrode patterning and deposition were done immediately after Cu metallization to minimize possible oxidation of Cu nanostructures.

The electrical conductivity of metallized nanostructures was measured using micromanipulator probes to connect two Au electrodes to a power source. The applied voltage and other parameters were controlled by LabVIEW and the current was measured with an Ithaco picoammeter (Ithaca, NY). The voltage set during measurements ranged from -100 to 100 mV.

3.3 RESULTS AND DISCUSSION

3.3.1 Pd seeding on DNA origami CC structures

A spin stretching method was used to put DNA origami on Si surfaces. The whole process took less than 10 min, which is faster and simpler than our previously reported work.[9] Seeding procedures were modified from our previous work.[15] I tested up to five Pd seeding steps to see what conditions yielded the best results on DNA origami on Si.

I studied the effects of different numbers of Pd seeding steps on DNA origami. **Figure 3.1** shows AFM height and 3D images of CC DNA origami both before and after several successive seeding steps. Compared unseeded DNA in **Figure 3.1A** with seeded samples in **Figure 3.1B-F**, it is clear that the DNA origami structures were able to retain their shape after seeding. Additionally, the surface background remained low even after 5 successive seedings, which indicates good selectivity. AFM images showed that seeding was discontinuous after the first seeding step (**Figure 3.1B**), but appeared more continuous with successive seeding steps (**Figure 3.1C-F**).

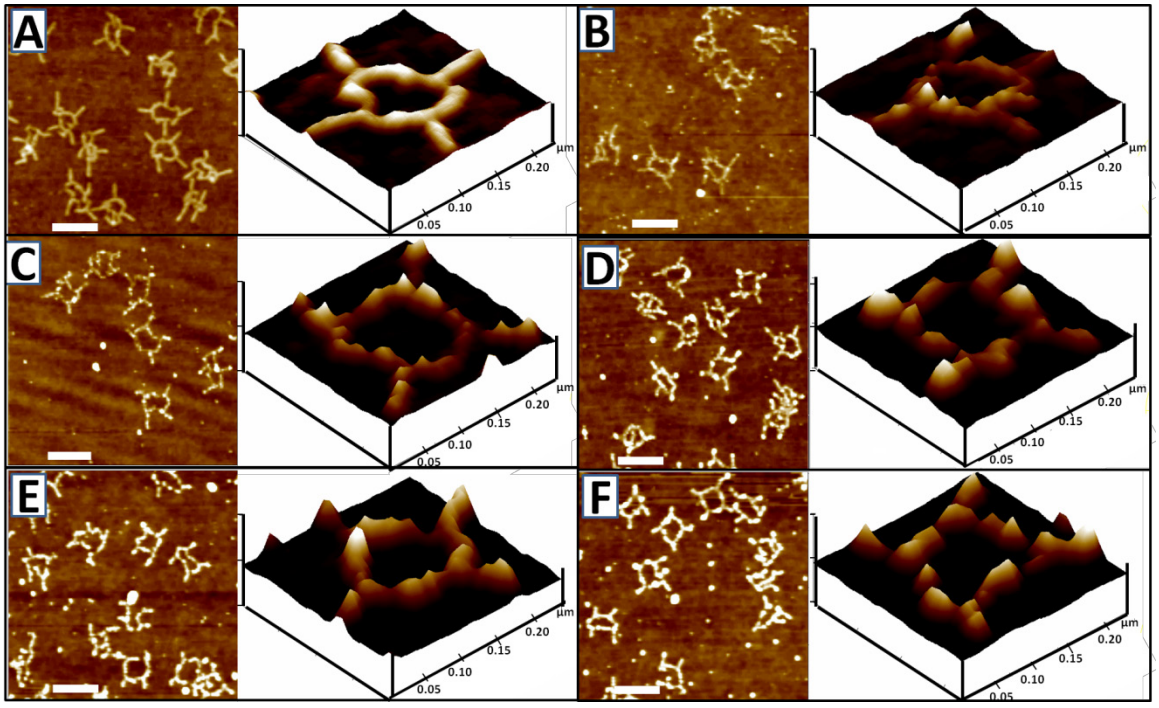

Figure 3.1 AFM height and 3D images of DNA origami CC structures on Si. (A) Unseeded structures. (B) 1, (C) 2, (D) 3, (E) 4, and (F) 5 palladium seedings. (Left) Height images; height scales: 6 nm; scale bars: 200 nm. (Right): 3D-view AFM images of individual structures. Height scale: 6 nm.

Because the AFM images provide a more subjective picture of seeding completeness, I used particle height distribution analysis to further characterize the seeding steps statistically (**Figure 3.2**). The data were obtained from AFM section analyses of particles on DNA molecules in

height images from several samples (**Figure 3.3**). For each seeding condition, I made more than 100 measurements to ensure adequate sampling. Histograms were generated from these data, and fitted to a Gaussian distribution. The mean particle height distribution increased going from one through five seeding steps (**Figure 3.2B-F**). Thus, the mean size of Pd seeds increased during these steps, which is consistent with the qualitative view from AFM height images in **Figure 3.1**.

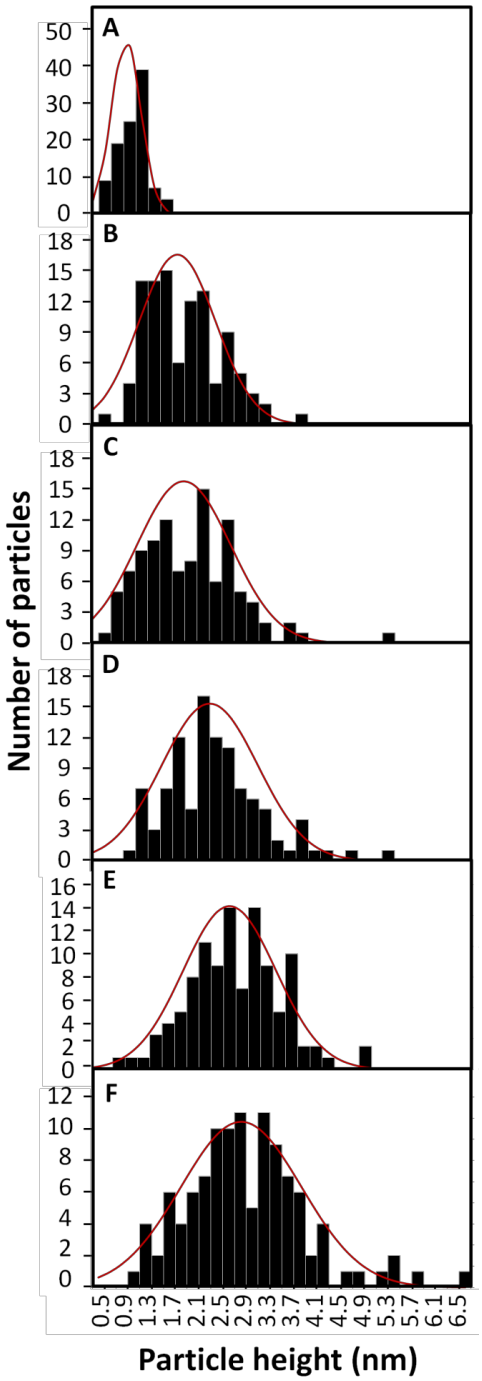

Figure 3.2 Height distribution analysis from AFM data before and after seeding steps. Data were obtained by AFM section analysis with more than 100 measurements for each seeding condition. (A-F) Histograms and Gaussian distribution for 0-5 seeding steps. The mean heights and standard deviations are (A) 1.0

Multiple seeding steps resulted in filling of the gaps between seeds, and improved the continuity and uniformity of seeding. Additionally, the histograms in **Figure 3.2** provide an estimate of the seed sizes after subtracting the unseeded DNA origami height (1.0 nm) from the resulting height after each seeding step. Thus, the mean thickness of metal deposited after 1-5 seeding steps was 0.9 nm, 1.0 nm, 1.4 nm, 1.9 nm, and 1.9 nm, respectively. Since no seed size change was observed between four and five repeated seedings but the height distribution was narrower for four seedings compared to five, four replicate seedings appeared to be the best number for subsequent experiments. The results above nicely demonstrate that multiple seeding steps lead to increased seed continuity and enlarged seed sizes.

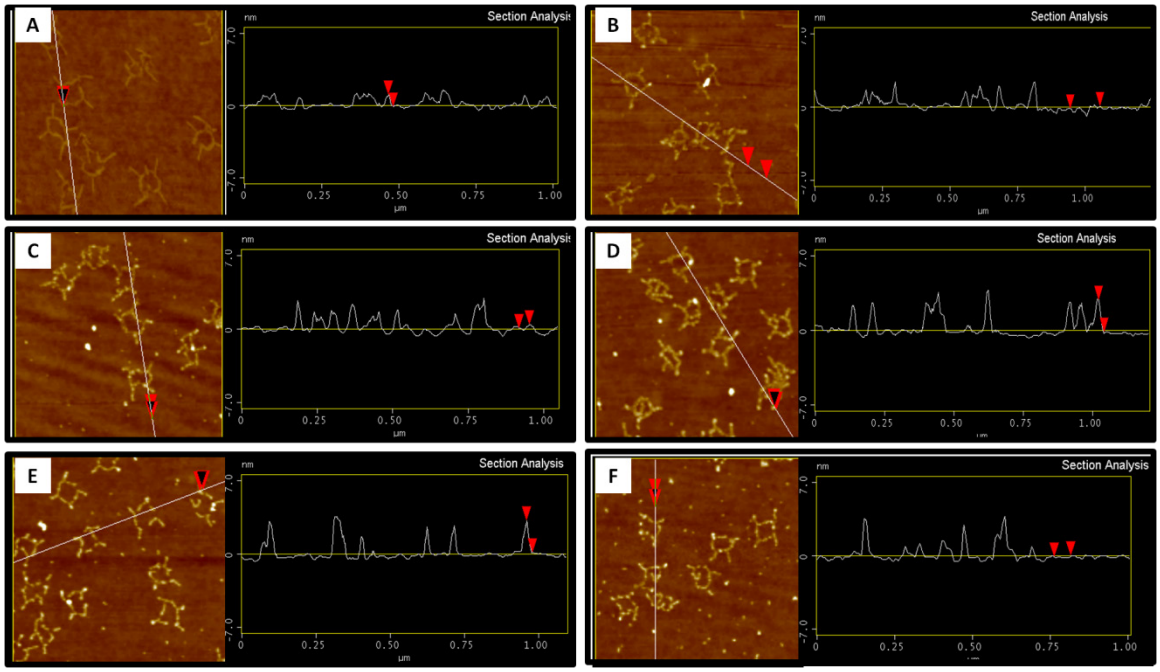

Figure 3.3 Examples of AFM section analyses for samples of (A-F) 0-5 Pd seedings. In total, more than 100 measurements were done for each condition, which were used for height distribution analysis in Figure 3.2.

3.3.2 Au electroless plating on DNA origami CC structures

To fabricate continuous metal nanostructures, a plating process is necessitated in which the metal grows and fully covers the Pd seeds. Here, I applied a commercial Au electroless plating solution on DNA origami CC structures that were Pd seeded from 1 up to 5 times to explore the effect of Pd seeding on the resulting plated structures. Each sample was exposed to 50 µL of plating solution for 10 min at room temperature, followed by water rinsing to quench the reaction. SEM images were then obtained to study the morphology of these samples (**Figure 3.4**). No fully metallized structures were observed for Au plated, singly seeded samples (**Figure 3.4A**), although in some areas, linear chains of nanoparticles could be seen. This result is consistent with the AFM seeding data (**Figure 3.1B**), where only discontinuous Pd seeds were seen after the first seeding step. The Au-plated structures that were seeded twice were more continuous and appeared more like the CC design (**Figure 3.4B**). However, there were still some regions of insufficient plating and continuity (see **Figure 3.4B**, inset). Based on the AFM data (**Figure 3.1C**) and height distribution (**Figure 3.2C**), this better result is likely due to both larger seed size and increased seed density. Plating continuity and uniformity were further improved for structures seeded 3-5 times (**Figure 3.4C-E**). This improvement can be explained based on the AFM images (**Figure 3.1**) in which the density of seeds increased, and the distribution analysis (**Figure 3.2**), in which the average height of Pd seeds increased. The data suggest that with increased seeding, there is a size threshold that must be exceeded for uniform Au plating. For the sample seeded five times (**Figure 3.4E**), the granularness and background after Au plating appeared to be slightly increased (**Figure 3.4E**). I attribute this to the increased background after 5 seeding steps (**Figure 3.1F**), and the larger standard deviation due to an increase in number of

larger seeds (> 5 nm) in the particle size distribution (**Figure 3.2F**). Width distribution analysis of Au plated samples was also applied (**Figure 3.5**), and the 4×Pd seeded samples had a slightly lower standard deviation than the 3× or 5× seeded samples. These results confirmed four Pd seeding steps as the best for 10-min Au plating.

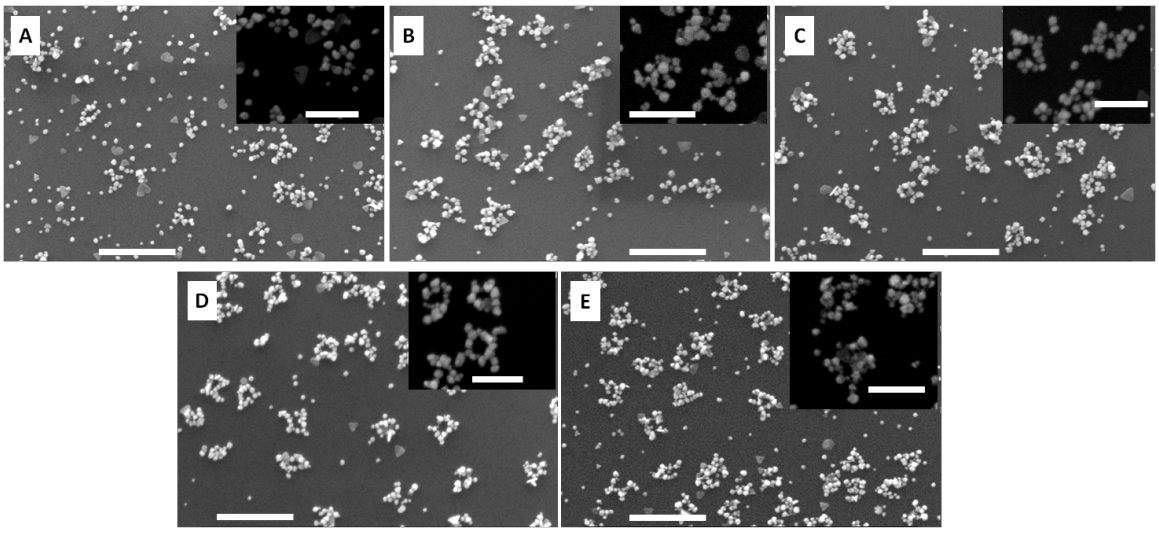

Figure 3.4 SEM images of CC DNA origami Au plated for 10 min for (A-E) 1-5 Pd seedings. Scale bars: 500 nm. Insets are zoomed in images for each condition. Scale bars for insets: 200 nm.

To see if alternative Au plating conditions would improve uniformity and continuity, I also carried out a second Au electroless plating step[9, 18] after the commercial Au plating process on 4×Pd seeded samples. As shown in **Figure 3.6**, the Au nanostructures after the second metallization step appeared somewhat more fused and enlarged compared with those after treatment with the commercial Au plating only. The average width was 30 nm for the single plating step and 35 nm for two Au platings. EDX spectra for both Au plating conditions exhibited an Au peak. Doubly plated structures had somewhat larger widths than singly plated ones, but the apparent continuity was essentially the same.

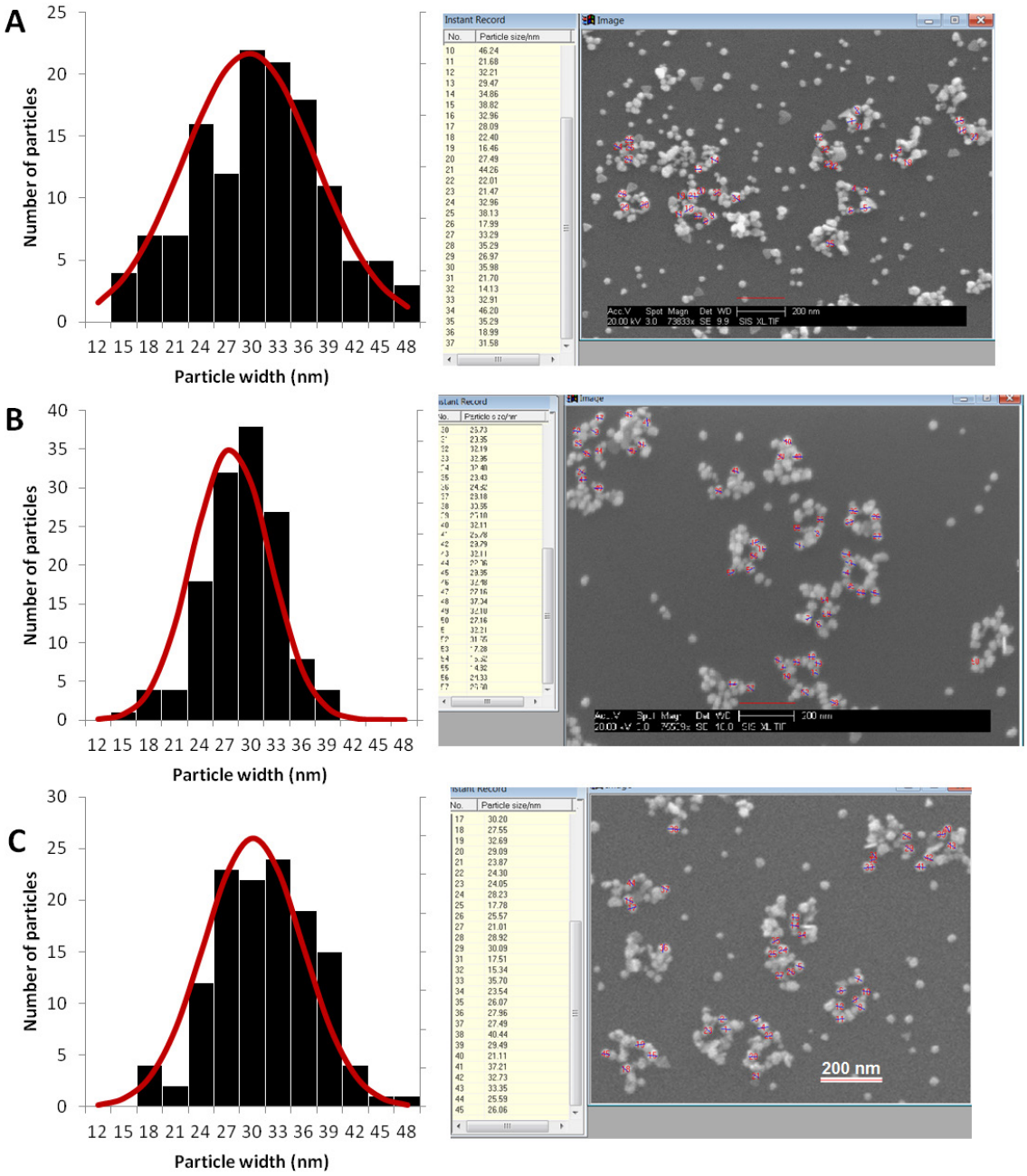

Figure 3.5 Width distribution on Au plated samples obtained from SEM images. Each condition had more than 100 measurements from different samples. 10 min commercial Au electroless plating on (A) 3, (B) 4 and (C) 5×Pd seeded samples. Mean particle widths and standard deviations were 29.6 ± 7.7nm, 27.6 ± 4.6 nm, and 30.0 ± 5.7 nm.

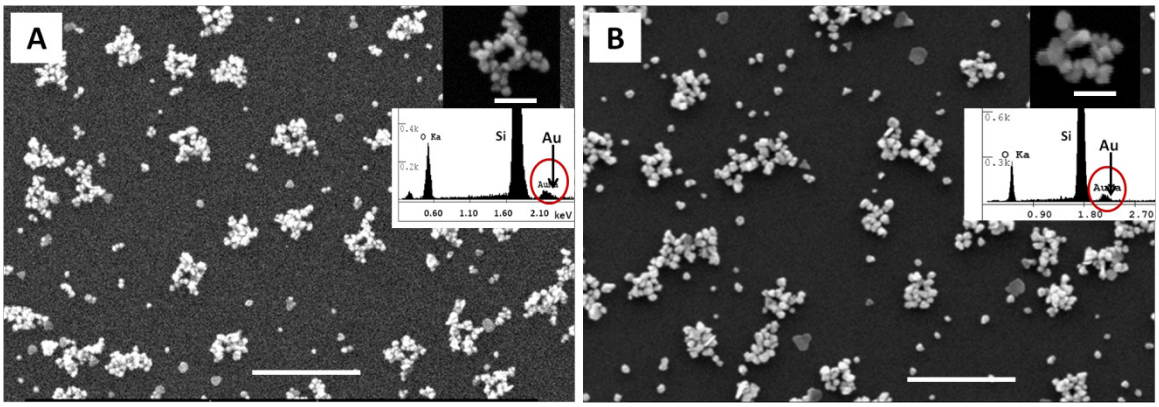

Figure 3.6 SEM images of Pd seeded CC structures made by (A) Au plating with a commercial solution only; or (B) Au plating with a commercial solution followed by Au plating using a published approach.[9, 18] Insets are highly zoomed images and EDX spectra of the zoomed region. Scale bars: 500 nm. Scale bars for insets: 100 nm.

3.3.3 Cu electroless plating on DNA origami CC structures

Cu was also plated on 4×Pd seeded DNA origami structures. The Pd seeded samples were first treated with the commercial Au plating solution for 10-15 s to enlarge the seed sizes. The nanoparticles grown on Pd seeds after this brief Au plating step were much smaller and clearly not continuous (**Figure 3.7A**), compared with the 10-min Au plating (**Figure 3.4D**). After 1 min of Cu electroless plating at room temperature, the structures appeared continuous and had the shape of the DNA origami (**Figure 3.7B**). A zoom-in SEM (**Figure 3.7C**) showed more detailed information on the Cu nanostructures. The Cu peak near 0.9 keV in the EDX spectrum (**Figure 3.7D**) for the red-circled structure in **Figure 3.7C** confirmed the Cu content of the metallized structures. In addition, a tiny peak of Au around 2.1 keV was also observed; this small Au signal was attributed to the short time of the Au plating (prior to Cu plating).The average diameter of the Cu lines in the plated DNA origami structures was ~40 nm.

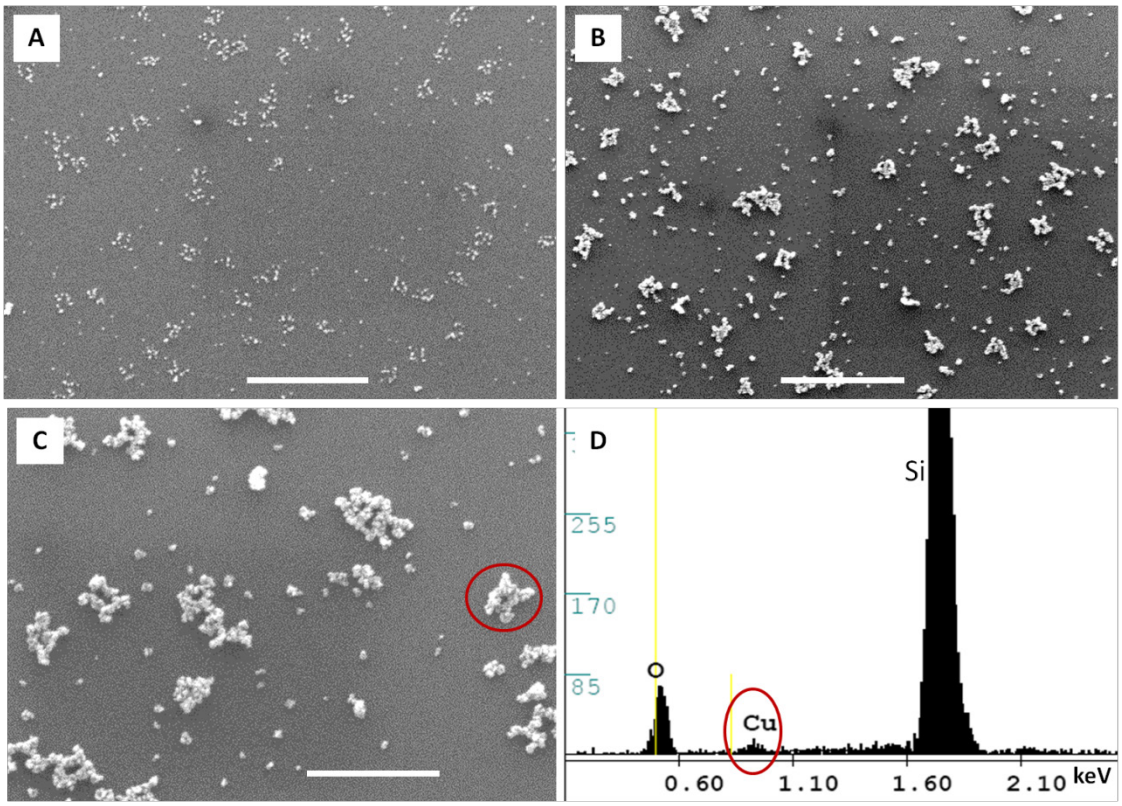

Figure 3.7 Characterization of metallized CC DNA structures on a Si surface. (A) SEM image of a 4×Pd seeded sample after 10 s of commercial Au plating solution treatment. (B-C) SEM images of structures plated with copper for 1 min after the Au plating pre-treatment in (A). (D) EDX of the circled structure in (C). Scale bars: (A-B): 1 μm; (C): 500 nm.

3.3.4 Electrical conductivity measurements on metallized DNA origami structures

Figure 3.8 shows SEM images of Au plated DNA origami CC structures interfaced with Au electrodes. The structures maintained the original DNA shape well in most cases (**Figure 3.8C-F**). Highly zoomed images (**Figure 3.8E-F**) indicate a good interfacial connection between the Au metallized DNA and the deposited electrodes. Electrical conductivity measurements were carried out to confirm the metallic nature of the plated DNA origami nanostructures using a similar experimental setup to one previously published.[9] Samples plated using the commercial plating solution only (**Figure 3.8A, C**) or two plating solutions (**Figure 3.8B, D**) were measured.

A current-voltage plot across an electrode pair having three structures bridging between electrodes 4 and 5 (**Figure 3.8D**) showed a resistance of 3.2 kΩ (**Figure 3.9A**). The results of a number of additional measurements on other Au-plated DNA origami between electrode pairs are shown in **Figure 3.9B**. SEM images of these electrode arrays are given in **Figure 3.10**. DNA origami were metallized using either the commercial Au plating solution alone (**Figure 3.9B**, devices 1-3, 6) or using the two-step plating approach (**Figure 3.9B**, devices 4, 5, 7 and 8). The lowest observed resistances (~1 kΩ) were obtained on DNA origami plated only with the commercial solution, but these also generally had more bridging DNA origami (3 to 4) between electrodes. The trend of the overall resistance increasing with a decreasing number of structures between electrodes is consistent with resistors in parallel in bulk materials and with our previous work.[9]

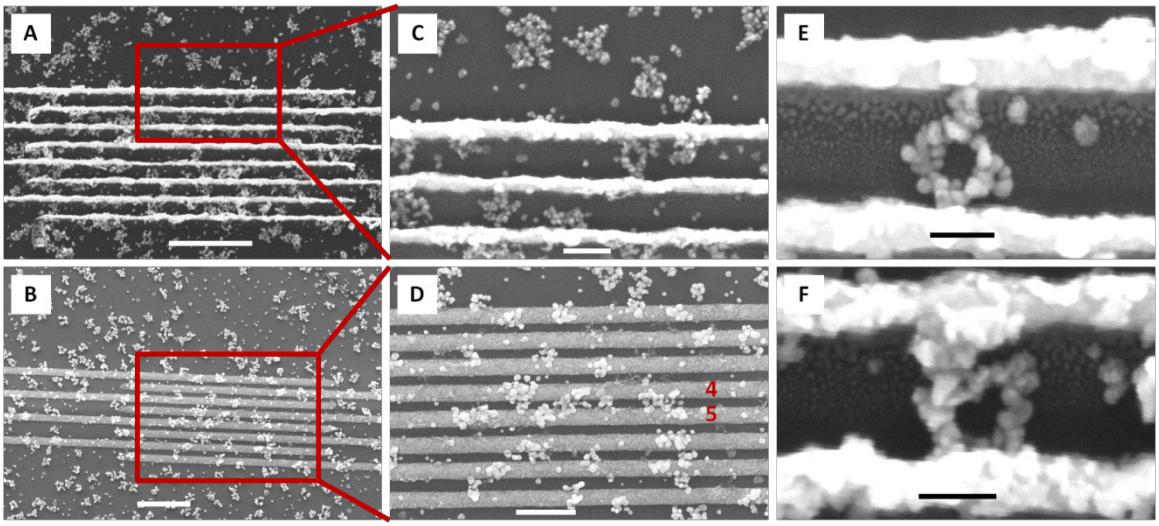

Figure 3.8 SEM images of Au metallized CC structures after depositing Au electrodes for electrical conductivity measurements. (A-B) Large area views of the surface after electrode deposition. (C-D) Zoomed-in images of selected areas in (A-B). (E-F) Highly zoomed views of Au CC structures between Au electrodes. Scale bars: (A-B): 1 μm; (C): 200 nm; (D): 500 nm; (E-F): 100 nm.

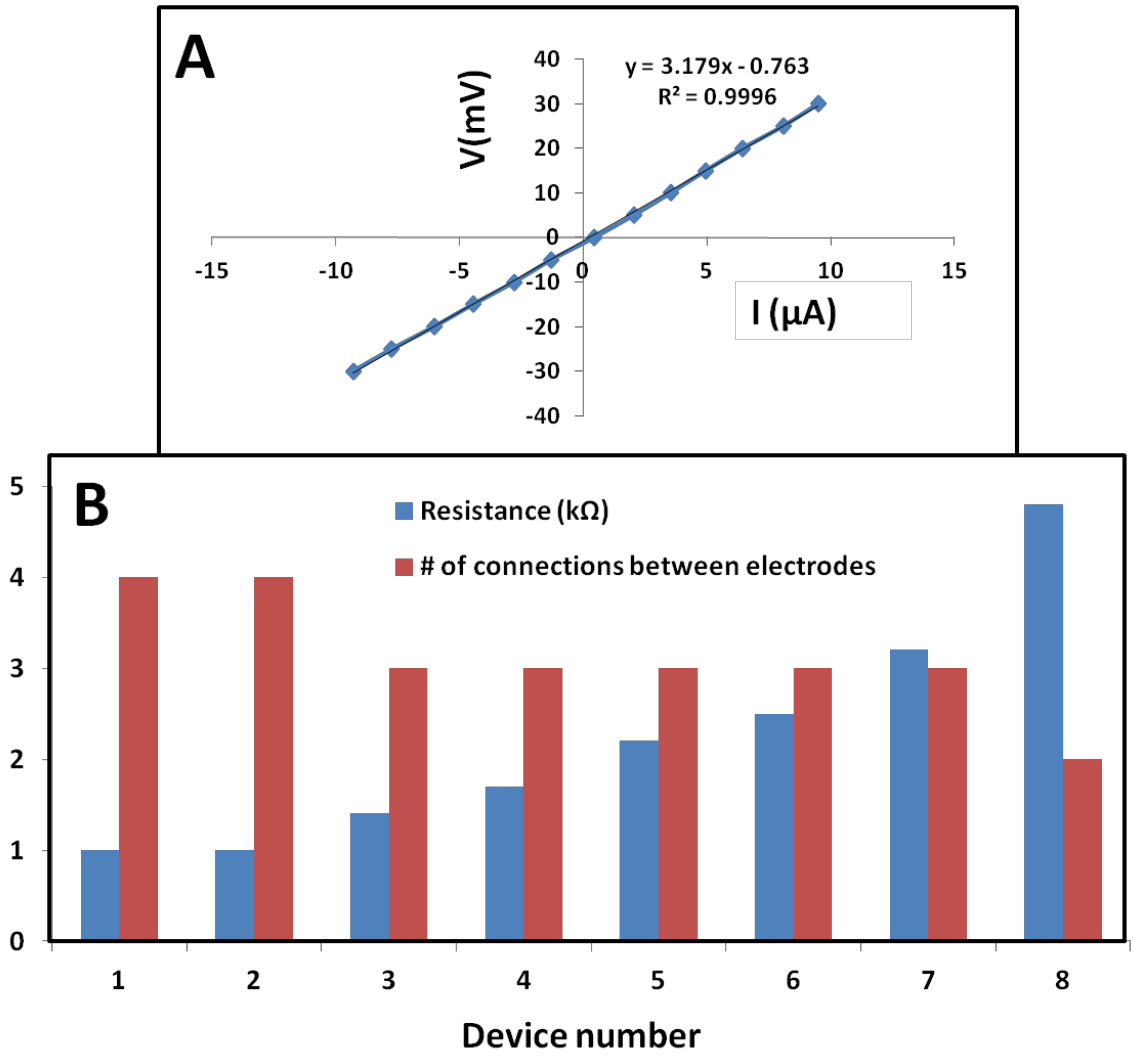

Figure 3.9 Conductance measurements on Au-plated DNA origami CC samples. (A) A typical current-voltage plot obtained of Au plated DNA origami bridging between Au electrodes. (B) Histogram of measured resistance values for 9 electrode pairs having Au-coated structures connecting them.

Conductance measurements were also performed on Cu metallized CC DNA origami. Compared with Au samples, the Cu structures were less well-defined between electrodes after their fabrication. **Figure 3.11** shows SEM images of Cu metallized structures after Au electrode deposition. A large area view of a sample surface, including metallized DNA structures and eight electrodes is shown in **Figure 3.11A**, along with zoomed view images (**Figure 3.11B-D**). Current-voltage plots were obtained by ramping the voltage from -100 to +100 mV. A sample

current voltage curve of metallized DNA origami between electrodes 4-5 in **Figure 3.12A** yielded an overall resistance of ~31 kΩ, as shown in **Figure 3.12C**. The zoomed in image (**Figure 3.12B**) shows one of the bridging structures of a total of 3 connections between the electrodes. I determined the number of connections between electrodes based on SEM images. Images of other electrode pairs measured are given in **Figure 3.13**. A summary of these resistance measurements is shown in **Figure 3.12D** for electrode pairs having one, three, or four Cu-metallized connections. The resistances for single bridging structures ranged from ~40-1000 kΩ (**Figure 3.12D**, devices 1-4), whereas resistances for electrode pairs having three or four connecting structures spanned from ~30-240 kΩ (**Figure 3.12D** devices, 5-10). One reason for the large variation in resistance measured is the ease of oxidation of Cu in air.[19]

I estimated the resistivity of plated DNA origami nanostructures using **Equation (3-1)**:

$$\rho = R\frac{A}{\ell}, \qquad \textbf{(3-1)}$$

Where

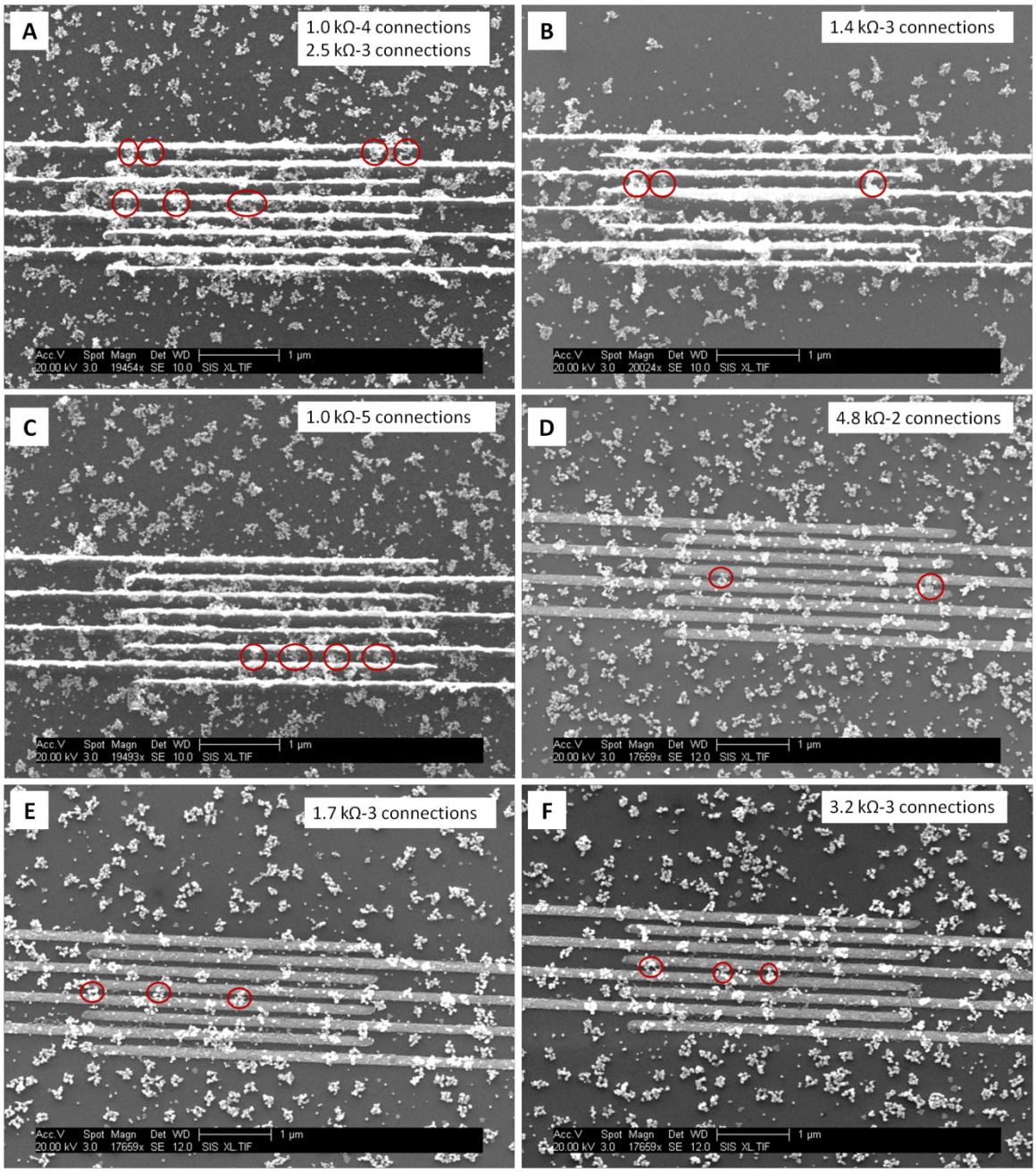

Figure 3.10 SEM images of Au-metallized DNA origami structures between electrode pairs. (A-C) Metallized using only commercial electroless plating solution. (D-F) Metallized using two plating steps.

The resistivity for Au and Cu metallized DNA origami structures was determined from the resistance, the radii of all bridging structures, and the lengths of the structures between the two electrodes, according to **Equation (3-2)**:

$$\rho = R \cdot \sum_n \frac{A_n}{\ell_n}, \qquad \textbf{(3-2)}$$

where R is the overall resistance between two electrodes, and $\sum_n \frac{A_n}{\ell_n}$ is the sum of the ratio of cross-sectional area to bridging length of each connection. I calculated the average resistivity of four singly Au plated samples using **Equation (3-2)** and the devices shown in **Figure 3.10A-C**, and obtained an average resistivity of 7.0×10^{-5} Ω•m with a standard deviation of 1.5×10^{-5} Ω•m and 95% CI of (5.2×10^{-5} Ω•m, 8.8×10^{-5} Ω•m). As with previous work, this value is larger than that of bulk Au (2.4×10^{-8} Ω•m) but is closer to that of linear Au plated DNA origami (6.2×10^{-6} Ω•m).[9] I also calculated the average resistivity for the 4 twice-Au-plated samples shown in **Figure 3.10D-F** and **Figure 3.8D**, obtaining an average resistivity of 11×10^{-5} Ω•m with a standard deviation of 5.4×10^{-5} Ω•m and 95% CI of (4.6×10^{-5} Ω•m, 17.4×10^{-5} Ω•m), which was somewhat larger than that of singly Au plated samples, but with a considerably larger standard deviation.

For Cu samples, equation (2) was also applied to calculate the resistivity. I chose the device that had the smallest resistance with only one connection (**Figure 3.13B**) to calculate the minimum resistivity with this fabrication approach: 3.6×10^{-4} Ω•m. This value is 4 orders magnitude greater than that of bulk Cu (1.7×10^{-8} Ω•m), most likely due to partial oxidation of the nanoscale Cu features in air in the brief time before resistance measurement[19, 20] or the effects of diffuse surface scattering, grain boundaries and line-edge roughness.[21-23]

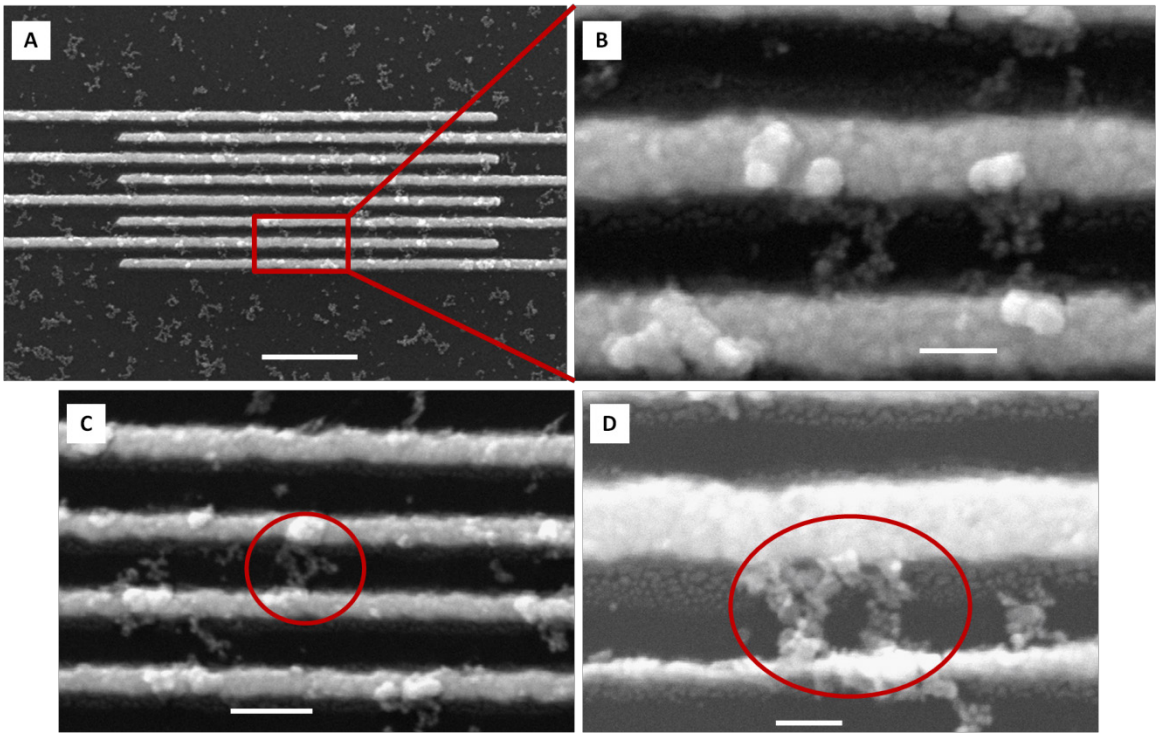

Figure 3.11 SEM images of Cu metallized DNA origami CC structures interfaced with Au electrodes for electrical conductivity measurements. (B) Zoomed-in view of (A). (C) Zoomed image of a single Cu metallized CC structure (circled in red) between electrodes. (D) A highly zoomed image of a Cu-CC structure circled in red. Scale bars: (A) 1 µm; (B, D) 100 nm; (C) 200 nm.

Even though the Cu structures had a higher resistivity than bulk, these measurements of electrical resistivity are the first on Cu metallized DNA samples or DNA origami. I recognize that the oxidation of Cu nanostructures might be decreased with a thin coating of another metal or material that has high oxygen resistance. I further note that the production of copper oxide with controlled oxidation nanostructures from the original copper metallized objects would be useful in making p-type semiconductors, which have potential uses such as field effect transistors.[24]

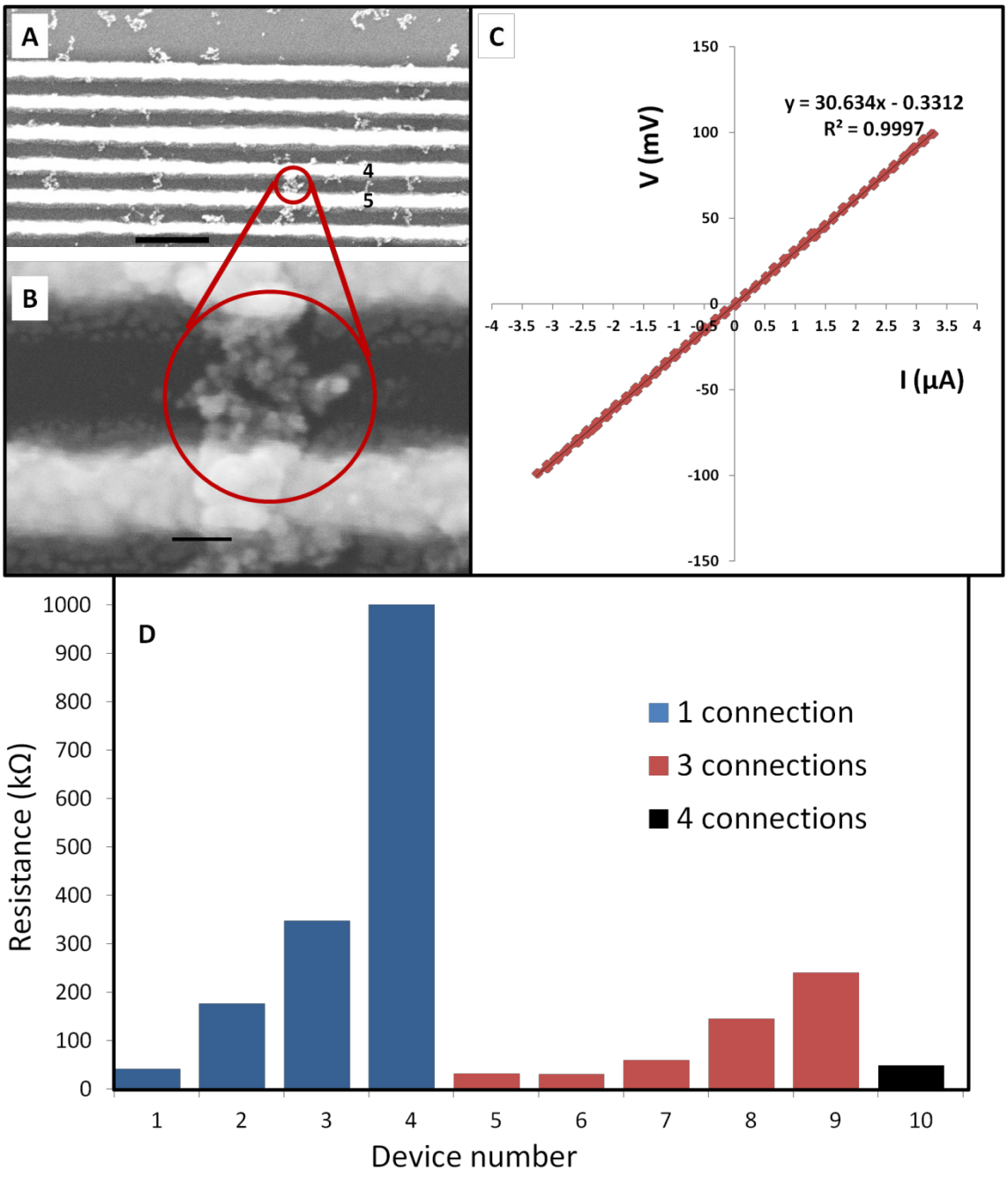

Figure 3.12 Conductance measurements on Cu plated CC DNA origami. (A-B) SEM images of Cu nanostructures between electrodes. Scale bars: (A) 500 nm; (B) 50 nm. (C) Current-voltage plot obtained between Au electrodes 4 and 5 in (A). (D) Histograms of measured resistance values between electrode pairs having a single structure (blue), three structures (red), or four structures (black) between electrodes.

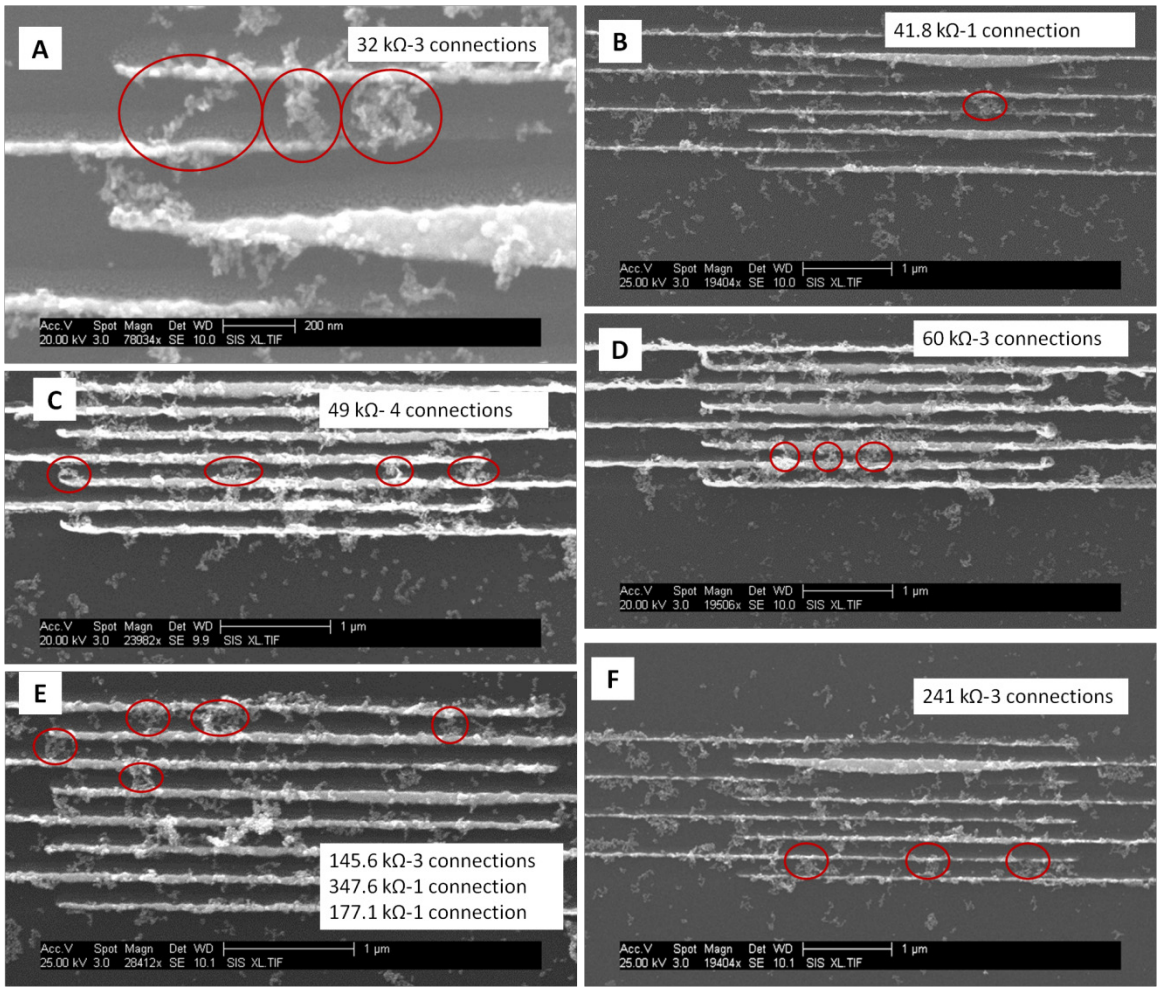

Figure 3.13 SEM images of several Cu-metallized DNA origami structures between electrode pairs. The connections are circled in red in each image.

3.4 CONCLUSIONS

I have demonstrated the metallization of DNA origami CC structures with both gold and copper after multiple Pd seedings. The number of successive seedings was studied and optimized based on several analyses including AFM, SEM, and particle distribution. The structures were continuous and well-defined after metallization. Additionally, I measured the electrical conductivity for these gold and copper DNA origami nanostructures. The resistivities were also calculated based on measured resistances and nanostructure dimensions. The resistivity for gold

samples was close to previously published work by the BYU group. Importantly, this is the first report on the conductivity of copper plated DNA origami templates. Our metallized DNA origami structures might be used as conducting interconnects to nanoscale objects. In addition, based on their surface characteristics, they may also find application in surface enhanced Raman scattering methods.[25]

Future work will focus on improving the conductivity of these metallized DNA origami by method such as thermal annealling. It has been reported that the conductivity of nanowires could be increased after annealling via sintering and fusing individual nanoparticles into a more continuous electrical path,[26] as well as reducing the number of defects in the nanowires.[27] For Cu metallized DNA origami, a less easily oxidized Ni[20] or Ag[28] coating could be deposited to prevent the oxidization of the Cu. Additionally, future work should address site-specific placement of semiconducting nanostructures on DNA origami coupled with site-selective metallization, which could lead to bottom-up transistor fabrication.

3.5 REFERENCES

1. Whitesides, G. M.; Grzybowski, B., Self-Assembly at All Scales. *Science* **2002,** *295* (5564), 2418-2421.
2. Seeman, N. C., Nucleic acid nanostructures and topology. *Angew Chem Int Edit* **1998,** *37* (23), 3220-3238.
3. Becerril, H. A.; Woolley, A. T., DNA-templated nanofabrication. *Chem Soc Rev* **2009,** *38* (2), 329-337.
4. Braun, E.; Eichen, Y.; Sivan, U.; Ben-Yoseph, G., DNA-templated assembly and electrode attachment of a conducting silver wire. *Nature* **1998,** *391* (6669), 775-778.
5. Yan, H.; Park, S. H.; Finkelstein, G.; Reif, J. H.; LaBean, T. H., DNA-Templated Self-Assembly of Protein Arrays and Highly Conductive Nanowires. *Science* **2003,** *301* (5641), 1882-1884.
6. Richter, J.; Mertig, M.; Pompe, W.; Monch, I.; Schackert, H. K., Construction of highly conductive nanowires on a DNA template. *Appl Phys Lett* **2001,** *78* (4), 536-538.

7. Nguyen, K.; Monteverde, M.; Filoramo, A.; Goux-Capes, L.; Lyonnais, S.; Jegou, P.; Viel, P.; Goffman, M.; Bourgoin, J. P., Synthesis of thin and highly conductive DNA-based palladium nanowires. *Adv Mater* **2008,** *20* (6), 1099-1104.
8. Ongaro, A.; Griffin, F.; Beeeher, P.; Nagle, L.; Iacopino, D.; Quinn, A.; Redmond, G.; Fitzmaurice, D., DNA-templated assembly of conducting gold nanowires between gold electrodes on a silicon oxide substrate. *Chem Mater* **2005,** *17* (8), 1959-1964.
9. Pearson, A. C.; Liu, J.; Pound, E.; Uprety, B.; Woolley, A. T.; Davis, R. C.; Harb, J. N., DNA Origami Metallized Site Specifically to Form Electrically Conductive Nanowires. *The Journal of Physical Chemistry B* **2012,** *116* (35), 10551-10560.
10. Rothemund, P. W. K., Folding DNA to create nanoscale shapes and patterns. *Nature* **2006,** *440* (7082), 297-302.
11. Pound, E.; Ashton, J. R.; Becerril, H. A.; Woolley, A. T., Polymerase Chain Reaction Based Scaffold Preparation for the Production of Thin, Branched DNA Origami Nanostructures of Arbitrary Sizes. *Nano Lett* **2009,** *9* (12), 4302-4305.
12. Ke, Y. G.; Douglas, S. M.; Liu, M. H.; Sharma, J.; Cheng, A. C.; Leung, A.; Liu, Y.; Shih, W. M.; Yan, H., Multilayer DNA Origami Packed on a Square Lattice. *J Am Chem Soc* **2009,** *131* (43), 15903-15908.
13. Dietz, H.; Douglas, S. M.; Shih, W. M., Folding DNA into Twisted and Curved Nanoscale Shapes. *Science* **2009,** *325* (5941), 725-730.
14. Liu, J. F.; Geng, Y. L.; Pound, E.; Gyawali, S.; Ashton, J. R.; Hickey, J.; Woolley, A. T.; Harb, J. N., Metallization of Branched DNA Origami for Nanoelectronic Circuit Fabrication. *ACS Nano* **2011,** *5* (3), 2240-2247.
15. Geng, Y. L.; Liu, J. F.; Pound, E.; Gyawali, S.; Harb, J. N.; Woolley, A. T., Rapid metallization of lambda DNA and DNA origami using a Pd seeding method. *J Mater Chem* **2011,** *21* (32), 12126-12131.
16. Pilo-Pais, M.; Goldberg, S.; Samano, E.; LaBean, T. H.; Finkelstein, G., Connecting the Nanodots: Programmable Nanofabrication of Fused Metal Shapes on DNA Templates. *Nano Lett* **2011,** *11* (8), 3489-3492.
17. Gu, Q.; Cheng, C. D.; Haynie, D. T., Cobalt metallization of DNA: toward magnetic nanowires. *Nanotechnology* **2005,** *16* (8), 1358-1363.
18. Musick, M. D.; Pena, D. J.; Botsko, S. L.; McEvoy, T. M.; Richardson, J. N.; Natan, M. J., Electrochemical properties of colloidal Au-based surfaces: Multilayer assemblies and seeded colloid films. *Langmuir* **1999,** *15* (3), 844-850.
19. Toimil-Molares, M. E.; Hohberger, E. M.; Schaeflein, C.; Blick, R. H.; Neumann, R.; Trautmann, C., Electrical characterization of electrochemically grown single copper nanowires. *Appl Phys Lett* **2003,** *82* (13), 2139-2141.
20. Rathmell, A. R.; Nguyen, M.; Chi, M. F.; Wiley, B. J., Synthesis of Oxidation-Resistant Cupronickel Nanowires for Transparent Conducting Nanowire Networks. *Nano Lett* **2012,** *12* (6), 3193-3199.
21. Graham, R. L.; Alers, G. B.; Mountsier, T.; Shamma, N.; Dhuey, S.; Cabrini, S.; Geiss, R. H.; Read, D. T.; Peddeti, S., Resistivity dominated by surface scattering in sub-50 nm Cu wires. *Appl Phys Lett* **2010,** *96* (4).
22. Wu, W.; Brongersma, S. H.; Van Hove, M.; Maex, K., Influence of surface and grain-boundary scattering on the resistivity of copper in reduced dimensions. *Appl Phys Lett* **2004,** *84* (15), 2838-2840.

23. Kim, T. H.; Zhang, X. G.; Nicholson, D. M.; Evans, B. M.; Kulkarni, N. S.; Radhakrishnan, B.; Kenik, E. A.; Li, A. P., Large Discrete Resistance Jump at Grain Boundary in Copper Nanowire. *Nano Lett* **2010,** *10* (8), 3096-3100.
24. Liao, L.; Zhang, Z.; Yan, B.; Zheng, Z.; Bao, Q. L.; Wu, T.; Li, C. M.; Shen, Z. X.; Zhang, J. X.; Gong, H.; Li, J. C.; Yu, T., Multifunctional CuO nanowire devices: p-type field effect transistors and CO gas sensors. *Nanotechnology* **2009,** *20* (8).
25. Bailo, E.; Deckert, V., Tip-enhanced Raman scattering. *Chem Soc Rev* **2008,** *37* (5), 921-930.
26. Kim, E. U.; Baeg, K. J.; Noh, Y. Y.; Kim, D. Y.; Lee, T.; Park, I.; Jung, G. Y., Templated assembly of metal nanoparticles in nanoimprinted patterns for metal nanowire fabrication. *Nanotechnology* **2009,** *20* (35).
27. Richter, J., Metallization of DNA. *Physica E* **2003,** *16* (2), 157-173.
28. Luo, X.; Gelves, G. A.; Sundararaj, U.; Luo, J.-L., Silver-coated copper nanowires with improved anti-oxidation property as conductive fillers in low-density polyethylene. *The Canadian Journal of Chemical Engineering* **2012**, n/a-n/a. DOI: 10.1002/cjce.21701.

CHAPTER 4: CONCLUSIONS AND FUTURE WORK

4.1 CONCLUSIONS

4.1.1 Rapid metallization of lambda DNA and DNA origami using a Pd seeding method

The use of Pd seeding and electroless plating to metallize lambda DNA and branched DNA origami on mica was described in Chapter 2. This method provides the advantage of a fast and simple process, as well as the ability to obtain a relatively high yield of metallized DNA origami nanostructures compared with prior work.[1] Using Pd seeding, continuous 28 nm tall Pd nanowires with good selectivity were successfully fabricated on lambda DNA; Au metallized branched structures were also formed using "T" shaped DNA origami with a length between 200-250 nm, and wire diameters of ~40 nm. Some factors including activation time and Mg^{2+} concentration that influence seeding and Au electroless plating were discussed.

For Pd seeding on lambda DNA templates, I studied the effect of Pd(II) activation time on the seed height and density. For the shortest activation times (2 min), Pd seeding density and height were low. As the time increased, the seeding density and average seed height also increased. When the activation time was lengthened beyond 10 min, the seeding density did not change significantly, and seed aggregation occurred, leading to an increase in the average size. The underlying DNA strands were also largely missing when the activation time was increased up to 3 h. Based on this analysis, a desirable activation time would be between 10 and 30 min, which was also appropriate for DNA origami metallization. In addition, I found that the addition of Mg^{2+} ion with the reducing agent or electroless plating solution could facilitate the surface retention of Pd seeded DNA as well as Au plated DNA structures. I also used double Pd seeding

steps to improve the seeding density on DNA origami. Both Pd metallized lambda DNA and Au metallized DNA origami were characterized by AFM, SEM and EDX, all of which indicated that DNA molecules were promising templates for metallic nanostructure fabrication. Moreover, the formation of Au metallized branched nanostructures showed progress towards the realization of nanoelectronics using DNA origami as the templates.

4.1.2 Electrically conductive Au and Cu metallized DNA origami nanostructures

Although metallization of DNA origami in Chapter 2 indicated promise for nanofabrication, it still needs to improve in some aspects: (1) a silicon surface instead of mica is preferred; (2) more complex DNA origami structures are needed to further illustrate the benefit of this templating method; and (3) electrical conductivity of these nanostructures should be confirmed. Therefore, in Chapter 3, I addressed these three issues. I used a "piranha" cleaned silicon substrate and a modified spin stretching method to put DNA origami on the surfaces, resulting in good retention of the structural shape. Moreover, this spin-coating method was faster than previously reported methods.[1, 2] Multiple Pd seeding steps were employed, and AFM images indicated that the seeded DNA origami remained on the surface and the background stayed low after multiple seeding steps. Distribution analysis of seed heights was used to study the influence of seeding steps on both average height and the uniformity of the seeds grown. An optimized process with four repeated palladium seedings was obtained from the AFM images, seed height distribution analysis, and Au electroless plating results after each seeding condition. Both Au and Cu metallized circular circuit design DNA origami were successfully produced with high yields and selectivity after electroless plating on the seeded samples. SEM results showed that most of these plated structures maintained their shapes, and the average diameters of Au and Cu samples were

~32 nm and 40 nm, respectively. Electrical conductivity measurements were carried out, and both the Au and Cu samples showed ohmic behavior under applied voltage. The resistivities were also estimated based on nanowire resistance and the size of the metallized structures. Although the resistivities obtained were larger than that of bulk metals, it is still promising progress on the metallization of complex DNA origami.

4.2 FUTURE WORK

In my dissertation, DNA origami have been used to form conductive metal nanostructures. However, there remain some matters for improvement: (1) efficient alignment and orientation of these metal structures on surfaces, and (2) the integration of metal nanostructures with other components for the realization of nanocircuitry. Here, I discuss some strategies that address these two problems.

4.2.1 Controlled DNA origami placement on surfaces

In my dissertation, I have succeeded in making relatively complex metal nanostructures on silicon surfaces using DNA origami templates; however, the structures are all randomly placed on the surface, which makes it difficult to integrate them into electronic circuits afterwards. To solve this problem, others have proposed some strategies. For example, Kershner et al.[3] reported the arrangement and orientation of individual DNA origami triangular structures on surfaces patterned by EBL and etched. It was most promising to place one individual DNA origami at a single binding site; when polygonal sites were designed to bind two origami per parallelogram, three per trapezoid, or up to six per hexagon, the frequency of random arrangements increased. I propose that this random arrangement problem could be solved by combining "origami of

origami"[4] discussed in **Section 1.6.1.2** with this arrangement technique. By integrating these two techniques, it should be possible to generate higher-order DNA origami templates for fabrication of nanocircuits. **Figure 4.1** illustrates this method schematically. The overall structure has four circuit units (1-4), each of which has 4 arms at each edge. The core sequences of these four structures (**Figure 4.1**, orange color) is the same, but different bridging sticky ends are attached on the 4 arms on each side. Thus, during the formation of individual subunits, I can use the same scaffold material. The staple strands used would be common for the circuit core, but the sticky-end parts would use different staple strands that are complementary to the sides of other circuit structures. Higher order DNA origami assembles could then be separated and purified by molecular weight. After DNA assembly, the EBL patterning method will be used for placement of the super DNA origami. Instead of units of triangular patterns on the surface, square structures with larger size will be made similarly based on the size of the super origami. Importantly, since the probability of hybridization between arms at each side of these 4 units should be the same, the final structure of the super origami should be close to square structures. The super origami itself is a symmetrical structure; thus, no rotational control is needed during alignment.

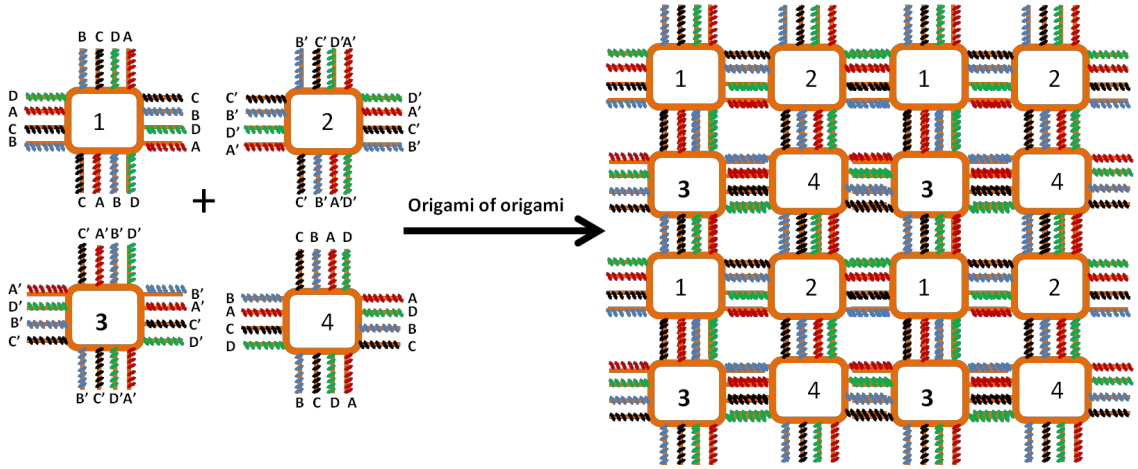

Figure 4.1 Origami of origami to form ordered circuit structure. Bridging strands (sticky ends) with different colors indicate different sequences. A-A', B-B', C-C', and D-D' are complementary with each other.

4.2.2 Integration of CNTs with metallized DNA origami

For DNA origami fabrication, staple strands modified by components such as biotin[5] or metal ions,[6] can be later used in DNA origami folding. Thus, it should be possible to site-specifically metallize the super DNA origami described above and integrate semiconducting CNTs. The biotin-streptavidin interaction can be used to assemble CNTs on a DNA template, which has been reported previously.[7] Here, staple strands modified with biotin would be used to attach CNTs in desired positions; and staple strands with Pd(II) bound could be used for metallization. Importantly, both modifications could be done prior to super DNA origami folding.

For CNT attachment, streptavidin would be attached biotin on the super DNA origami template, defining the binding sites for CNTs; then, CNTs with the correct length will be wrapped using biotin-modified DNA strands; finally, through biotin-streptavidin interaction, CNTs will be placed on the desired locations on the super origami.

For metallization, some staple strands will be incubated with Pd(II) solution, during which the staples are activated and coordinated with Pd^{2+} ions. Excessive Pd(II) not bound to the staple strands will be removed through ion exchange (**Figure 4.2**). The already bound Pd(II) can be reduced and catalyze the electroless plating step, to provide a continuous metal coating.

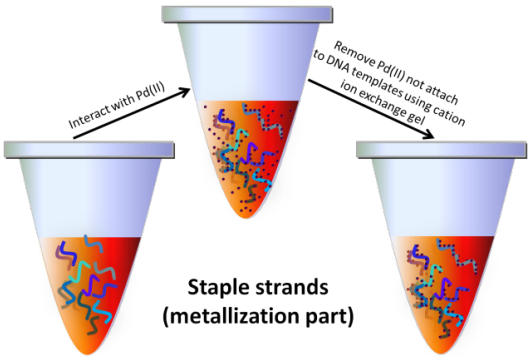

Figure 4.2 Schematic for modification of staple strands with Pd(II) and purification.

A schematic of the whole process is illustrated in **Figure 4.3**. DNA origami units are first fabricated using scaffolds and staple strands with proper modifications of either biotin or Pd(0) (**Figure 4.3A-B**). These are then mixed and annealed to form super DNA origami as shown in **Figure 4.1**, followed by streptavidin binding (**Figure 4.3C**), which then helps placement of biotin-bound CNTs (**Figure 4.3D**). DNA origami templates would then undergo electroless plating metallization (**Figure 4.3E**). The complexity of super DNA origami association with diverse functionalized locations should allow the formation of multiple connections for nanoelectronic circuit fabrication. The resulting structures would have multiple metallized parts serve as conducting wires that integrated with semiconducting CNTs.

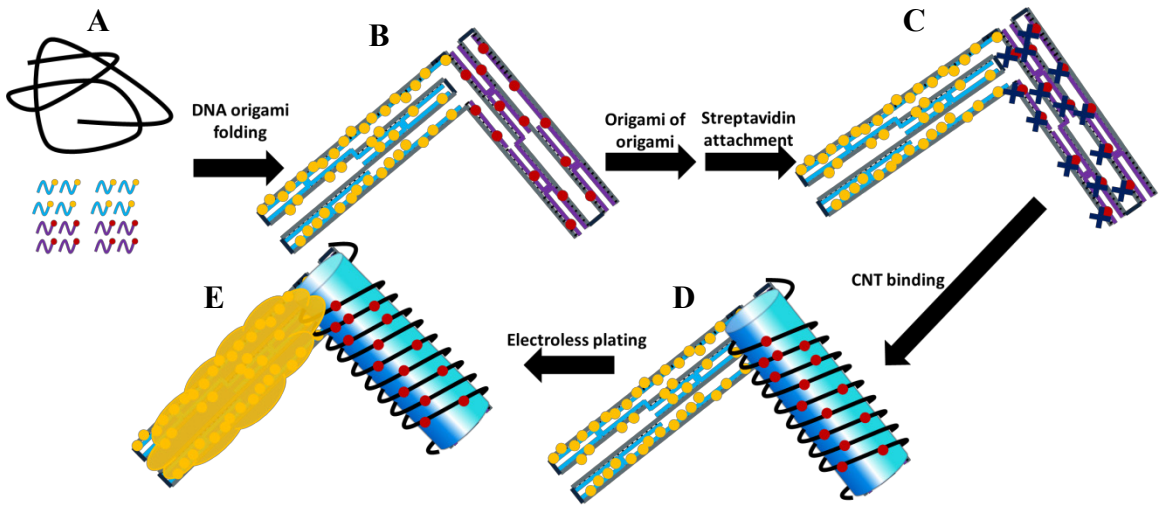

Figure 4.3 Schematic of metallization of CNT attached super DNA origami structures. (A-B) DNA origami formation in which four different DNA origami are folded individually, with specific locations having Pd(0) or biotin. (C) Further super DNA origami folding and then attachment of streptavidins onto biotin sites. (D) CNT binding onto DNA origami site selectively. (E) Electroless plating of the seeded part of DNA origami.

To conclude, in my dissertation I have developed a Pd seeding method to successfully obtain metal nanostructures on both lambda DNA and DNA origami templates on mica and silicon

surfaces. Future studies on metallized super DNA origami structures integrated with CNTs should be beneficial towards the realization of ordered nanocircuit fabrication.

4.3 REFERENCES

1. Liu, J. F.; Geng, Y. L.; Pound, E.; Gyawali, S.; Ashton, J. R.; Hickey, J.; Woolley, A. T.; Harb, J. N., Metallization of Branched DNA Origami for Nanoelectronic Circuit Fabrication. *ACS Nano* **2011,** *5* (3), 2240-2247.
2. Pilo-Pais, M.; Goldberg, S.; Samano, E.; LaBean, T. H.; Finkelstein, G., Connecting the Nanodots: Programmable Nanofabrication of Fused Metal Shapes on DNA Templates. *Nano Lett* **2011,** *11* (8), 3489-3492.
3. Kershner, R. J.; Bozano, L. D.; Micheel, C. M.; Hung, A. M.; Fornof, A. R.; Cha, J. N.; Rettner, C. T.; Bersani, M.; Frommer, J.; Rothemund, P. W. K.; Wallraff, G. M., Placement and orientation of individual DNA shapes on lithographically patterned surfaces. *Nat Nanotechnol* **2009,** *4* (9), 557-561.
4. Zhao, Z.; Liu, Y.; Yan, H., Organizing DNA Origami Tiles into Larger Structures Using Preformed Scaffold Frames. *Nano Lett* **2011,** *11* (7), 2997-3002.
5. Voigt, N. V.; Torring, T.; Rotaru, A.; Jacobsen, M. F.; Ravnsbaek, J. B.; Subramani, R.; Mamdouh, W.; Kjems, J.; Mokhir, A.; Besenbacher, F.; Gothelf, K. V., Single-molecule chemical reactions on DNA origami. *Nat Nano* **2010,** *5* (3), 200-203.
6. Ford, W. E.; Harnack, O.; Yasuda, A.; Wessels, J. M., Platinated DNA as precursors to templated chains of metal nanoparticles. *Adv Mater* **2001,** *13* (23), 1793-1797.
7. Eskelinen, A. P.; Kuzyk, A.; Kaltiaisenaho, T. K.; Timmermans, M. Y.; Nasibulin, A. G.; Kauppinen, E. I.; Torma, P., Assembly of Single-Walled Carbon Nanotubes on DNA-Origami Templates through Streptavidin-Biotin Interaction. *Small* **2011,** *7* (6), 746-750.